# Processing Study of in-situ Bonded Scarf Repairs for Composite Structures

Kavish Bujun

Master of Engineering

Department of Mechanical Engineering

McGill University

Montreal, Quebec

15th August 2014

A thesis submitted to McGill University in partial fulfillment of the requirements of the degree of Master's in Engineering

# Abstract

Composites, particularly, carbon fibre reinforced polymers (CFRP), are widely used in the aerospace industry because of their superior properties compared to their metallic counterparts. These structures eventually undergo damage during operation due to their long service life and the hazardous operating environment. In-situ bonded repairs offer a promising approach to restore the strength of the damaged composite structure. This repair is achieved in one step by simultaneously curing the repair patch and the adhesive film onto the parent laminate using a one sided heat source, such as a heating blanket. However, several issues remain unaddressed and present a challenge during the repair process, such as the temperature heterogeneity within the repair patch and the bondline, which arises during curing. This temperature heterogeneity is associated with thermochemical phenomena that significantly influence the final quality of the repair patch and adhesive. Furthermore, lack of instrumental access within the repair patch prevents in-situ monitoring of this temperature gradient. To efficiently implement a bonded repair, it is crucial to fully understand the thermal response of these repairs, which can henceforth improve their processing, and ultimately the design of repair methodologies and guidelines for composite structures. The objective of this thesis is to develop an approach that can predict this inevitable temperature gradient during curing of a monolithic composite structure. First, an analytical platform is developed using the existing heat transfer theory to study any subsequent dependent physical and chemical phenomena. Second, graphical tools are presented to capture the thermal response of this repair patch configuration. Third, the derived heat transfer model is experimentally validated. The experimental results showed agreement with the analytical model. Finally, the influence of the induced temperature field on the governing thermo-chemical behaviour of the material is analyzed using the derived analytical platform. Through this study, it was found the recommended cure cycle for the material under study (Cycom 5320) required adjustments in the cure cycle to ensure a fully cured repair patch with minimum void content. These adjustments consist of high initial ramp rates, extended dwell periods and careful selection of ramp rates for the post cure section. The influence of heat sinks has also been studied experimentally.

# Sommaire

Les matériaux composites, en particulier, les polymères à fibres de carbone (FC), sont largement utilisés dans l'industrie aérospatiale en raison de leurs propriétés supérieures par rapport à leurs homologues métalliques. Ces structures, éventuellement, subissent des dommages pendant leur fonctionnement en raison de leur longue durée d'opération et de l'environnement hasardeux dans lesquelles elles opèrent. Cependant, restaurer l'intégrité de ces structures composites demeure l'un des principaux défis. Des réparations composites collées *in-situ* offrent une approche prometteuse pour restaurer l'intégrité d'une structure composite endommagée. Cette technique de réparation est réalisée en faisant polymériser simultanément la pièce de réparation et le film d'adhésif sur la structure endommagée à l'aide d'une source de chaleur appliquée sur une seule face, par exemple une couverture chauffante. Cependant, cette source de chaleur non symétrique génère une distribution hétérogène de température au sein de la pièce de réparation et à la ligne de liaison au cours du processus de polymérisation, dont les effets de ce phénomène thermique ont reçu une attention limitée dans la littérature. De plus, cette hétérogénéité de la température est associée à des phénomènes thermochimiques qui influencent de manière significative la qualité finale de la pièce de réparation et de l'adhésif. En outre, le manque instrumentation dans la pièce de réparation empêche une surveillance *in situ* de l'évolution de ce gradient de température. Pour appliquer efficacement une réparation collée *in-situ*, il est donc essentiel de bien comprendre le comportement et la réaction thermique de ces réparations qui ont le potentiel d'améliorer leur traitement et, éventuellement, la conception de méthodologies et de directives pour les réparations des structures composites en général. L'objectif de cette thèse est de développer une approche qui peut prédire ce gradient de température inévitable lors de la polymérisation de la pièce de réparation collée sur une structure composite monolithique. Premièrement, une plate-forme d'analyse analytique est développée en utilisant la théorie de transfert de chaleur pour, ensuite, étudier des phénomènes physiques et chimiques dépendants. Deuxièmement, des outils graphiques sont présentés pour facilement prédire le comportement et la réaction thermique de cette configuration de réparation. Troisièmement, le modèle dérivée de transfert de chaleur est expérimentalement validé. Les résultats expérimentaux concordent avec les prédictions de température du modèle analytique. Enfin, l'influence du champ de température

induite sur le comportement thermochimique du matériau composite est analysée en utilisant la plate-forme d'analyse dérivée. Selon cette étude, il a été constaté que le cycle de polymérisation recommandé pour le matériau composite à l'étude (Cycom 5320) nécessite des ajustements pour faire que la pièce finale de réparation est complètement polymérisée avec une porosité minimale. Ces ajustements consistent en des taux initiaux de rampe élevés, des périodes prolongées pour la section du plateau et une soigneuse sélection de rampe pour la section de polymérisation postérieure. L'influence des puits de chaleur a également été étudiée expérimentalement.

# Acknowledgments

I would like to sincerely thank my supervisor, Professor Pascal Hubert, for his mentorship and support. Throughout my masters, he provided constructive input and guidance while preserving and promoting intellectual independence. Additionally, his ability to lend a global perspective to any research topic has greatly benefited my learning experience as a graduate student.

I would like to thank Natural Sciences and Engineering Research Council of Canada (NSERC) for their financial support, as well as all the industrial and academic partners for their funding and resources: Bombardier, L3, CRIAQ, CREPEC, Université de Laval, Polytechnique de Montréal, and McGill University.

I collaborated with Mathieu Préau and Nadine Auda on this research project, and I am really grateful for their valuable contributions. Furthermore, I would like to specially thank Dr. Arthur Lévy who helped me with the modelling aspect of my work, and Surabhi Joshi for her invaluable help with the concepts of partial differential equations.

The very interactive and involved atmosphere created by the members of Structures and Composites Materials Laboratory made my graduate experience smooth and enjoyable, for which I am really thankful.

Finally, I would like to thank my parents and sister for their love and support.

# Table of Contents

**Abstract** ..... I
**Sommaire** ..... II
**Acknowledgments** ..... IV
**Table of Contents** ..... V
**List of Figures** ..... VII
**List of Tables** ..... XI
**Chapter 1: Introduction and Literature Review** ..... 1
**1.1 Introduction** ..... 1
1.1.1 Repair Overview ..... 4
**1.2 Theory and Literature Review** ..... 5
1.2.1 Bonded Repair ..... 5
1.2.2 Processing of In-Situ Bonded Repairs ..... 10
1.2.3 Heat Transfer Phenomenon for Bonded Repairs ..... 12
1.2.4 Thermo-Chemical Phenomena ..... 13
1.2.5 Conclusion ..... 15
**1.3 Thesis Objectives and Structure** ..... 16
1.3.1 Thesis Objectives ..... 16
1.3.2 Thesis Structure ..... 17
**Chapter 2: Heat Transfer Modelling** ..... 18
**2.1 Problem Definition** ..... 18
2.1.1 Simplifications and Assumptions ..... 19
**2.2 Analytical Solution** ..... 26
2.2.1 Boundary Conditions ..... 27
2.2.2 Heat Transfer during Ramp ..... 28
2.2.3 Heat Transfer during Dwell ..... 33
2.2.4 Comparison of Analytical Solution with the Finite Element Model ..... 34
**2.3 Application: Heat Transfer Charts** ..... 36
2.3.1 Non-Dimensionalization of Heat Equation ..... 36
2.3.2 Heat Charts ..... 38
**2.4 Summary** ..... 49
**Chapter 3: Experiments and Model Validation** ..... 50

**3.1 Manufacturing Process** ..... **50**
3.1.1 Materials ..... 51
3.1.2 Manufacture of Parent Laminates ..... 52
3.1.3 Preparation of Repair Patch and Adhesive Film ..... 54
**3.2 Apparatus and Instrumentation** ..... **54**
3.2.1 Hot-Bond System ..... 54
3.2.2 Data Acquisition System ..... 56
**3.3 Experimental Setup** ..... **56**
**3.4 Measurement of Heat Transfer Coefficient** ..... **58**
3.4.1 Thermal Map Methodology ..... 59
3.4.2 In-Situ Estimation of the Heat Transfer Coefficient ..... 63
**3.5 In-Situ Bonded Repair Experiment** ..... **66**
3.5.1 Implementation of Repair Process ..... 67
3.5.2 Comparison of Experimental Results and Analytical Solution ..... 69
**3.6 Summary** ..... **73**
**Chapter 4: Analysis of Thermo-Chemical Phenomena and Heat Sinks** ..... **74**
**4.1 Thermo-Chemical Analysis** ..... **74**
4.1.1 Cure Kinetics ..... 75
4.1.2 Resin Viscosity and Degree of Impregnation ..... 80
4.1.3 Glass Transition Temperature ..... 86
4.1.4 Summary of Thermo-Chemical Analysis ..... 89
4.1.5 Modified Cure Cycle for Repair ..... 90
**4.2 Thermal Response Analysis with Heat Sinks** ..... **94**
4.2.1 Experimental Study of the Influence of Heat Sinks ..... 94
4.2.2 Experimental Results ..... 97
4.2.3 Analysis of Heat Sinks ..... 99
4.2.4 Summary of Heat Sink Analysis ..... 100
**Chapter 5: Conclusions and Future Work** ..... **102**
**5.1 Conclusions and Contributions** ..... **102**
**5.2 Future Work** ..... **104**
**References** ..... **106**
**Appendix** ..... **110**

# List of Figures

Figure 1.1: Schematic showing typical location of damage on an aircraft fuselage (Airbus A320) during service. The different types of damage and impact energies are also shown [8]. .....3

Figure 1.2: Pictures showing the common types of damage on an aircraft usually encountered while in service: (a) lightning strike [9], (b) runway debris, (c) ground vehicle impact. Image courtesy of Boeing. .....3

Figure 1.3: Schematic showing the various types of bonded repairs used on composite structures [14]: (a) scarf bonded repair, (b) stepped bonded repair, (c) overlap bonded repair . .....5

Figure 1.4: X-ray micrographs of OOA prepregs laminate at different stages in their processing cycle [26]. (a) shows the stack of laminate without any consolidation or heat. The dark areas represent the dry regions and the light grey areas represent the resin rich areas and the fibres. (b) shows the consolidated stack of laminate under vacuum without any heating. (c) shows a fully cured, fully impregnated laminate when both vacuum and heat is applied.....8

Figure 1.5: Pictures showing the main steps involved when performing an in-situ bonded scarf repair [29]. (a) damage removal and scarfing, (b) adhesive and repair patch application, (c) heating blanket application. .....9

Figure 1.6: Schematic showing a typical bagging arrangement for the in-situ bonded repair process. .....9

Figure 1.7: Graph showing the evolution of various key thermo-chemical phenomena when subjected to an imposed temperature and time cycle during the curing process. The consolidation vacuum pressure is constant at 101 kPa during the entire curing process.....14

Figure 2.1: Schematic showing the heat transfer modelling for in-situ bonded scarf repairs of monolithic composite panels. The heat source is applied on one side and the other side is exposed to the ambient air.....19

Figure 2.2: Schematic showing the axisymmetric heat transfer modelling of the repair patch. .....20

Figure 2.3: Temperature and heat flux distribution throughout a composite repair patch during the curing process by considering a 2D analysis. .....22

Figure 2.4: Schematic describing the two characteristic zones for the heat transfer phenomena during the cure of a repair patch: the 1D conduction zone and the edge effect zone. The overlap distance is also shown. .....24

Figure 2.5: Contour plot of the overlap distance for the 1D dimensional approximation of the heat transfer problem for in-situ bonded repair process. The different contours represent different Biot numbers. The area surrounded by the dashed blue line represents the typical range of values of the overlap distance for a composite repair patch.....25

Figure 2.6: A schematic showing a one-dimensional model representation of the heat transfer problem of the repair process through the thickness, and subjected to two different boundary conditions. .....27

Figure 2.7: Graph showing the comparison between the finite element and the analytical model used to estimate the temperature field within the repair patch subjected to a one-side heat source.....35

Figure 2.8: Schematic showing the key characteristics of the thermal response during the cure of an in-situ repair patch. .....39

Figure 2.9: Graph showing the temperature lag between the heated side and the non-heated side during the initial ramp of the cure cycle. The contours represent the temperature lag for various Biot numbers. The dashed line illustrates the representative case study considered. ..... 43

Figure 2.10: Graph showing the ratio of the ramp rate of the non-heated side to the imposed ramp rate (on the heated side) during the initial ramp of the cure cycle. The contours represent various Biot numbers. The dashed line illustrates the representative case study considered. ..... 44

Figure 2.11: Graph showing the dimensionless time for which the non-heated side has reached 95% of the steady state temperature during the dwell section of the cure cycle. The contours represent the various Biot numbers. The dashed line illustrates the representative case study considered. ..... 45

Figure 2.12: Graph showing the steady state temperature of the non-heated side during the dwell section of the cure cycle. The dashed line illustrates the representative case study considered. ..... 46

Figure 2.13: A contour plot of the relative deviations (in percentage) in (a) the ramp rate of the non-heated side, $R_L$, and (b) the steady state temperature of the non-heated side, $T_{ss}$, from the baseline temperature is shown for a range of values of heat transfer coefficient, $h$, and repair patch thickness, $L$. ..... 48

Figure 3.1: Schematic showing the bagging arrangement used for the manufacture of the parent laminate with the integrated scarfed cavity. ..... 53

Figure 3.2: Picture showing the cured parent structure with the integrated scarfed cavity which was manufactured using the ply drop off technique. The close-up area of the scarfed cavity shows the rough terraced texture obtained from the ply drop off and the use of a peel ply. ..... 53

Figure 3.3: Picture showing (a) the uncured repair patch used for the in-situ bonded repair. (b) The ring shaped adhesive film that was placed between the repair patch and the scarfed cavity. ..... 54

Figure 3.4: Schematic showing the layout of the electrical circuit for the hot bond system. The PID controller is used to control the temperature of the heating blanket via a solid state relay. ..... 55

Figure 3.5: Picture of the experimental setup used to perform the in-situ bonded repair for the validation of the heat transfer model. ..... 57

Figure 3.6: Picture of the parent laminate vertically supported in the experimental setup. The heating blanket was applied on one side and the other side was exposed to ambient air. ..... 58

Figure 3.7: (a) Cross section of the representative thermal map setup used to estimate the transverse heat flux through the parent laminate subjected to a one sided heat source. (b) Thermocouple layout onto both sides of the silicone sheet ..... 60

Figure 3.8: Schematic of the cross-section of the silicone sheet showing three different thermocouples embedded throughout the silicone blanket for the thermal map application. This configuration aims at reducing the percentage error in estimating the value of the heat transfer coefficient. ..... 63

Figure 3.9: Schematic of the cross-section of the damaged parent structure showing the bagging arrangement used for the thermal map assembly. ..... 64

Figure 3.10: Graph showing the typical measurements of the 18 embedded thermocouples within the silicone sheet during the thermal map sensing process. ..... 65

Figure 3.11: Schematic of the cross-section of the parent structure showing the bagging arrangement for the in-situ bonded repair process. It is noted that a vacuum bag was also placed on the non-heated side to provide consolidation pressure for the repair patch and prevent the flow of air through the repair patch. ..... 68

Figure 3.12: Schematic of the repair patch and parent laminate showing the locations of the thermocouples used to capture the thermal response of the repair patch during curing. ..... 69

Figure 3.13: A temperature plot showing the temperature distribution through the thickness of the repair patch during the curing process for Case Study 1 (4.1 mm thick); the thermocouple measurements were collected every second. For better clarity, the temperature at locations 1 and 2 of the repair patch is shown. The temperature at the rest of the thermocouple locations are shown in the Appendix. ..... 70

Figure 3.14: A temperature plot showing the temperature distribution through the thickness of the laminate during the cure of the repair patch for Case Study 2 (14mm thick) ); the thermocouple measurements were collected every second. For better clarity, the temperature at locations 1 and 2 of the repair patch is shown. The temperature at the rest of the thermocouple locations are shown in the Appendix. ..... 71

Figure 4.1: Graph showing the temperature and the predicted degree of cure of the heated and non-heated side of the repair patch during the curing process for Case study 1(top) and Case Study 2(bottom). Case Study 1 and 2 involve a 4.1mm thick (5320/PW) and 14mm thick (5320/8HS) parent laminate respectively..... 78

Figure 4.2: Graph showing the temperature and the predicted resin viscosity of the heated and non-heated side of the repair patch during the curing process for Case study 1(top) and Case Study 2(bottom). Case Study 1 and 2 involve a 4.1mm thick (5320/PW) and 14mm thick (5320/8HS) parent laminate respectively..... 83

Figure 4.3: Graphs showing the temperature and the predicted degree of impregnation of the heated and non-heated side of the repair patch during the curing process for Case study 1(top) and Case Study 2(bottom). Case Study 1 and 2 involve a 4.1mm thick (5320/PW) and 14mm thick (5320/8HS) parent laminate respectively. ..... 84

Figure 4.4: Graph showing the temperature and the predicted glass transition temperature of the heated and non-heated side of the repair patch during the curing process for Case study 1(top) and Case Study 2(bottom). Case Study 1 and 2 involve a 4.1mm thick (5320/PW) and 14mm thick (5320/8HS) parent laminate respectively. ..... 88

Figure 4.5: Graph showing the temperature evolution, the predicted resin viscosity (top) and degree of impregnation (bottom) of the heated and non-heated side of the repair patch when the modified cure cycle is imposed for Case Study 1. It involves a 4.1mm thick (5320/PW) parent laminate. ..... 91

Figure 4.6: Graph showing the temperature evolution, the predicted degree of cure (top) and glass transition temperature (bottom) of the heated and non-heated side of the repair patch when the modified cure cycle is imposed for Case Study 1. It involves a 4.1mm thick (5320/PW) parent laminate. ..... 92

Figure 4.7: A micrograph of the cross-section of the monolithic panel (Case Study 1) restored using the in-situ bonded repair technique. The low void content (less than 1%) in the bondline and within the repair patch indicate a good quality repair. ..... 93

Figure 4.8: Schematic showing the two different types of aluminum stiffeners attached to the parent laminate:(a) represents a flat stiffener (Heat Sink Case Study 1) and (b) represents a long L-shaped stiffener (Heat Sink Case Study 2). ..... 95

Figure 4.9: Schematic of the cross section of the repair patch showing the locations of the thermocouples used to capture the thermal response of the repair patch for the two heat sink case studies: Heat Sink Case Study 1 (top) and Heat Sink Case Study 2 (bottom).....97

Figure 4.10: Graphs showing the thermal response of the repair patch for a 4.1mm thick parent laminate (5320/PW) in the presence of two different kinds of metallic stiffeners: a thin flat stiffener in Heat Sink Case Study 1 (top) and a long L-shaped stiffener in Heat Sink Case Study 2 (bottom).....98

Figure A.1: Schematic of the repair patch and parent laminate showing the locations of the thermocouples used to capture the thermal response of the repair patch during curing.....110

Figure A.2: A temperature plot showing the temperature distribution through the thickness of the repair patch during the curing process for Case Study 1 (4.1 mm thick). The temperature at locations 1, 2,3,4,5 and 6 of the repair patch is shown.....110

Figure A.3: A temperature plot showing the temperature distribution through the thickness of the repair patch during the curing process for Case Study 2 (14 mm thick). The temperature at locations 1,2,3,4, 5 and 6 of the repair patch is shown.....111

Figure A.4: Heat chart showing the extracted values of the steady state temperature for the non-heated side of the repair patch ($T_{ss}$) for the experimental Case Studies 1 and 2 discussed in Chapter 3.....112

Figure A.5: Heat chart showing the extracted values of the ramp rate of the non-heated side of the repair patch ($R_L$) for the experimental Case Studies 1 and 2 discussed in Chapter 3.....113

Figure A.6: A contour plot of the relative deviations in (a) $\Delta T$ ,in °C, and (b) $t_{ss}$ , in hours, from the baseline imposed cure cycle is shown for a range of values of heat transfer coefficient, $h$, and repair patch thickness, $L$.114

# List of Tables

Table 2.1: Model Parameters used for comparing the analytical solution with the finite element model [25]. ..... 35

Table 2.2: Material properties and heat transfer parameters for the representative case study [25]. ..... 41

Table 2.3: Thermal response data extracted from the heat charts for the representative case study ..... 47

Table 3.1: Properties of Cycom 5320/PW and 5320/8HS prepregs [2, 48]. ..... 51

Table 3.2: Thermo-physical properties of the composite materials used in the experimental validation [25]. ..... 52

Table 3.3: Sensing data for post processing of thermal-map for repair Case Study 1. ..... 66

Table 3.4: Specifications of the parent laminates used for the experimental validation. ..... 67

Table 3.5: Material properties of CYCOM 5320 and the heat transfer parameters for the two case studies [25] ..... 70

Table 3.6: Thermal response data for the two case studies. Both the experimental and predicted values are shown for comparison. ..... 72

Table 4.1: Cure kinetics model parameters for Cycom 5320 [25]. ..... 77

Table 4.2: Viscosity model parameters for Cycom 5320 [25]. ..... 81

Table 4.3: Degree of impregnation model parameters for Cycom 5320/PW and Cycom 5320/8HS [2]. ..... 82

Table 4.4: Dimensions of the two types of metallic stiffener. ..... 95

# Chapter 1

# Introduction and Literature Review

## 1.1 Introduction

The emergence of composite materials and processes over the past decades is predominantly justified by the needs of the aerospace industry where there is a constant demand for improved performance. Composite materials are engineered to fit the specialized needs of the aerospace industry: they offer improved performance compared to conventional materials and significantly lower the manufacturing and operational costs of aircrafts [1, 2]. The general trend in manufacturing composite materials consists of combining at least two different materials to generate one final material that exceeds the performance of its individual constituents [1, 3]. Most aerospace grade composite materials are designed to out-perform conventional metallic alloy materials.

Carbon Fibre Reinforced Polymer (CFRP) is a commonly used material in the aerospace industry that offers a high specific strength and stiffness with improved fatigue resistance. These enhanced properties results from the light but strong uniformly oriented carbon fibres, which are usually embedded in an epoxy matrix. Under loading, the matrix and fibres work together to maintain the shape of the structure in addition to sharing the load to obtain the best-combined performance. Additionally, the epoxy resin plays an important role in transferring loads between

the fibres, reducing wear and tear of the fibres, and resisting interlaminar shear between the fibres[1, 4].

Another unique feature of composite materials is their anisotropic nature, i.e., their properties are directionally dependent, thereby enabling versatile design options for the manufacturing of composites. For instance, structures made out of composite materials can be optimized for efficiency by tailoring the material properties to support specific directional loads.

With the development of composite materials, the manufacturing processes of aircraft structures have also experienced an innovative shift in the general practice. The ability of the composite materials to be joined by simply overlapping the plies and to conform to complex mold shapes in their uncured state has enabled a minimum-step manufacturing process. Large composite structures with integrated complex parts and curvatures can now be manufactured in one go, resulting in a significant reduction of joining operations and the use of fasteners. These characteristics produce a faster, improved, and cost effective manufacturing process.

Overall, composite materials offer an ideal balance between performance and cost savings to sustain the growth of the aerospace industry. Consequently, these attractive properties of composite materials have led to a dramatic increase in the use of CFRPs in aerospace in the recent years. For, instance, the composite content of several aircraft frames has even exceeded 50 % by weight [5]. However, as the number of aircraft components made out of composite materials is escalating, the probability of these structures experiencing damage during operation is increasing simultaneously.

Despite their enhanced properties, composite structures, inevitably, still experience damage and operational usage while in service. These damages are becoming particularly prominent in aircraft structures due to a combination of long service life and the hazardous environment in which an aircraft constantly operates. For instance, Figure 1.1 shows the typical locations and the types of damage commonly seen on a fuselage structure. They include ground service vehicle bumps, tool drop during maintenance, and other unavoidable circumstances such as in-flight

lightning strikes and cyclical damage to the material due to the environment [6, 7]. Figure 1.2 shows the various kinds of damage often experienced during operation.

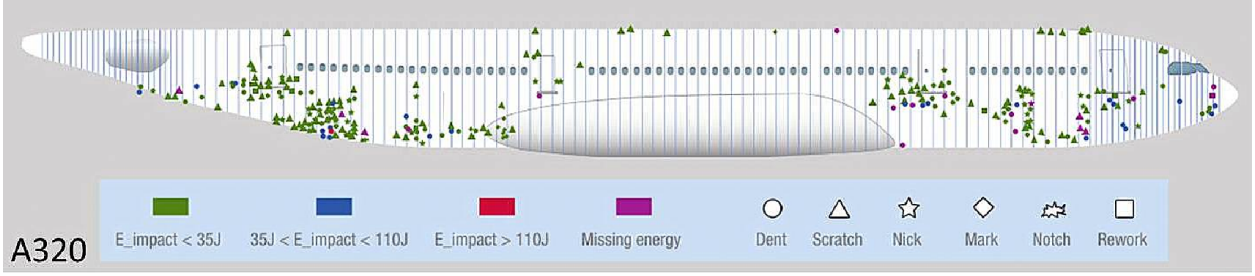


**Figure 1.1:** Schematic showing typical location of damage on an aircraft fuselage (Airbus A320) during service. The different types of damage and impact energies are also shown [8].


**(a)** **(b)** **(c)**

**Figure 1.2:** Pictures showing the common types of damage on an aircraft usually encountered while in service: **(a)** lightning strike [9], **(b)** runway debris, **(c)** ground vehicle impact. Image courtesy of Boeing.

After inspection, if the strength of the damaged composite structure has been found to be compromised, repair actions are required to restore the strength the component instead of replacing it, which would be costly and therefore intentionally avoided. The development of a robust repair methodology following damage requires the union of expertise from several different areas [10]. As of now, unfortunately, the aerospace industry lacks this multi-disciplinary expertise with regard to the repair process of these newly developed composite materials [10]. Consequently, there is an increasing need for researchers to develop certifiable repair methodologies and protocols for new composite aircraft structures.

### 1.1.1 Repair Overview

Over the past few decades, the repair processes of conservative metallic structures have been well researched and mastered. Unfortunately, because the damage mechanisms differ, these practices and procedures cannot be mapped as-is from metallic to composite structures. Consequently, composite structures require repair techniques that are different from their metallic counterparts [10]. Baker and Hart-Smith have shown that composite bonded repairs can achieve better strength restoration and fatigue resistance compared to conventional bolted repairs because of the absence of stress concentrations due to fasteners on the parent structure [11, 12]. Furthermore, bonded repairs are low-weight and have the ability to maintain an aerodynamic profile, which are desirable characteristics for aircraft structures.

Nonetheless, carrying out a bonded repair is complex and involves numerous challenges that need to be addressed to ensure bond integrity and maximum strength restoration. One of these difficulties arises during the processing of bonded composite repairs and has received limited attention in the literature. In order to efficiently implement a bonded repair, especially for primary and secondary structures, it is crucial to fully understand the processing of bonded repairs, and design repair methodologies and guidelines for composite structures accordingly [13].

## 1.2 Theory and Literature Review

In this section, a concise review of relevant background theory and literature on the processing of composite repairs for aircraft structures is presented. The governing physical phenomena that influence the processing of bonded repairs are identified along with areas that require further investigation.

### 1.2.1 Bonded Repair

Damaged composite structures can be repaired using numerous bonded repair configurations; scarf, stepped and overlap, as shown in Figure 3.1.

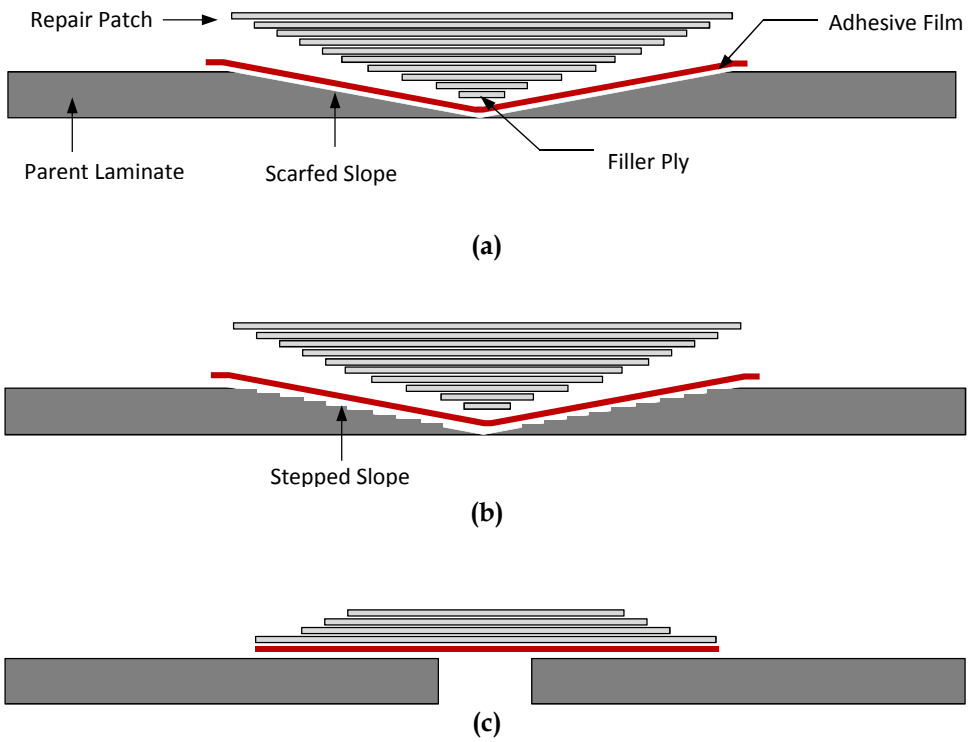


**Figure 1.3:** Schematic showing the various types of bonded repairs used on composite structures [14]: **(a)** scarf bonded repair, **(b)** stepped bonded repair, **(c)** overlap bonded repair .

All these repair techniques can be implemented directly onto the damaged structure especially when we lose the ability to remove the component to place it into an autoclave or conventional oven. However, when high strength recovery is crucial, or when there is a requirement for a flush surface to satisfy the aerodynamic profile, the choice is limited to only bonded scarf or stepped

lap repairs which are also referred as flush structural repair [14] . Gunnion has shown that an optimum-designed scarf or stepped lap joint is significantly stronger than an optimum lap joint, with failure occurring in the adherend outside of the joint instead of adhesive peel or shear failures [15-17]. Both bonded scarf and stepped lap repairs restores full structural properties by forming a joint between the prepared repair area and the repair patch. The repair process is implemented by replacing each ply of the parent structure that has been removed from the damaged area and by placing an adhesive film at the interface of the new and old material [14].

The only variation between scarfed and stepped lap repairs lies in the way the damaged material is removed from the parent structure. Stepped lap is achieved by removing a precise area of material per ply, resulting in a terraced slope versus a smooth slope of a scarfed area. However, in the context of processing of the repair, both configurations are similar.

Within the bonded scarf/stepped lap repair configuration, there are two main approaches in implementing this type of repair process. The first technique involves a co-bonded pre-cured hard patch, where a previously cured hard patch is bonded using an adhesive film onto the scarfed cavity in the parent structure. This process is also known as secondary bonding where two cured laminate are bonded together. The second technique is often referred to as an in-situ co-cured soft patch configuration, which consists of simultaneously curing the prepreg repair patch and adhesive film onto the parent structure. Each technique has their respective advantages and disadvantages.

The hard patch configuration offers the advantage of using autoclave grade material, which has been pre-processed under optimum conditions in an autoclave for the repair process. Consequently, to achieve a successful repair process, the only concern is to ensure that the adhesive has been adequately cured to get a pristine bondline during the bonding process. However, one drawback of this practice is that it is a two-step procedure (the repair patch has to be manufactured prior to bonding and then bonded to the scarfed area) which can significantly delay the repair process. In addition, since every repair is different, a specific cast mold is required to achieve the right dimension and shape of the repair patch, especially in intricate areas.

On the other hand, in-situ bonded repair is a one step process, and can be easily made to conform to the shape of the parent structure. Nevertheless, with in-situ soft patch repairs, it is crucial that the quality of both the repair patch and the bondline, which are being processed simultaneously, meet the aerospace norms. This includes a fully cured patch and bondline, without damaging any surrounding areas and with minimum overall void content.

Since the procedure for implementing a softpatch configuration does not permit the use of an autoclave to consolidate the repair patch, this technique is restricted to the use of only Out-of Autoclave (OOA) prepregs, where vacuum-bag-only pressure in the presence of a localized heat source is used. Also, during the recent years, significant improvements in the vacuum-bag-only processing of OOA composite materials have further increased the popularity of in-situ co-cured repair patch for bonded repairs [18-20].

**Out of Autoclave Materials and Processing**

Out-of Autoclave prepreg materials and processes are engineered to produce high quality parts using vacuum-bag-only (VBO) consolidation and in the presence of a heat source [18, 19]. During the processing of OOA prepregs, it is crucial that any entrapped air is evacuated from the laminate stack to produce a final low porosity, good quality part. However, the reduced pressure differential during consolidation in the VBO process compared to autoclave pressure represents a challenge for collapsing voids within the laminate. Consequently, these innovative materials are designed to feature engineered vacuum channels (eVaCs) for removing the entrapped air which would otherwise remain as void [21].

The microstructure of the OOA prepregs consists of semi-impregnated fibres, which are divided into dry areas and areas that contain excess resin. The eVaCs channels are represented by the dry fibre regions and allow the gases to escape during early stages of the processing when the laminate is placed under vacuum hold for several hours. These eVaCs channels are responsible for the in-plane breathing capabilities of OOA materials. However, the physical constraints at the extremities of in-situ bonded repair patches demand a few modifications to allow the use of these in-plane breathing capabilities during vacuum bag only processing, which are explained in

Section 1.2.2. When heat is applied, the resin viscosity is lowered and infiltrates the dry fibres to produce a fully impregnated, high quality with low porosity laminate [22-24]. This chemical phenomenon significantly depends on the imposed cure cycle, which has to be carefully designed and optimized to create a high quality part [25]. Figure 1.4 shows the micrographs of OOA materials at the different stages of processing.

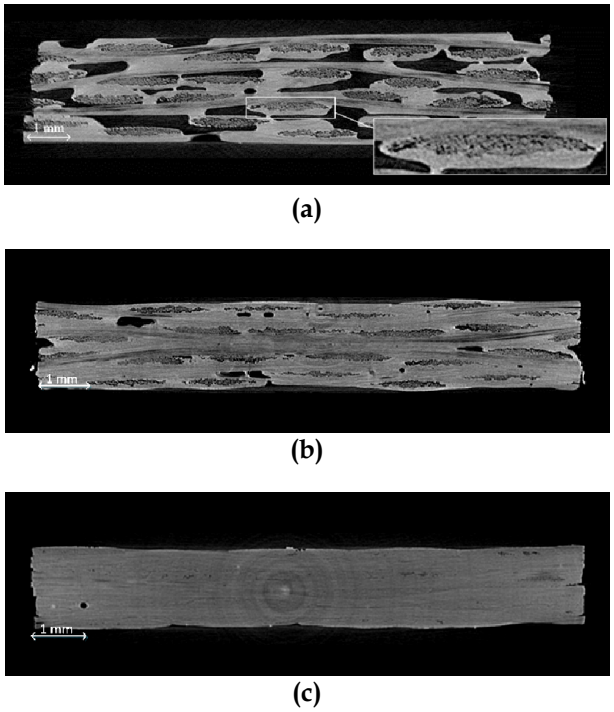


**Figure 1.4:** X-ray micrographs of OOA prepregs laminate at different stages in their processing cycle [26]. **(a)** shows the stack of laminate without any consolidation or heat. The dark areas represent the dry regions and the light grey areas represent the resin rich areas and the fibres. **(b)** shows the consolidated stack of laminate under vacuum without any heating. **(c)** shows a fully cured, fully impregnated laminate when both vacuum and heat is applied.

### Outline of the In-Situ Bonded Repair Process

There are a series of steps involved in implementing an in-situ bonded repair. They can be divided in five main tasks: damage removal, surface preparation, patch application and consolidation, curing process, and finally non-destructive inspection [14, 27]. The first step in a repair process of a composite structure includes the removal of any material surrounding the damage as shown in Figure 1.5 (a). A scarf angle of 3° is usually maintained while sanding out the parent laminate for maximizing the strength restoration [7]. Typically, a couple of plies are left on the parent structure during material removal to ensure a back pressure to maintain

consolidation when vacuum is applied, as shown in Figure 1.6. Alternatively, if the damage is through the entire thickness of the parent structure, a metallic cap or a vacuum bag can be placed on one side to maintain the required consolidation pressure. Subsequently, the scarfed surface of the parent structure is activated using standardized surface preparation techniques to enhance its adhesivity [7]. For cases where a high moisture content is present in the parent laminate, a heating blanket is placed over the scarfed structure to dry out most of the moisture thereby improving the quality of the bond [28].

**(a)** **(b)** **(c)**

**Figure 1.5:** Pictures showing the main steps involved when performing an in-situ bonded scarf repair [29]. **(a)** damage removal and scarfing, **(b)** adhesive and repair patch application, **(c)** heating blanket application.

The next step involves preparing the softpatch that will be placed in the scarfed cavity. First the adhesive film is placed on the scarfed surface (see Figure 1.5 (b)). Next, the plies of the soft patch are carefully positioned in place to match the lay-up orientation of the parent laminate. Once the softpatch is in place, the repair setup is bagged and consolidated under vacuum pressure. A schematic of the bagging arrangement is shown in Figure 1.6.

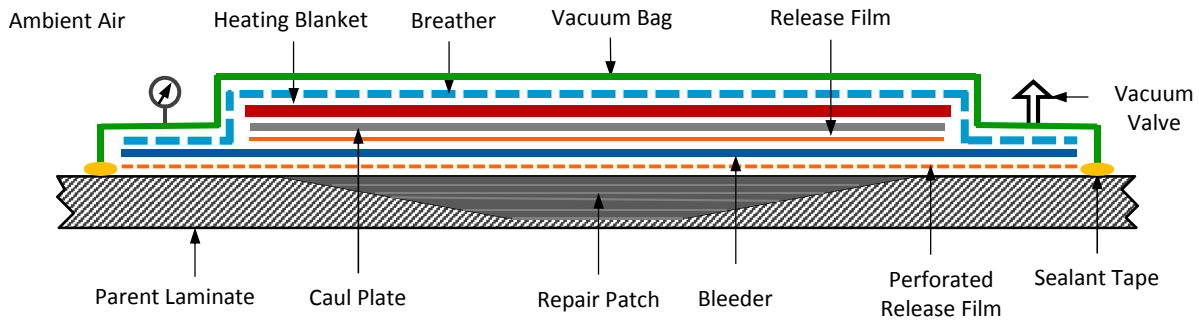


**Figure 1.6:** Schematic showing a typical bagging arrangement for the in-situ bonded repair process.

A silicone-heating blanket is used to provide the necessary heat to cure the epoxy resin in the soft patch as well as the adhesive film (see Figure 1.5 (c)). A proportional-integral-derivative (PID) controller that uses feedback thermocouples, placed only on the top of the repair patch, maintains the temperature of heating blanket according to a specified cure cycle. This imposed cure cycle cures the adhesive film and the repair patch.

### 1.2.2 Processing of In-Situ Bonded Repairs

OOA materials and processing techniques represent a viable approach for implementing high quality in-situ co-cured bonded repairs. However, there are numerous challenges associated with in-situ processing of an OOA repair patch for bonded scarf repairs.

#### Air Evacuation

The in-plane direction, which is more effective and dominantly used to extract the entrapped air in OOA materials [30, 31], is not an option for processing of bonded scarf joint repairs. The in-plane air evacuation is restricted by the sloped cavity of the parent laminate. In a recent study, Preau et al. investigated various breathing solutions to produce a low porosity repair patch and bondline for the scarf repair configuration [32]. This approach uses an inter-leaf fabric along the bondline to create a continuous network of evacuation channels in the in-plane direction for the entrapped air to escape. A combination of this modified in-plane and through thickness air channels was able to evacuate the entrapped air within the repair patch and at the bondline, reducing the overall void content.

#### Curing Process

The curing process of the in-situ co-cured repair patch is one of the most crucial steps in performing a high-quality repair and continues to pose a significant challenge, as summarized by [7]. As described earlier, the heat source for the in-situ bonded repair configuration under study is applied on only one side of the repair patch due to inaccessibility to the other side of the structure. This method of heating adds further complexity to the curing process of both the repair patch and the adhesive film.

In a global heating system such as conventional autoclave or regular oven, the heat source surrounds the entire part enabling the part to attain cure temperature homogeneity during the curing process [33]. On the contrary, the one sided heat source (typically a heating blanket) used for the repair process, induces a temperature gradient within the repair patch and along the bondline, especially for thick primary composite structures and in the presence of substructures such as ribs and stiffeners [7, 33, 34]. This temperature heterogeneity adds a pervasive aspect in the processing of in-situ bonded repairs which can lead to severe risks of damage from overheating or undercuring of both the adhesive film and the repair patch, therefore being detrimental to the repair [7, 33].

Additionally, numerous thermo-chemical phenomena that critically dictate the final part quality of OOA materials, are highly dependent on the temperature distribution within the part: degree of cure, resin viscosity, glass transition temperature, cure time of the epoxy resin and adhesive, escapes of volatiles, resin flow before gelation and the thermal residual stresses [22, 25, 35]. Subsequently, for in-situ bonded repairs, the final quality of the repair patch and the bondline is significantly dependent on the evolution of these thermo-chemical phenomena of both the prepreg and the adhesive film. Therefore, to effectively and accurately control these phenomena, an accurate knowledge of the temperature evolution within the repair patch during the curing process is essential [25, 35].

During the repair process, the in-situ monitoring of the thermal response, which is defined as the temperature distribution of the repair patch, implies instrumenting the repair patch with numerous thermocouples. However, the presence of the thermocouples throughout the repair patch intrudes the structural integrity of the patch by creating stress concentration areas and is therefore avoided. Consequently, the only way to know the temperature distribution is to predict the thermal response of the repair patch during the curing process from the imposed temperature-time profile (cure cycle). Only then, the cure cycle can be adjusted to accommodate for any repair scenario. The cure cycle can be adapted to ensure full homogenous cure of the repair patch, without causing any overheating damage and control the resin flow to achieve minimum overall void content. In doing so, the processing induced defects are significantly minimized, thereby improving the processing integrity of the repair.

### 1.2.3 Heat Transfer Phenomenon for Bonded Repairs

While researchers have been concentrating on assessing the mechanical behavior of scarf-bonded repairs, only a few studies looked into the applied knowledge for performing a repair and the heat transfer phenomenon (being one of the processing fundamentals). Papathanasiou et al. proposed an analytical approach to study the in-plane heat conduction phenomena during the repair of a metallic structure with a composite patch [36]. This model was further coupled with a genetic optimization algorithm to optimize the cure cycle for this repair patch configuration [37]. However, with regard to bonded repairs of a composite structure, the transverse heat conduction is more critical than its behavior in the in-plane direction since it is the cause of the heterogeneous temperature distribution in the repair patch.

In an attempt to create a homogenous temperature distribution at the bondline and hence a homogeneous cure for the adhesive, Rider et al. looked into using a thin resistive metallic mesh at the entire bondline which provided the required heat to cure the adhesive [38]. However, this approach is not feasible if the repair patch and the adhesive require curing. Bestley et al. modeled a 3D representation of the scarf repair patch in finite element and coupled the main thermo-chemical phenomena [39]. They were able to track and understand the thermal response for a specific case but because their approach involves the use of finite element modeling for every repair case, it lacks versatility for in-field repairs, where the finite element expertise and the resources are not necessarily at hand.

The various issues associated with the influence of substructures on heat transfer phenomenon of in-situ bonded repair process have also been reported in the literature [33, 40]. Emery et al. showed that the temperature gradient within the repair patch is amplified in the presence of a metallic stringer attached to the non-heated side of the monolithic parent structure [40]. His study also aimed at estimating the magnitude of the heat losses for different configuration of parent structures undergoing repair. Any substructure connected to the parent laminate undergoing repair acts as a heat sink that enhances heat losses to the surroundings or conducts heat to unwanted areas of the structure [33]. As a result, this increases the temperature gradient

within the repair patch during the one-side in-situ curing process and could potentially lead to detrimental undercured regions.

Every repair case is different in terms of material, geometry (thickness variation) and the environment in which the repair is performed. These variations in the repair scenario can influence the heat transfer phenomena during the repair process and in some cases require adjustments on the imposed cure cycle. One approach to quickly study and predict the influence of variation in parameters on a heat transfer problem uses parametric heat transfer charts. Rasekh et al. exploited this methodology to capture the thermal response of composite structures cured in an oven [41].They presented and validated experimentally modified Heisler charts [42] to predict various key characteristics of the thermal response of any composite part during curing. Similarly, this approach can be adapted for in-situ bonded repair process to predict the influence of several parameters on the thermal response of the repair patch due to one-sided heating.

### 1.2.4 Thermo-Chemical Phenomena

Cure of the thermoset resin and adhesive is a chemical process that depends on the temperature - time profile of the composite part [25, 43, 44]. Numerous studies have shown that having a clear understanding and control over the chemical reactions taking place during the curing process is the route towards producing high quality composite parts using OOA prepregs [2, 30, 44]. These chemical reactions can be indirectly controlled by selectively imposing a specific temperature profile. In the processing of OOA materials, there are four main thermo-chemical phenomena that are essential to control: resin viscosity, degree of impregnation, degree of cure, and glass transition temperature. The definitions of these thermo-chemical phenomena are not presented in this section. Instead, they are fully defined in the Chapter 4 where their influence on the final part quality is described in detail; it is also shown that some of these thermo-chemical parameters are functions of each other.

There are several models in the literature to study the evolution of these thermo-chemical processes with respect to temperature and time for commonly used aerospace grade materials [25, 43, 44]. Previous studies of these models show that two main sections of the cure cycle dictate these phenomena; the initial ramp and the following initial dwell, as shown in Figure 1.7.

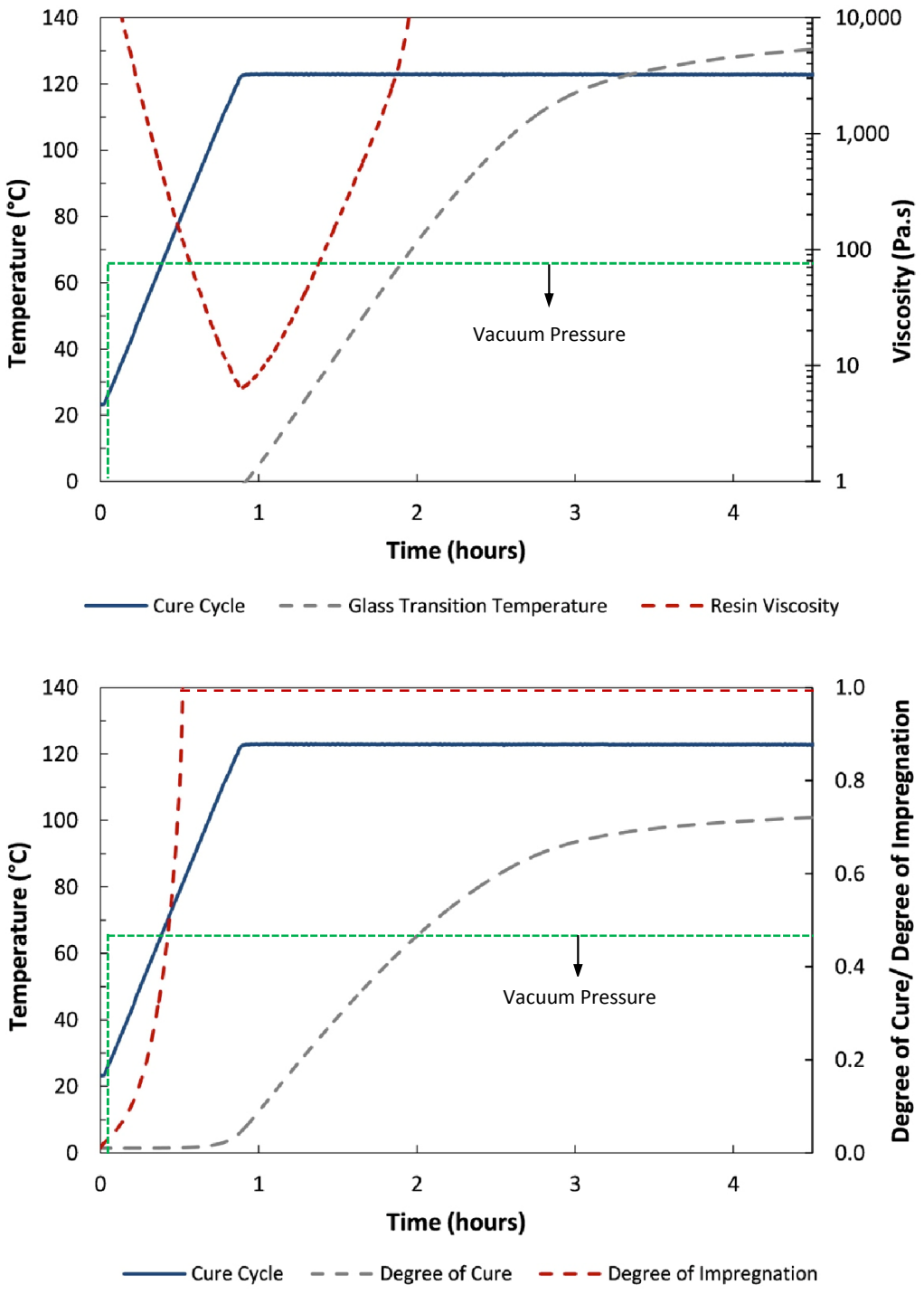


**Figure 1.7:** Graph showing the evolution of various key thermo-chemical phenomena when subjected to an imposed temperature and time cycle during the curing process. The consolidation vacuum pressure is constant at 101 kPa during the entire curing process.

The initial ramp rate mainly dictates the lowest attainable resin viscosity level (see Figure 1.7 Top) [22]. The degree of impregnation depends on several parameters, such as fibre properties, capillarity, applied pressure, time, and the resin viscosity (which is a function of temperature and time). Figure 1.7 shows the explicit influence of resin viscosity on the degree of impregnation for a repair process, where the remaining parameters were kept constant. The evolution of the degree of cure and the glass transition temperature of the resin is dictated by a combination of both the initial ramp and dwell characteristics of the cure cycle (see Figure 1.7) [25].

The dependency of these key thermo-chemical phenomena on the temperature-time profile of the part mandates the need to predict the temperature field evolution within the repair patch (particularly during the initial ramp and dwell sections of cure cycle). This approach can help in controlling the evolution of these phenomena during the bonding process to achieve a final fully cured and high quality part.

In an assessment of the in-situ bonded composite repair process, Tomblin et al. mentioned the development of cure envelopes of adhesives and prepregs to provide guidance in the design of the repair process [33]. The cure envelopes constitute a graphical representation of the flexibility in the variation of the cure cycle of the materials. These cure envelopes can be potentially used in conjunction with the parametric graphs that estimate the thermal response of the repair patch to quickly and confidently assess and design the repair process.

### 1.2.5 Conclusion

A concise summary of the existing literature on the current status of the in-situ bonded repair process of composite structures reveals numerous gaps. These gaps, if addressed properly, can significantly improve the repair process. In regards to the processing of in-situ bonded repairs, there is a lack of understanding of the heat transfer phenomena during curing. Many researchers recognized that knowledge of the thermal phenomena within the repair patch and at the bondline is key to implementing a robust repair [33, 35]. However, this repair configuration does not permit any in-situ instrumentation (thermocouples) within the repair patch to monitor the induced temperature gradient during cure. Consequently, a predictive approach is cornerstone. Presently, no heat transfer study was found for the in-situ repair configuration to predict the

temperature variation throughout the repair patch. Additionally, in-field repairs demand a quick, accurate, and easy-to-use analytical tools to design a confident repair process, eliminating an approximation approach.

## 1.3 Thesis Objectives and Structure

### 1.3.1 Thesis Objectives

In an attempt to address the missing links related to the processing of the in-situ bonded scarf joint repairs, the overall aim of this thesis is to gain better understanding of the curing process of this repair configuration, more specifically the thermal behaviour of the repair patch and the various physical phenomena involved. To achieve this goal, this study has three main objectives.

**1.** The first objective is to bridge the gap between the existing tools of heat analysis and the processing of in-situ bonded scarf joint repairs to create an analytical platform to study any subsequent dependent physical and chemical phenomena.

**2.** The second goal is to develop analytical graphical tools to provide guidelines and ease the assessment, design and optimization of the curing process of the repair patch.

**3.** The final objective is to provide insight into the final properties of the repair patch from the perspective of thermally driven phenomena. However, both surface preparation and thermal phenomena play a key role in the strength restoration of the overall repair. The considered study is a first step towards understanding the quality of the repair by examining the influence of the governing thermal process.

### 1.3.2 Thesis Structure

The objectives of this study described above are fulfilled using a series of steps as per the following chapters:

**Chapter 2** focuses on applying the fundamentals of heat transfer to model the transient heat transfer phenomena during the curing process of an in-situ bonded repair patch configuration on a monolithic composite panel. The heat transfer problem along with the key governing parameters is defined, and a methodology to solve for the induced temperature field analytically is proposed. A parametric representation of the solution is also depicted graphically.

**Chapter 3** presents an experimental validation study of the heat transfer model derived in Chapter 2. A detailed experimental approach to perform the repair is described. Finally, the measured thermal response of the repair patch during the repair process is validated against both the analytical model and the graphical solution.

**Chapter 4** analyzes the influence of the induced temperature field on the various governing thermo-chemical behavior of the material. The models of these thermo-chemical phenomena are implemented in conjunction with the heat transfer platform derived in Chapter 2. Additionally, the effect of metallic stiffener on the heat transfer phenomena is studied experimentally and the key governing parameters are identified.

By completing the tasks described in the above chapters, it is expected that this study will provide tools and insights to assist the design and optimization of robust in-field repairs from a processing perspective, particularly driven by the governing heat transfer phenomenon.

# Chapter 2

# Heat Transfer Modelling

In this chapter, an analytical solution to capture the thermal response of an in-situ repair patch is presented. The heat transfer problem is defined, the governing parameters are identified, and a methodology to develop an analytical solution using suitable assumptions is proposed. This analytical solution is used to perform a parametric study to examine the influence of the governing parameters on the thermal response of the repair patch. This parametric study is represented graphically in the form of heat charts, which can be used to assess the temperature field throughout the repair patch for in-field repairs.

## 2.1 Problem Definition

Let us consider the problem of defining the heat transfer taking place within the repair of a monolithic composite panel. The in-situ bonded repair process can be represented by the simplified 2D schematic, as shown in Figure 2.1. The temperature of the upper side of the patch is maintained according to the imposed cure cycle; the lower side is exposed to ambient air. The model does not consider the materials (consumables) between the heating blanket and the upper side of the repair patch because the temperature of this upper side is directly controlled, as shown in Figure 2.1. During the curing process, a specified cure cycle is imposed on the heated side and

there is a heat flux exchange with the air on the other (non-heated) side. This unsymmetrical heating induces a temperature gradient through the patch, which can be modeled by the fundamental theory of heat conduction.

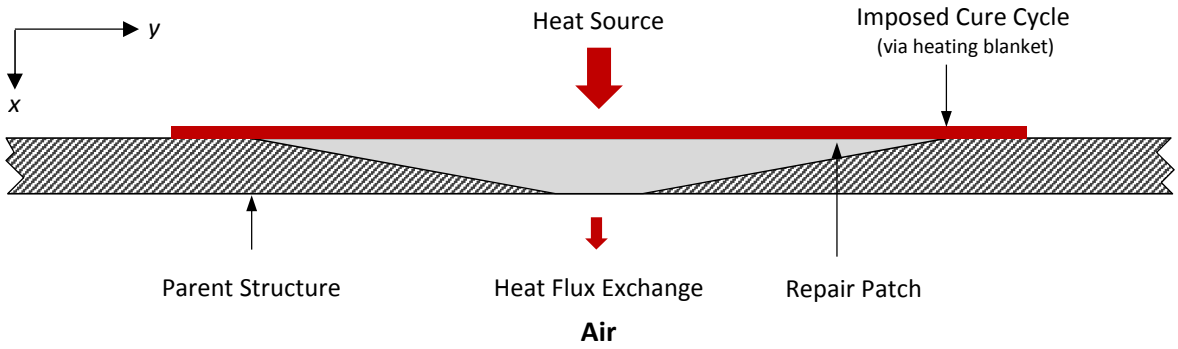


**Figure 2.1**: Schematic showing the heat transfer modelling for in-situ bonded scarf repairs of monolithic composite panels. The heat source is applied on one side and the other side is exposed to the ambient air.

The conservation of energy in a thermally conductive medium is applied in this case, and is given by [45],

$$\rho c_p \frac{\partial T(\vec{r},t)}{\partial t} = \nabla \cdot \left[ \overline{\overline{k}} \, \nabla T(\vec{r},t) \right] + g(\vec{r},t) \tag{2.1}$$

where $t$ is the time and $\vec{r}$ the space coordinate, $\rho$ is the density of the material, $c_p$ its specific heat capacity, $\overline{\overline{k}}$ is the thermal conductivity tensor of the material and $g(\vec{r},t)$ represents the heat generation term. The temperature field, $T(\vec{r},t)$ , is a function of space and time.

Equation (2.1) represents a general case of heat conduction. However, for a composite repair patch, this equation can be further simplified.

### 2.1.1 Simplifications and Assumptions

#### A. Heat Generation

The heat conduction Equation (2.1) consists of a heat generation term $g(\vec{r},t)$. This function accounts for any heat generated within the system. In a composite patch, the exothermic reaction during cure can be modelled using this term. The amount of heat generated during the curing

process of the composite patch depends on its resin content; typically, OOA prepregs have a resin content of about 30 - 40% [2]. However, during the in-situ curing process, the latent heat of reaction generated by this resin content of the repair patch is relatively low compared to the amount of heat supplied by the heating blanket [40]. For instance, the heat flow supplied by a 12" x 12" heating blanket during curing typically averages to 55 W [46], which is two orders of magnitude larger than the maximum heat flow due to the exothermic reaction of the resin cure, which is in the range of 0.02 – 0.04 W [25]. Consequently, the heat generation term can be safely neglected for a composite repair patch, which is of interest in this research.

### B. One-Dimensional Approximation

In Section 2.1, the thermal response of the in-situ repair process is modeled as a 2D phenomenon. We can take advantage of the symmetry in this problem and describe the heat transfer using an axisymmetric representation, as shown in Figure 2.2.

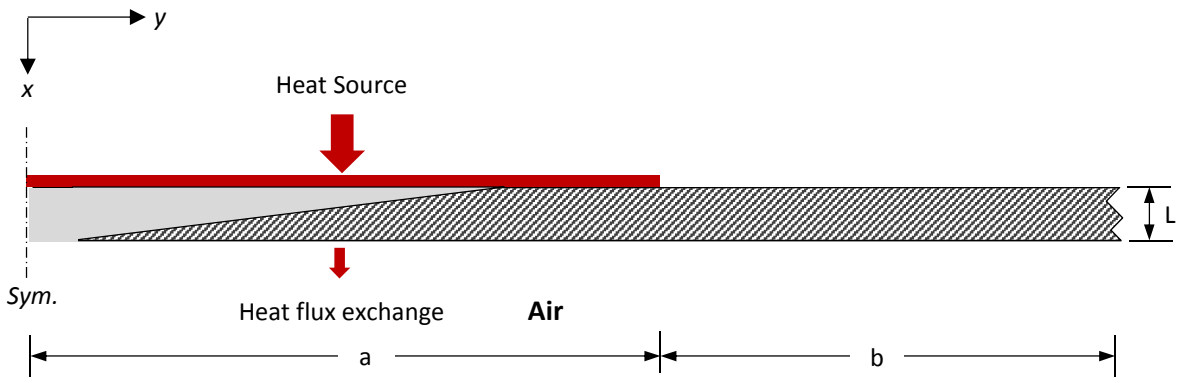


**Figure 2.2:** Schematic showing the axisymmetric heat transfer modelling of the repair patch.

Using assumption **A** and neglecting the heat generation term, the equation governing the heat transfer phenomena simplifies to:

$$\rho c_p \frac{\partial T}{\partial t} = k_x \frac{\partial^2 T}{\partial x^2} + k_y \frac{\partial^2 T}{\partial y^2} \tag{2.2}$$

In Equation (2.2), $k_x$ is the transverse and $k_y$ is the in-plane thermal conductivity of the repair patch material. The parent laminate in this case is assumed to have the same thermo-physical properties as the repair patch. The temperature distribution within the repair patch is denoted by $T(x,y,t)$, which is a function of space and time.

This 2D heat transfer problem is subjected to 4 different boundary conditions. These boundary conditions are given by Equations (2.3) to (2.6).

$$T(0,y,t) = f(t), \quad 0 < y < a, \quad t > 0 \tag{2.3}$$

$$k_x \frac{\partial T(L,y,t)}{\partial x} = -h\left[T(L,y,t) - T_\infty\right], \quad 0 < y < a+b, \quad t > 0 \tag{2.4}$$

$$k_x \frac{\partial T(0,y,t)}{\partial x} = 0, \quad a < y < a+b, \quad t > 0 \tag{2.5}$$

$$k_y \frac{\partial T(x,y,t)}{\partial y} = 0, \quad 0 < x < L, \quad y = a+b, \quad t > 0 \tag{2.6}$$

where *h* is the heat transfer coefficient of the ambient air, and $T_\infty$ is the ambient temperature.

As denoted by the boundary condition in Equation (2.3), the function $f(t)$ represents the temperature variation with time imposed by the heating blanket on the top of the repair patch. It follows a typical cure cycle, which consists of ramps followed by dwells.

The boundary condition given by Equation (2.5) is valid as long as the parent laminate is well insulated on the heated side which is usually feasible for this repair configuration. Furthermore, Equation (2.6) assumes that a combination of the low in plane thermal conductivity of composite materials and the high length to thickness ratio of the parent structure leads to no heat transfer in the in plane direction at $y=a+b$.

This 2D representation of heat transfer was first modeled in COMSOL Multiphysics 4.3a, a finite element software (FEA), to gather an initial understanding of the heat transfer problem. The boundary conditions, Equations (2.2)-(2.6), were fed into the FE model. A constant temperature

of 121 °C was imposed for $f(t)$ and a steady state analysis was performed. The extracted solution for the temperature and heat flux field in the repair patch at $x = L$ is shown in Figure 2.3.

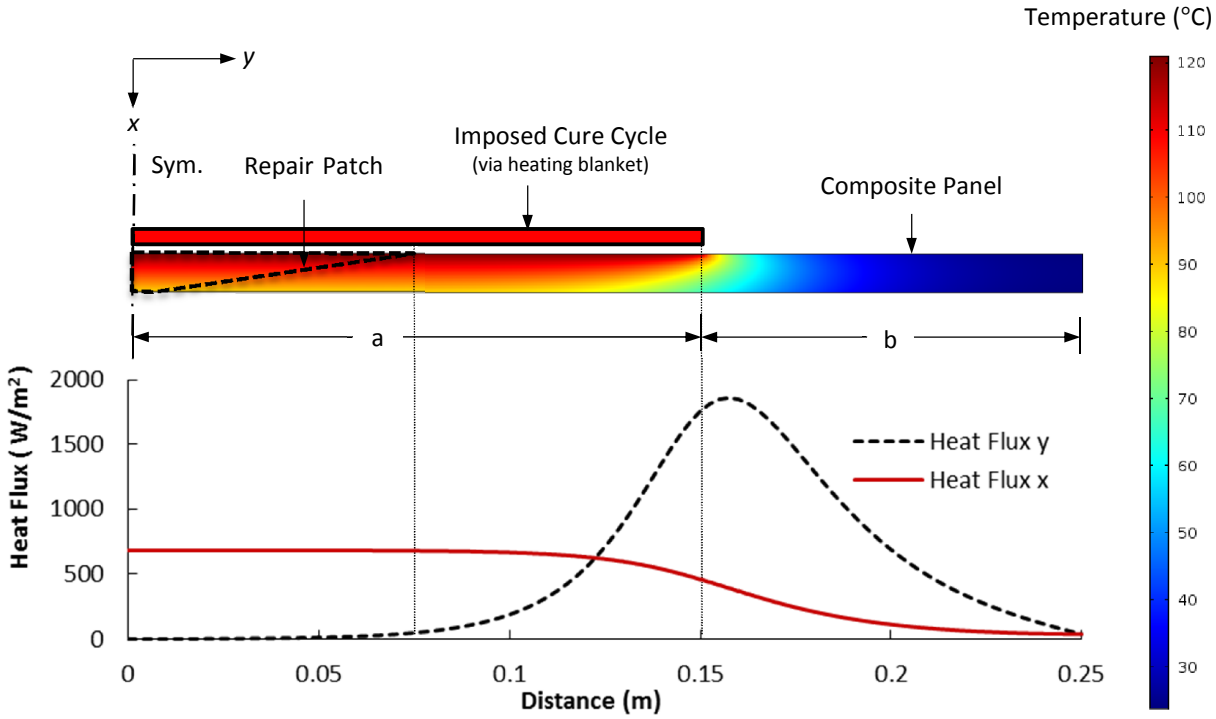


**Figure 2.3:** Temperature and heat flux distribution throughout a composite repair patch during the curing process by considering a 2D analysis.

The plots of the heat flux and temperature field show that the heat transfer phenomenon is primarily dominant in the transverse direction when the heat is applied on only one side of the repair patch except for region close to the finishing edge of the heating source ($y$=$a$). To verify this further, the governing parameters that dictate the heat transfer are identified. A dimensional analysis is first performed to reduce the number of parameters in the original set of Equations (2.3) to (2.6), by introducing a dimensionless temperature defined as $\theta_{2D} = (T - T_\infty)/(T_d - T_\infty)$ and two dimensionless lengths, $X = x/L$ and $Y = y/W$ in the transverse and the in-plane direction respectively, where $W = a + b$. These dimensionless parameters are then substituted in the governing equation and boundary conditions.

It is worthy to note that a steady state analysis was considered for this dimensional analysis instead of the original time dependent one because the former analysis was sufficiently accurate

to capture the trend in the heat fluxes that we are interested in. Moreover, the given transverse and in-plane heat fluxes under steady state conditions form an upper limit; the resulting steady state analysis using the considered boundary conditions therefore produces a conservative estimate and is used instead of the transient study.

The resulting non-dimensional system of equations that described the heat transfer in the repair patch is now given by:

**Governing Equation**

$$\frac{k_x}{L^2}\frac{\partial^2\theta_{2D}}{\partial X^2}+\frac{k_y}{W^2}\frac{\partial^2\theta_{2D}}{\partial Y^2}=0 \tag{2.7}$$

**Boundary Conditions**

$$\begin{aligned}&\theta_{2D}=1, \quad X=0, \quad 0<Y<a/W\\ &\frac{\partial\theta_{2D}}{\partial X}=-\frac{hL}{k_x}, \quad X=1, \quad 0<Y<1\end{aligned} \tag{2.8}$$

By performing the dimensional analysis on the governing equations, the number of independent parameters and variables is reduced from 9 to 3. The simplified representation of the system makes it easier to assess and isolate the influence of each parameter. From Equations (2.7) and (2.8), the parameters dictating the temperature distribution are $k_x/L^2$, $k_y/W^2$, and $hL/k_x$, which is also known as the Biot number. Considering the geometry of a composite panel, which is typically thin and long, the length, $W$, can be assumed to be relatively greater than the thickness, $L$. Consequently, the coefficient, $k_y/W^2$, is negligible compared to $k_x/L^2$. This simple analysis implies that the dominant heat transfer phenomenon can be assumed to be in the transverse direction.

Similar observations regarding the dominant heat transfer direction can be made if we revisit Figure 2.3, which shows the heat flux distribution in the repair patch. Consequently, the heat transfer within the composite laminate can be divided into two zones; the heat fluxes in each

zone have different magnitudes in the transverse and in-plane direction. In the first zone, more than 95% of the total heat flux is contributed by its transverse component. The heat transfer in this region can therefore be safely simplified to a one-dimensional problem in the transverse direction. In the second zone, the ratio of the transverse to the in-plane heat flux is less that 95%. This region consists of a mixed contribution of both directions of heat fluxes and therefore has to be represented by a 2D heat transfer phenomenon. It is denoted by the edge effect zone in Figure 2.4.

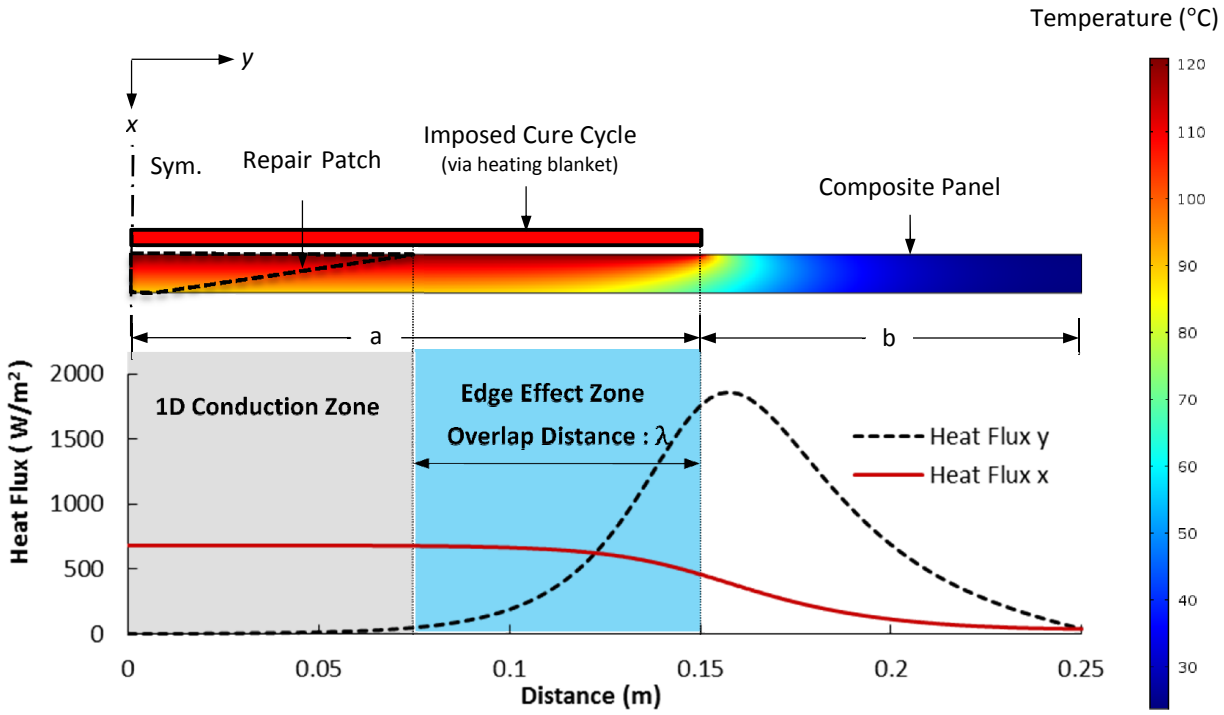


**Figure 2.4:** Schematic describing the two characteristic zones for the heat transfer phenomena during the cure of a repair patch: the 1D conduction zone and the edge effect zone. The overlap distance is also shown.

In conclusion, for the 1D approximation to be representative and valid for the heat transfer during the curing process of a repair patch, it is important that heating blanket overlaps the repair patch by a distance, $\lambda$, defined by the edge effect zone (Figure 2.4). This distance, $\lambda$, is referred further on by the term overlap distance.

By considering the parameters that govern the magnitude of $\lambda$, a parametric study is performed and the results are represented graphically in Figure 2.5. It can be used to estimate the overlap

distance for any general repair scenario. Using the material properties and dimensions of the repair patch, and the heat transfer coefficient of air, the ratios, $0.25k_x/L^2k_y$ and $hL/k_x$ are first calculated. It is important to note that the value of $W^2$ was fixed at 0.25m$^2$ since it represents a sufficiently wide length of the parent structure for this type of repair. These two ratios are then identified on the contour plot in Figure 2.5 and the corresponding value of the overlap distance is extracted.

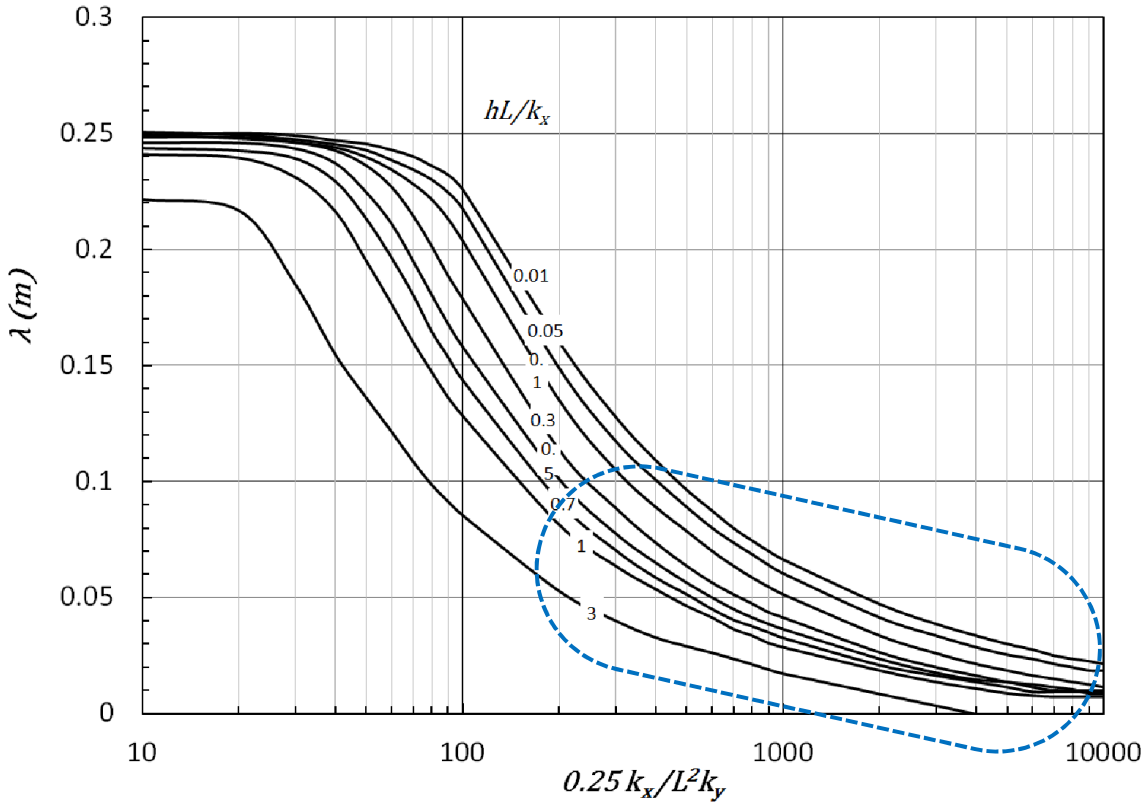


**Figure 2.5:** Contour plot of the overlap distance for the 1D dimensional approximation of the heat transfer problem for in-situ bonded repair process. The different contours represent different Biot numbers. The area surrounded by the dashed blue line represents the typical range of values of the overlap distance for a composite repair patch.

The contour plot in Figure 2.5 can be used as a quick tool to estimate the overlap distance between the heating blanket and the repair patch that ensures a dominant heat flux in the transverse direction for the curing of the repair patch and adhesive film. This condition ensures a uniform in-plane temperature distribution throughout the repair patch during cure.

This completes the definition of our heat transfer problem along with the appropriate assumptions. The methodology to solve the heat transfer problem analytically is addressed in the next section.

## 2.2 Analytical Solution

In this section, a methodology to solve the governing set of equations that defines the heat transfer problem is described. By implementing the assumptions mentioned in section 2.1.1, the heat condition equation for this problem can be summarized as follows.

The governing one-dimensional heat conduction equation is given by:

$$\frac{1}{\alpha}\frac{\partial T(x,t)}{\partial t}=\frac{\partial^2 T(x,t)}{\partial x^2} \tag{2.9}$$

where $\alpha = k/\rho c_p$ is the thermal diffusivity and $k$ is the transverse thermal conductivity of the composite material.

The two boundary conditions that dictate the heat transfer are:

**a)** The imposed temperature on the heated side $x$=0:

$$T(0,t)=f(t), \quad t>0 \tag{2.10}$$

where $f(t)$ is a time dependent function which follows a specific cure cycle.

**b)** The heat flux exchange with the surrounding air on the colder side $x$=$L$:

$$k\frac{\partial T(L,t)}{\partial x}=-h\left[T(L,t)-T_\infty\right], \quad t>0 \tag{2.11}$$

where $T_\infty$ is the ambient temperature, $h$ is the heat transfer coefficient to the surrounding air and $L$ is the laminate thickness.

The initial condition for the heat transfer problem is given by,

$$T(x,0)=T_i, \quad 0<x<L \tag{2.12}$$

where $T_i$ is the initial temperature.

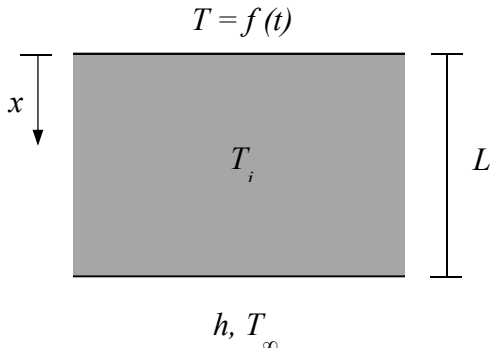


**Figure 2.6:** A schematic showing a one-dimensional model representation of the heat transfer problem of the repair process through the thickness, and subjected to two different boundary conditions.

In this repair scenario, the repair patch is made from the same material as the parent structure. Consequently, both the repair patch and the parent structure have the same thermal and physical properties.

### 2.2.1 Boundary Conditions

The one dimensional heat transfer problem is subjected to two different boundary conditions. The side in contact with the heating source has a time dependent boundary condition where the imposed temperature profile is dictated by a cure cycle. The opposite side is subjected to the ambient air. These two boundary conditions are described mathematically in Equations (2.11) and (2.12).

For the in-situ curing process, a typical cure cycle imposed on the heated side consists of an initial ramp, followed by a dwell. This characteristic of the cure cycle can be represented as a time dependent, discontinuous function. Therefore, during the ramp, $f(t) = Rt + T_\infty$, where $R$ is the initial ramp rate. During the dwell, $f(t) = T_d$, where $T_d$ is a constant temperature.

### 2.2.2 Heat Transfer during Ramp

**Preliminary Steps**

The system of partial differential equations (PDEs) and the corresponding boundary conditions for the initial ramp section of the cure cycle are given by Equations (2.9) to (2.12), where $f(t) = Rt + T_\infty$. An analytical approach to solve for the temperature field during this initial ramp is discussed below.

First, we set,

$$T_{ramp}(x,t) = U(x,t) + V(x,t) + T_\infty \tag{2.13}$$

where, $U(x,t)$ satisfies homogenous boundary conditions given by,

$$\begin{aligned} U(0,t) &= 0, \quad t > 0 \\ k\frac{\partial U(L,t)}{\partial x} + hU(L,t) &= 0, \quad t > 0 \end{aligned} \tag{2.14}$$

and the initial condition is extracted from Equations (2.12) and (2.13) and is given by,

$$U(x,0) = T_i - T_\infty, \quad 0 < x < L \tag{2.15}$$

The governing equation for $U(x,t)$ is given by,

$$\frac{1}{\alpha}\frac{\partial U(x,t)}{\partial t} = \frac{\partial^2 U(x,t)}{\partial x^2} \tag{2.16}$$

The solution to $U(x,t)$ can be obtained using the method of separation of variables [47], $U(x,t) = X(x)\Gamma(t)$, because of the homogeneous boundary conditions given by Equation (2.14). This gives the solution,

$$U(x,t) = \sum_n^\infty \frac{F(T_i - T_\infty)(1 - \cos(\mu_n L))e^{-\alpha\mu_n^2 t}\sin\mu_n x}{\mu_n} \tag{2.17}$$

where, $F = \dfrac{2\left[\mu_n^2 + \left(\dfrac{h}{k}\right)^2\right]}{L\left[\mu_n^2 + \left(\dfrac{h}{k}\right)^2 + \dfrac{h}{k}\right]}$ and $k\mu_n + h\tan(L\mu_n) = 0$; an expression for the eigenvalue, $\mu_n$

Next, let us consider the solution to $V(x,t)$. The governing equation for $V(x,t)$ is given by,

$$\frac{1}{\alpha}\frac{\partial V(x,t)}{\partial t} = \frac{\partial^2 V(x,t)}{\partial x^2} \tag{2.18}$$

The boundary conditions of $V(x,t)$ are given by Equation (2.19).

$$\begin{aligned} V(0,t) &= f(t) - T_\infty, \quad t > 0 \\ k\frac{\partial V(L,t)}{\partial x} + hV(L,t) &= 0, \quad t > 0 \end{aligned} \tag{2.19}$$

and the initial condition is,

$$V(x,0) = 0, \quad 0 < x < L \tag{2.20}$$

Due to the complex nature of the time dependent, discontinuous boundary condition at $x = 0$, Duhamel's Theorem is used to find an analytical solution to this heat transfer problem. This methodology is discussed in the next section.

**Duhamel's Theorem**

Duhamel's theorem provides a convenient approach for developing solutions to linear heat conduction problems with time dependent boundary conditions. It is based on the principle of superposition [45]. In the case of in-situ bonded repair, this time-dependent boundary condition refers to the imposed temperature variation on one side of the repair patch by means of the heating blanket. This temperature profile (cure cycle) is a piecewise linear function to which the Duhamel's theorem can be applied to find an analytical solution to the heat transfer problem defined previously.

The general formulation of the Duhamel's theorem involves solving the heat transfer problem by assuming time-independent boundary conditions. The corresponding solution, $V'(x,t)$ is then used to perform integration with respect to time according to the equation,

$$V(x,t)=\int_{\tau=0}^{t} V'(x,t-\tau)\frac{dB(\tau)}{dt}d\tau + B_{t=0}V'(x,t) \tag{2.21}$$

where $B(\tau)$ is the imposed time-dependent condition, and $V(x,t)$ is the solution to the heat transfer problem with time-dependent boundary condition.

The first step in applying the Duhamel's theorem is to assume the time-independent boundary conditions and solve the governing heat transfer equations. This is defined by the function $V'(x,t)$. The boundary conditions of $V'(x,t)$ are set to be time-independent: the boundary condition at $x=0$ for $V'(x,t)$ is set to 1 and the second boundary condition at $x=L$ and initial condition are both set to 0, as shown in Equation (2.22) ,

$$\begin{gathered} V'(0,t)=1, \quad t>0 \\ k\frac{\partial V'(L,t)}{\partial x}+hV'(L,t)=0, \quad t>0 \\ V'(x,0)=0, \quad 0<x<L \end{gathered} \tag{2.22}$$

Due to the non-homogenous boundary condition at $x=0$, we introduce a slave function, $V_s(x)$, such that,

$$V'(x,t)=V_s(x)+\phi_r(x,t) \tag{2.23}$$

where the slave function, $V_s(x)$ is solely a function of $x$, and $\phi_r(x,t)$ is a function with homogeneous boundary conditions.

Let us consider the solution to $V_s(x)$. Since, it is only a function of *x*, the governing equation for $V_s(x)$, reduces to,

$$\frac{d^2V_S(x)}{dx^2} = 0 \tag{2.24}$$

This results is a simple, linear solution,

$$V_s(x) = Ax + B \tag{2.25}$$

Applying the boundary conditions given in Equation (2.22) we obtain,

$$V_s(x) = \frac{-h}{k + hL}x + 1 \tag{2.26}$$

The function $\phi_r(x,t)$ has homogeneous boundary conditions, given by

$$\begin{aligned} \phi_r(0,t) &= 0, \quad t > 0 \\ k\frac{\partial\phi_r(L,t)}{\partial x} + h\phi_r(L,t) &= 0, \quad t > 0 \end{aligned} \tag{2.27}$$

The initial condition of $\phi_r(x,t)$ is extracted from Equations (2.22), (2.23) and (2.26) and is given by,

$$\phi_r(x,0) = \frac{hx}{k + hL} - 1, \quad 0 < x < L \tag{2.28}$$

The solution can be solved using separation of variables leading to a series solution, which is given by,

$$\phi_r(x,t) = \sum_n^{\infty} B_k \sin(\mu_n x)e^{-\alpha\mu_n^2 t} \tag{2.29}$$

where $k\mu_n + h\tan(L\mu_n) = 0$, and provides an expression for the eigenvalue, $\mu_n$

By using Equations (2.28) and (2.29), we can solve for $B_k$, the coefficient of a Fourier sine series, which is given by,

$$B_k = F \int_0^L \left( \frac{hx}{k + hL} \right) \sin \mu_n x \, dx \tag{2.30}$$

where $F = \dfrac{2\left[ \mu_n^2 + \left( \dfrac{h}{k} \right)^2 \right]}{L\left[ \mu_n^2 + \left( \dfrac{h}{k} \right)^2 + \dfrac{h}{k} \right]}$

The complete expression for $V'(x,t)$ can now be written as,

$$V'(x,t) = 1 - \frac{hx}{k + hL} + \sum_n^{\infty} B_k \sin(\mu_n x) e^{-\alpha \mu_n^2 t} \tag{2.31}$$

Now, we substitute Equation (2.31) into the mathematical expression of Duhamel's theorem given by Equation (2.21). This gives us,

$$V(x,t) = R\left[ \left( 1 - \frac{hx}{k + hl} \right) t + \sum_n^{\infty} \frac{B_k \sin(\mu_n x)\left(1 - e^{-\alpha \mu_n^2 t}\right)}{\alpha \mu_n^2} \right] + V'(x,t)\left[T_i - T_\infty\right] \tag{2.32}$$

Therefore, Equations (2.13), (2.17) and (2.32) form a complete solution to the heat transfer problem in a repair patch when one side is exposed to an imposed linear temperature variation, which is referred to as the ramp of the cure cycle. In the next section, we consider the heat transfer during the dwell section of the repair process.

### 2.2.3 Heat Transfer during Dwell

The dwell of a cure cycle occurs when a constant temperature is maintained after ramping it up from the initial temperature. The governing equation of this section and the corresponding boundary and initial conditions are given by Equations (2.33) and (2.34)

$$\frac{1}{\alpha}\frac{\partial T_{dwell}(x,t)}{\partial t} = \frac{\partial^2 T_{dwell}(x,t)}{\partial x^2} \tag{2.33}$$

where the boundary and initial conditions are given by,

$$T_{dwell}(0,t) = f(t) = T_d \ , \quad t > t_d$$

$$k\frac{\partial T_{dwell}(L,t)}{\partial x} = -h\left[T_{dwell}(L,t) - T_\infty\right], \quad t > t_d \tag{2.34}$$

$$T_{dwell}(x,0) = T_{ramp}(x,t_d), \quad 0 < x < L$$

where $t_d$ is the time duration of the initial ramp, and is also defined as the starting time at which the dwell temperature is imposed.

Since the boundary condition at $x = 0$ is nonhomogeneous, we introduce a slave function, $T_{ds}(x)$ , to account for this inhomogeneity,

$$T_{dwell}(x,t) = T_{ds}(x) + \phi_d(x,t) + T_\infty \tag{2.35}$$

where $\phi_d(x,t)$ satisfies homogenous boundary conditions.

Let us first solve for the slave function, $T_{ds}(x)$. Since, it is only a function of *x*, the governing equation for $T_{ds}(x)$, reduces to,

$$\frac{d^2 T_{ds}(x)}{dx^2} = 0 \tag{2.36}$$

The corresponding boundary conditions are,

$$\begin{aligned} T_{ds}(0) &= T_d - T_\infty \\ k\frac{dT_{ds}(L)}{dx} + hT_{ds}(L) &= 0 \end{aligned} \tag{2.37}$$

Equation (2.36) results in a simple, linear solution,

$$T_{ds}(x) = Ax + B \tag{2.38}$$

Applying the boundary conditions given by Equation (2.37) we obtain,

$$T_{ds}(x) = T_{d\infty}\left(1 - \frac{hx}{k + hL}\right) \tag{2.39}$$

where $T_{d\infty} = T_d - T_\infty$.

The function, $\phi_d(x,t)$, can be solved using the concept of separation of variables and Fourier sine series. This results in,

$$\phi_d(x,t) = \sum_n^\infty D_k e^{-\alpha\mu_n^2 t}\sin(\mu_n x) \tag{2.40}$$

where $D_k = \frac{F}{e^{-\alpha\mu_n^2 t_d}}\left[\int_0^L\left(\theta_{ramp}(x,t_d) + T_{d\infty}\left(\frac{hx}{k+hL} - 1\right)\right)\sin(\mu_n x)dx\right]$, $\theta_{ramp}(x,t_d) = T_{ramp}(x,t_d) - T_\infty$

Equations (2.35), (2.39) and (2.40) completely define the heat transfer within a repair patch during the dwell section of the cure cycle.

### 2.2.4 Comparison of Analytical Solution with the Finite Element Model

The analytical solution is compared to a finite element analysis of a specific repair case and a graphical representation of both the solutions is shown in Figure 2.7. One term approximation is used to evaluate the analytical solution. The input parameters for the FE model and the analytical solutions are listed in Table 2.1.

**Table 2.1:** Model Parameters used for comparing the analytical solution with the finite element model [25].

| Model Parameters | Symbol | Value |
|---|---|---|
| Thermal Conductivity, (W/m·K) | $k$ | 0.21 |
| Density, (kg/m$^3$) | $\rho$ | 1310 |
| Specific Heat Capacity, (J/kg·K) | $c_p$ | 1260 |
| Laminate thickness, (mm) | $L$ | 10 |
| Heat Transfer Coefficient, (W/m$^2$·K) | $h$ | 10 |
| Ambient Temperature, (°C) | $T_\infty$ | 21 |
| Initial Temperature, (°C) | $T_i$ | 21 |
| Ramp Rate, (°C/min) | $R$ | 2 |
| Dwell Temperature, (°C) | $T_d$ | 121 |

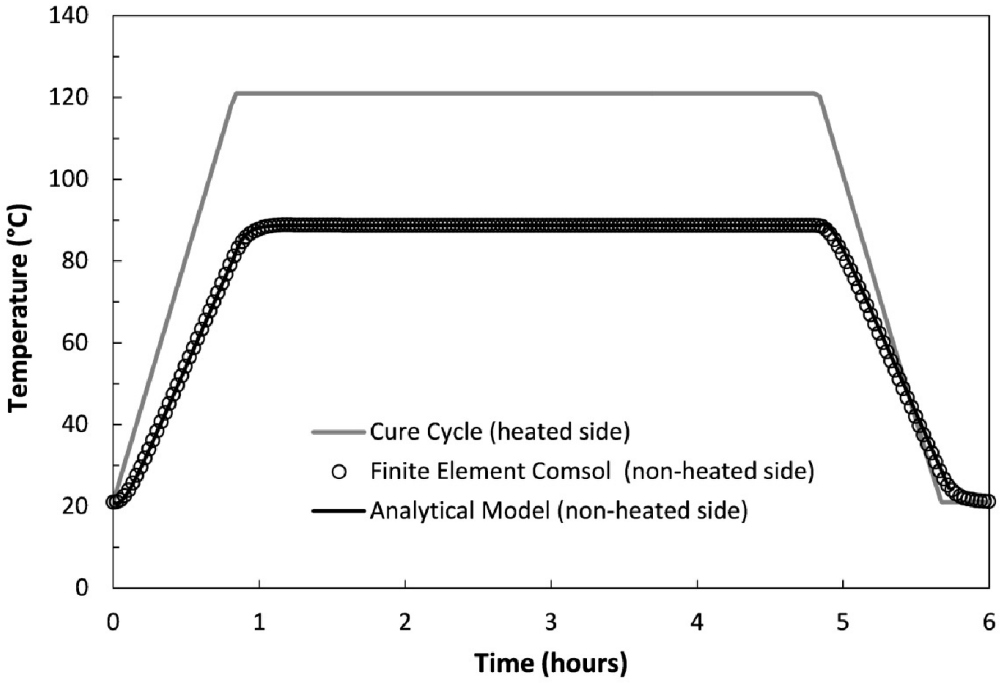


**Figure 2.7:** Graph showing the comparison between the finite element and the analytical model used to estimate the temperature field within the repair patch subjected to a one-side heat source.

There is a close match between the FE model and the analytical solution, as shown by Figure 2.7. This shows that the analytical solution with a one-term approximation to the Fourier series is sufficient to capture the thermal response of the in-situ repair patch. It must be noted that the

strong agreement in the numerical and analytical results of the thermal response was obtained for an in-situ repair patch configuration; this provides confidence in the range of properties typically encountered for this type of repair since we do not anticipate a lot of drastic change in the variables shown in Table 2.1. This enables a simple extension of the developed analysis to any in-situ bonded repair process.

By implementing Duhamel's theorem, an analytical solution to the heat transfer problem for an in-situ bonded repair scenario was found. This analytical solution can be used to predict and evaluate the influence of various parameters on the temperature distribution throughout the repair patch such as the ambient temperature, the heat transfer coefficient, the laminate thickness etc. Furthermore, this solution can be flexibly used to design any in-situ monolithic composite repair process by selecting suitable process parameters. In the next section, an application of this analytical solution is presented. It involves developing heats charts that graphically represent the thermal response of the in-situ bonded repair process for monolithic composite panels.

## 2.3 Application: Heat Transfer Charts

The design process can be enforced graphically with the help of heat charts, which represent the results of the analytical solution of Section 2.2 on 2D graphs thereby providing easy access and estimation for in field repairs. However, a 2D graphical representation can be achieved only if the thermal response of the repair patch is a function of a maximum number of two independent parameters. The above heat transfer problem for in-situ bonded repairs includes nine independent variables and parameters: $L$, $k$,$\alpha$, $h$, $T_\infty$, $x$, $t$, $R$, and $T_i$. To reduce the total number of parameters while still capturing the heat transfer phenomena, a dimensional analysis is performed.

### 2.3.1 Non-Dimensionalization of Heat Equation

In order to non-dimensionalize the heat transfer equation, we first introduce a non-dimensional temperature and length. Let us define the dimensionless temperature as $\theta = \left(T - T_\infty\right)\alpha / RL^2$ and the dimensionless length as $X = x/L$. By substituting these two dimensionless variables in the

governing Equation (2.9), the boundary conditions (Equations (2.10) – (2.11)) and the initial condition (Equation (2.12)), the heat transfer problem simplifies to:

$$\frac{\partial^2 \theta}{\partial X^2} = \frac{L^2}{\alpha}\frac{\partial \theta}{\partial t} \tag{2.41}$$

where the boundary and initial conditions are:

$$\begin{aligned} \theta(0,t) &= t\,, \quad t > 0 \\ \frac{\partial \theta(1,t)}{\partial X} &= \frac{-hL}{k}\theta(1,t)\,, \quad t > 0 \\ \theta(X,0) &= 0\,, \quad 0 < X < 1 \end{aligned} \tag{2.42}$$

Equations (2.41) and (2.42) can be further simplified by isolating two non-dimensional numbers: the Biot number, $Bi = hL/k$, and the Fourier number, $\tau = \alpha t / L^2$. Consequently, the dimensionless governing equations, boundary conditions and initial conditions are given by:

**Governing Equation:**

$$\frac{\partial \theta(X,\tau)}{\partial \tau} = \frac{\partial^2 \theta(X,\tau)}{\partial X^2} \tag{2.43}$$

**Boundary Conditions and Initial Conditions:**

$$\begin{aligned} \theta(0,\tau) &= \tau\,, \quad \tau > 0 \\ \frac{\partial \theta(1,\tau)}{\partial X} &= -Bi\left[\theta(1,\tau)\right], \quad \tau > 0 \\ \theta(X,0) &= 0\,, \quad 0 < X < 1 \end{aligned} \tag{2.44}$$

Therefore, by performing a dimensional analysis of the original heat transfer problem, the number of variables and parameters is reduced to three instead of nine. The temperature field throughout the repair patch can now be expressed as a function of three dimensionless variables and numbers, $\theta(X,\tau) = f(Bi,\tau,X)$. This particular representation of the heat equation makes it feasible to display the results of a parametric study on the thermal response of the repair patch in

a graphical form. In the next section, details of the approach used to represent this parametric study graphically, in the form of heat charts, are discussed.

### 2.3.2 Heat Charts

Heats charts are developed to represent the thermal response of any general in-situ bonded repair patch during the curing process. It involves performing a parametric study to investigate how the thermal response of the patch is influenced when the governing parameters vary. Before performing a parametric study, it is important to first identify the key characteristics of the thermal response that are dominant during the cure.

**Key Characteristics of Thermal Response**

Numerous characteristics of the thermal response dictate the processing of a repair patch and determine its feasibility, as discussed in Chapter 1. Furthermore, these characteristics of the thermal response are crucial to the design and optimization of the in-situ bonded repair patch process. By taking into consideration the various thermo-chemical phenomena, as seen in Chapter 1, the key characteristics of the thermal response are defined as follows: (i) the difference in temperature, $\Delta T$, between the heated sided and the non-heated side during the ramp; (ii) the ramp rate of the non-heated side, $R_L$; (iii) the steady state temperature of the non-heated side, $T_{ss}$; and (iv) $t_{ss}$, the time taken to reach 95% of this steady state temperature during the dwell section. These regions of interest are illustrated in Figure 2.8.

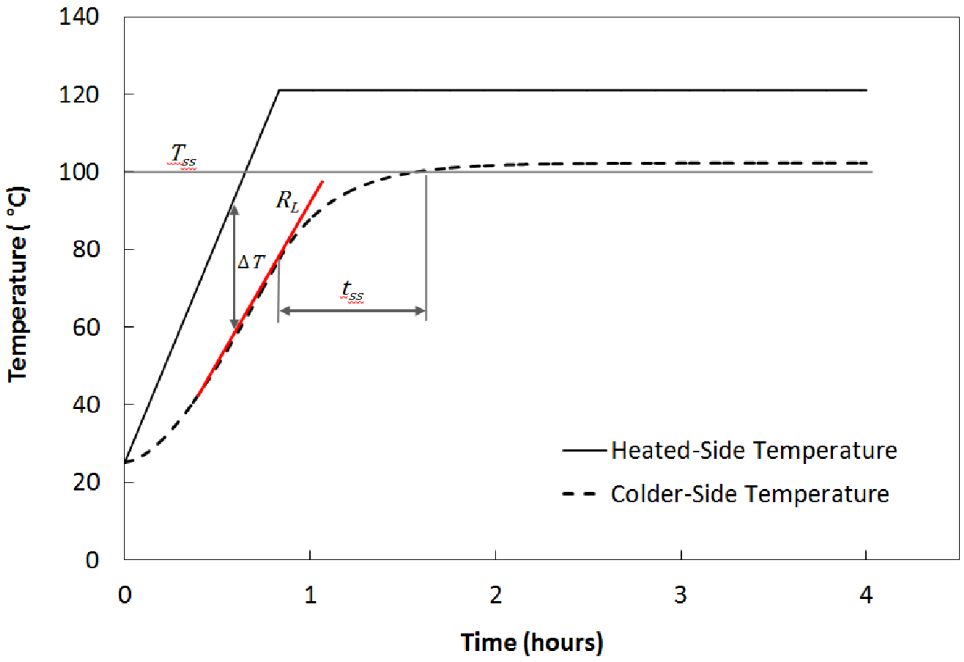


**Figure 2.8:** Schematic showing the key characteristics of the thermal response during the cure of an in-situ repair patch.

During the cure of an in-situ bonded repair patch, it is of interest to capture the largest lag between the temperature in the part and the imposed cure cycle applied on the heated side of the patch [7]. In the case of one-sided heating, the coldest regions are the furthest from the heated side. Consequently, the temperature at location, $X = 1$, in the repair patch is analyzed.

By fixing the dimensionless length, $X = 1$, the dimensionless temperature, $\theta(1, \tau)$, becomes a sole function of Biot and Fourier number, and hence can be represented graphically on a 2D graph. The key characteristics of the thermal response, ($\Delta T$ , $R_L$ , $T_{ss}$ , $t_{ss}$), can now be expressed in terms of the dimensionless numbers.

**Mathematical Representation of the Key Characteristics of the Thermal Response.**

The four key characteristics of the thermal response, as described graphically in Figure 2.8, are expressed mathematically in terms of the Biot and Fourier number.

$\Delta T$ represents the temperature difference between the heat side and the non-heated (coldest) side of the repair patch during the ramp section. It can be expressed in terms of the dimensionless constants as follows:

The dimensionless temperature difference is given by $\theta_{X=0} - \theta_{X=1}$ and it can be further expressed as $\left(T(0,t) - T(L,t)\right)\alpha / RL^2$. Subsequently, we obtain $\Delta\theta = \Delta T\left(\alpha / RL^2\right)$, which is dependent on the Biot and the Fourier number.

$R_L$ is defined as the ramp rate of the non-heated side. It can be represented by $\partial T(L,t)/\partial t$. By expressing the latter in terms of the dimensionless temperature, we get $\partial\theta/\partial\tau = R_L/R$, where $R$ is the imposed ramp rate on the heated side.

$T_{ss}$ is the steady state temperature of the non-heated side *(X = 1)* during the dwell section of the cure cycle. It is represented by $(T_{ss} - T_\infty)/(T_d - T_\infty) = 1/1 + \text{Biot}$.

$t_{ss}$ is the time taken by the non-heated to reach 95% of its steady state temperature after the ramp. It can be expressed in terms of the dimensionless time as $\alpha t_{ss}/L^2$ which is a function of the dimensionless dwell temperature, $\alpha(T_d - T_\infty)/RL^2$ and the Biot number.

Now that all the key characteristics of the thermal response have been defined in terms of the dimensionless variables and numbers, the heats charts can be generated using the analytical model. The heat charts depicting the thermal response during the cure of a repair patch and the approach taken to predict its key characteristics are shown below.

## Heat Charts Illustration

In this section, the different heat charts that are used to extract the thermal response data of an in-situ bonded repair patch are presented. To illustrate how the thermal response data is extracted from heat charts, a representative example of an in-situ bonded repair process is considered. The case study involves a repair patch with the following process parameters and material properties as described in Table 2.2.

**Table 2.2:** Material properties and heat transfer parameters for the representative case study [25].

| **Material Properties** | |
|---|---|
| Thermal Conductivity, (W/m·K) | 0.21 |
| Density, (kg/m$^3$) | 1310 |
| Specific Heat Capacity, (J/kg·K) | 1260 |
| **Heat Transfer Process Parameters** | |
| Laminate thickness, (mm) | 4 |
| Heat Transfer Coefficient, (W/m$^2$·K) | 8 |
| Ambient Temperature, (°C) | 18 |
| Ramp Rate, (°C/min) | 2 |
| Dwell Temperature, (°C) | 123 |

The following steps are undertaken to extract the desired thermal response data ( $\Delta T$ , $R_L$ , $t_{ss}$ and $T_{ss}$ ) from the heat charts.

*i)* First, calculate the Biot number $\left(hL/k\right)$ of the system.

*ii)* To compute $\Delta T$ and $R_L$ , calculate the Fourier number $\left(\alpha t/L^2\right)$ , which is located on the *x* axis of the heat charts in Figure 2.9 and Figure 2.10. Using the calculated Biot and Fourier numbers, the corresponding value of $\Delta T$ and $R_L$ can be identified from Figure 2.9 and Figure 2.10.

*iii)* To compute $t_{ss}$, calculate the dimensionless dwell temperature $\left(\alpha\left(T_d - T_\infty\right)/RL^2\right)$, which is located on the *x* axis of the heat charts in Figure 2.11. Using the calculated

Biot and dimensionless dwell temperature, the corresponding value of $t_{ss}$ can be identified from Figure 2.11.

*iv)* To estimate the value of $T_{ss}$, we can use the Biot number, which is located on the *x* axis of the heat chart in Figure 2.12, to extract the corresponding $T_{ss}$.

For the representative case study, the corresponding Biot number is 0.15 and the Fourier number at 50 minutes into the imposed cure cycle is 12.5. The dimensionless dwell temperature is 23.1.

The four different heat charts are shown in Figure 2.9 to Figure 2.12. The dashed line shows the thermal response data for the representative case study.

**Heat Chart - 1:** ***Temperature difference between the heated side (at x = 0) and the non-heated side (at x = L) during the initial ramp of the cure cycle.***

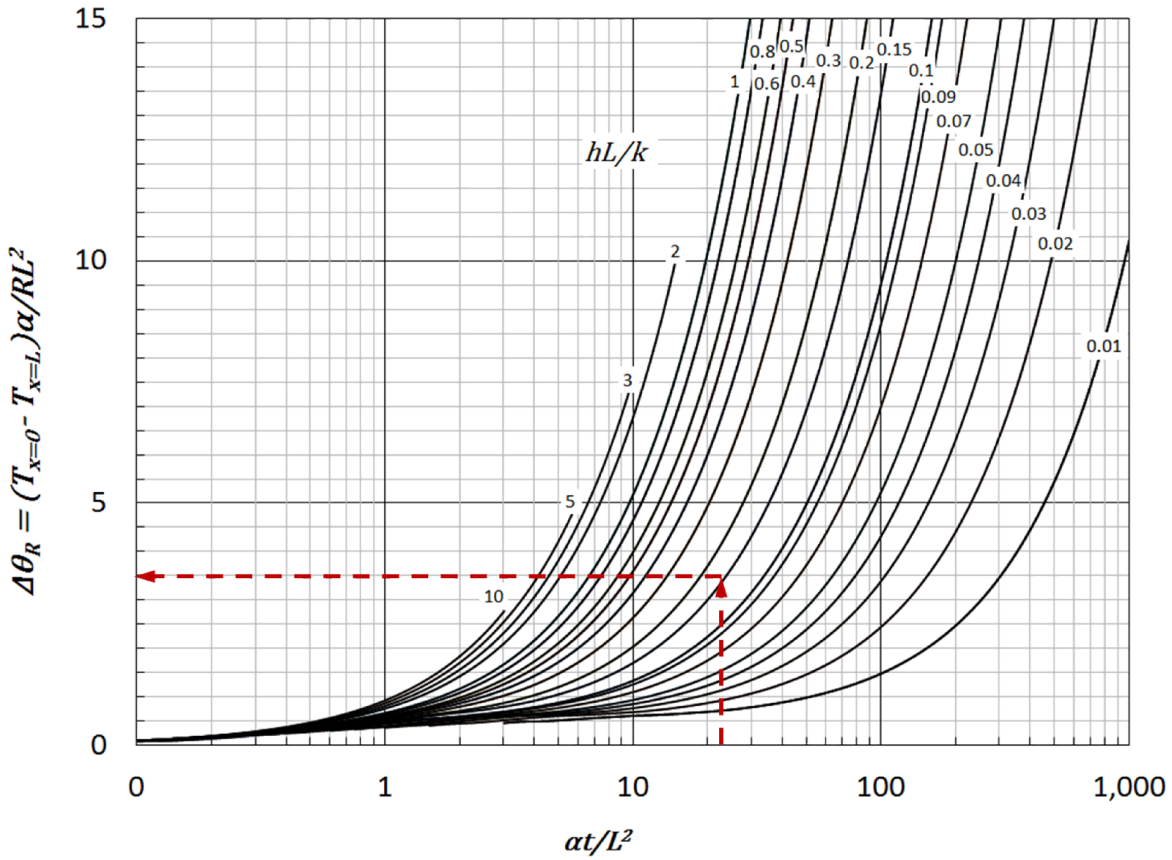


**Figure 2.9:** Graph showing the temperature lag between the heated side and the non-heated side during the initial ramp of the cure cycle. The contours represent the temperature lag for various Biot numbers. The dashed line illustrates the representative case study considered.

**Heat Chart - 2:** ***Ramp rate of the non-heated side (at x = L) during the initial ramp of the cure cycle.***

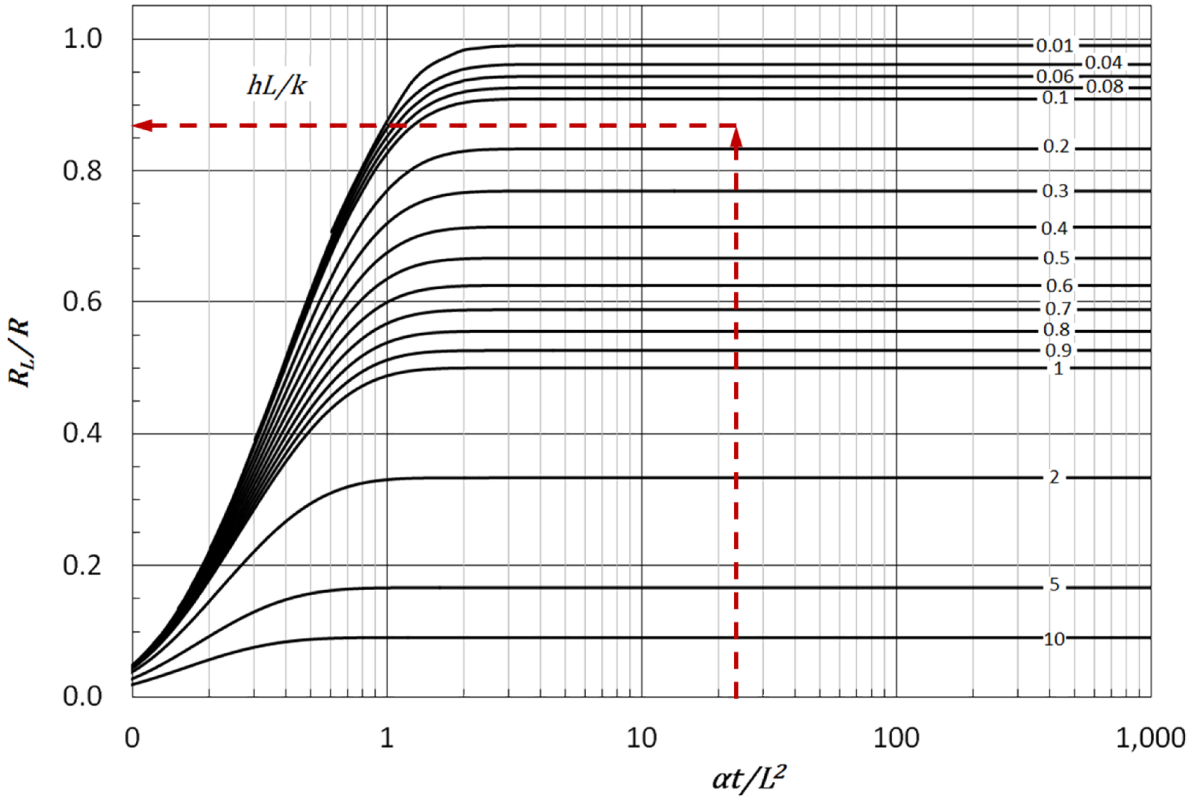


**Figure 2.10:** Graph showing the ratio of the ramp rate of the non-heated side to the imposed ramp rate (on the heated side) during the initial ramp of the cure cycle. The contours represent various Biot numbers. The dashed line illustrates the representative case study considered.

**Heat Chart - 3:** ***Time taken for the non-heated side (at x = L) to reach 95% of the steady state temperature during the dwell section of the cure cycle.***

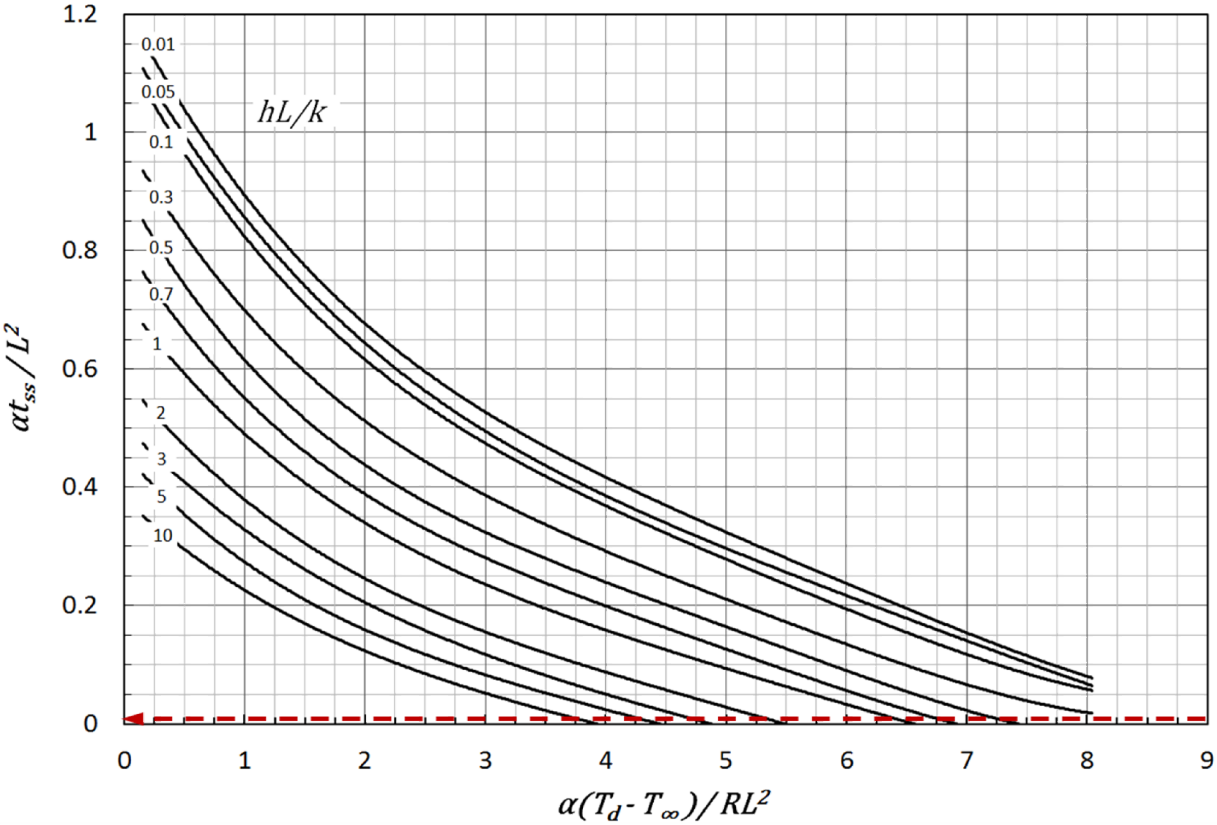


**Figure 2.11:** Graph showing the dimensionless time for which the non-heated side has reached 95% of the steady state temperature during the dwell section of the cure cycle. The contours represent the various Biot numbers. The dashed line illustrates the representative case study considered.

* For the considered representative case, the *x*-axis value is 23.1 (not shown in graph), which corresponds to a *y*-axis value of 0. The red dashed line therefore does not intersect any curve. This implies that for this representative case study, the time taken to reach 95% of the steady state temperature during dwell is 0 s, and is therefore instantaneous.

**Heat Chart - 4:** ***Steady state temperature of the non-heated side (at x = L) during the dwell section of the cure cycle.***

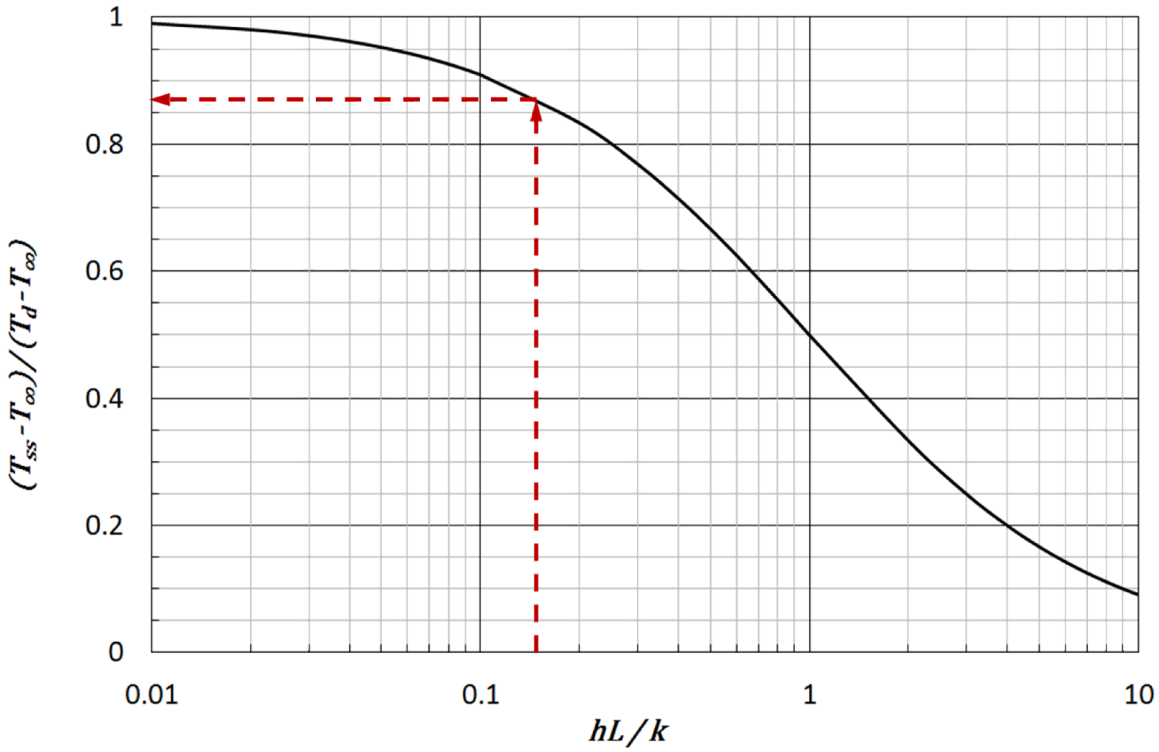


**Figure 2.12:** Graph showing the steady state temperature of the non-heated side during the dwell section of the cure cycle. The dashed line illustrates the representative case study considered.

The thermal response data for the representative case study extracted from heat charts 1- 4 are summarized in Table 2.3:

**Table 2.3:** Thermal response data extracted from the heat charts for the representative case study

| **Thermal Response Data for the Case Study** | |
|---|---|
| $\Delta T$ (°C) at *t=3000s* | 14.5 |
| $R_L$ (°C/min) | 1.8 |
| $t_{ss}$ (min) | 0.0 |
| $T_{ss}$ (°C) | 108.8 |

Similarly, the heat chart procedure described above can be used to predict the four key characteristics of the thermal response for a given in-situ bonded repair patch configuration during cure without any elaborate modelling of the heat transfer phenomenon.

Furthermore, using the heat charts, it is possible to capture certain trends in the key characteristics of the thermal response for a repair patch. Amongst the nine variables in the governing heat transfer problem, the variables, $h$ (heat transfer coefficient) and $L$ (repair patch thickness), undergo noticeable changes in a typical repair process and are therefore important to study; these two parameters can be seen in the system of PDEs that describe the governing heat conduction, Equations (2.9)-(2.12). Ideally, the temperature distribution throughout the repair would be equal to the imposed temperature during cure, and is taken as the baseline for the temperature of the repair patch. However, the one sided heat source induces a temperature gradient throughout the repair patch. To illustrate this departure from the ideal behavior described above, we plot trends showing the influence of $h$ and $L$ on two key characteristics of the thermal response: $R_L$ and $T_{ss}$. These two characteristics are selected because they undergo perceptible deviations from the baseline case. However, for completeness, the influence of $h$ and $L$ on the remaining two characteristics of the thermal response, $\Delta T$, and $t_{ss}$, are shown in the Appendix.

The corresponding trends showing the relative deviations in $R_L$ and $T_{ss}$ from the baseline temperature are shown in Figure 2.13 using a range of values for $h$ and $L$, which is typical for

this repair configuration; the range of $L$ includes both thick and thin laminates, and the range of $h$ provides both low and high heat transfer coefficients. In Figure 2.13, the baseline temperature used is the same imposed cure cycle considered in the representative case study (Table 2.1), which consists of an initial ramp of 2 °C/min from room temperature to 121 °C and a dwell at 121 °C for a period of 4 hours, and finally a cooling rate of 2 °C/min back to room temperature. It must be noted that this baseline is a typical cure cycle commonly used in the industry for manufacturing composite parts [48].

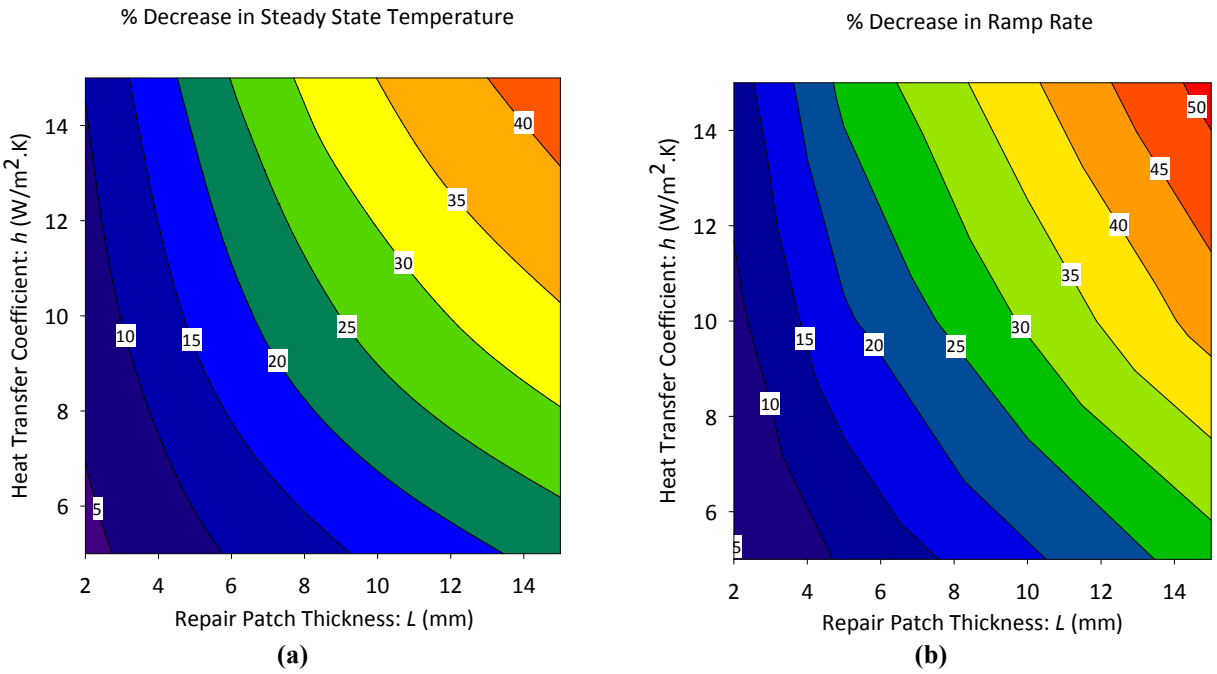


**Figure 2.13:** A contour plot of the relative deviations (in percentage) in **(a)** the ramp rate of the non-heated side, $R_L$, and **(b)** the steady state temperature of the non-heated side, $T_{ss}$, from the baseline temperature is shown for a range of values of heat transfer coefficient, $h$, and repair patch thickness, $L$.

## Observations and Discussions

The percentage decrease in $R_L$ and $T_{ss}$ is shown in Figure 2.13 (a) and (b) respectively. It is observed that the deviations are larger when the repair patch is thicker and the heat transfer coefficient with ambient air is greater. This is expected because the high heat transfer coefficient results in faster cooling on the non-heated side of the repair patch, leading to a greater temperature gradient. In addition, the large thickness increases the thermal mass of the system, contributing to a slower thermal response and greater lag, which further amplifies the

temperature gradient. The trends shown in Figure 2.13 (a) and (b) represent the extracted results of the heat charts and can provide estimates of the deviation in $R_L$ and $T_{ss}$ experienced when performing an in-situ repair process with respect to $h$ and $L$.

## 2.4 Summary

The heat transfer phenomenon during the curing process of an in-situ bonded repair patch was modelled. The governing heat transfer equation was simplified using suitable assumptions, which were discussed and justified. A methodology to solve the governing heat conduction equation subjected to a time-dependent and discontinuous boundary condition was presented. Consequently, an analytical solution to predict temperature field throughout the repair patch and at the bondline was developed. In addition to solving the heat transfer problem, a dimensional analysis was performed to reduce the total number of independent parameters in the system of equations. This enabled a graphical representation of the solution in the form of heat charts, which can be used to extract the key characteristics of the thermal response of the repair patch during the curing process. They are easy to implement, as was demonstrated using a representative case study. These heat charts present a potential tool to assess the feasibility as well as to facilitate the design process for in-field bonded repairs.

# Chapter 3

# Experiments and Model Validation

In this chapter, the heat transfer model developed for the in-situ bonded repair process is validated using experiments. First, the methodology to manufacture the parent laminate and the repair patch is outlined. The experimental setup including all the apparatus and instrumentation is also described. A simple experimental approach to determine the heat exchange coefficient with air for in-field repairs is presented.

For this experimental validation, two case studies are considered using two different thicknesses of the parent laminate. To validate the heat transfer model, both the analytical solution and the thermal response data extracted from the heat charts are compared with the measured thermal response of the two representative repair patches.

## 3.1 Manufacturing Process

In this section, the primary aspects of the manufacture of the representative parent structure and the repair patch are highlighted. The useful material properties are also described.

### 3.1.1 Materials

For this study, two Out-of-Autoclave (OOA) prepreg materials were used to manufacture the parent structure as well as the repair patch. The materials are commercially known as CYCOM 5320/PW and CYCOM 5320/8HS and are manufactured by Cytec Engineered Materials. Both of them have the same toughened epoxy resin systems and carbon fibres but have different fibre architecture: CYCOM 5320/8HS plies are relatively thicker and heavier than the CYCOM 5320/PW plies. The properties of the different materials are shown in Table 3.1 .

For the bonded repair patch, Cytec FM 300-2M adhesive film was also used. It constitutes of a thin polyester carrier which has been impregnated with the adhesive. It has a 293 $g/m^3$ areal weight and its uncured average nominal thickness is 0.25 mm [49].

**Table 3.1:** Properties of Cycom 5320/PW and 5320/8HS prepregs [2, 48].

| Material Properties | Cycom 5320/PW | Cycom 5320/8HS |
|---|---|---|
| Resin | 5320 | 5320 |
| Resin content | 36 % | 36 % |
| Out-life | 21 days | 21 days |
| Fabric | T650-3K PW | T650-3K 8HS |
| Areal weight | 195 $g/cm^3$ | 370 $g/cm^3$ |
| Tow count | 3k | 3k |

### Thermal Properties of Material

The thermal response of the in-situ bonded repair patch is dependent on the thermo-physical properties of the material. These properties include the thermal conductivity, the specific heat capacity and the density of the material. They are used as input parameters in both the heat transfer model and with the heat charts to predict the thermal response of a bonded repair patch during the curing process. The specific heat capacity and the density of the material (CYCOM 5320/PW and CYCOM 5320/8HS) were provided in the manufacturer's data sheet; however, its transverse thermal conductivity was measured experimentally according to ASTM E1225

standard. Table 3.2 summaries the thermo-physical properties of the composite materials used for the experiments.

It must be noted that the two composite materials used differ in their fibre architecture. However, this difference does not influence their thermo-physical properties. Both composite materials constitute of the same kind of resin and carbon fibres in the same proportion and are therefore expected to have similar thermo-physical properties.

**Table 3.2:** Thermo-physical properties of the composite materials used in the experimental validation [25].

| **Material Properties** | **Cycom 5320** (PW and 8HS) |
|---|---|
| Density (kg/m$^3$) | 1310 |
| Specific heat capacity (J/kg·K) | 1260 |
| Thermal conductivity (W/m·K) | 0.21 |

### 3.1.2 Manufacture of Parent Laminates

Two parent laminates were manufactured from the OOA prepreg plies and each measured 20" x 20". The first parent laminate was a 20 plies lay-up with 5320/PW, used for Case Study 1 whereas the other parent laminate was a 40 plies lay-up with 5320/8HS, used for Case Study 2. To avoid the sanding process in creating the scarfed cavity in the representative parent structure, a method of ply drop-off was used during the lay-up process. Each ply of the parent structure had a hole cut into it such that when stacked on top of each other, it created a ply drop-off that simulated a scarfed hole in the parent structure (see Figure 3.2). The size of each hole was calculated such that a scarf angle of 3 degrees is maintained for the 20 plies parent laminate and 10 degrees for the 40 plies parent laminate to avoid the excess use of materials. It is worthy to note that the scarf angle is not a governing parameter in the thermal response of the system. A $[0/90]_s$ layup was used and the laminates were processed according to the recommendations provided by the manufacturer [48]. The vacuum bag arrangement is shown in Figure 3.1. It consisted of the parent laminate over the tool plate (Aluminum, 13 mm thick), a nylon peel ply (silicone coated) over the scarfed area of the laminate; a non-perforated release film above the laminate (model number: A4000R-001-60-41 7-SHT, supplier: Airtech); edge breathing dams

made of sealant tape wrapped in fibreglass cloth; and, one layer of breather material (Airweave N10, 340g/m$^2$ , supplier: Airtech) and the vacuum bag (model number: WL7400-002-60-1000-SHT, 0.002" thick).

The uncured laminate was subjected to a 4 hour vacuum-hold at 20 °C before it was cured in a convection oven. The cure cycle consisted of an initial ramp of 2 °C/min to 121 °C and maintained at this dwell temperature for 4 hours. The structure was then post cured at 180 °C for 2 hours and cooled down to 25 °C. A picture of the cured parent structure is shown in Figure 3.2.

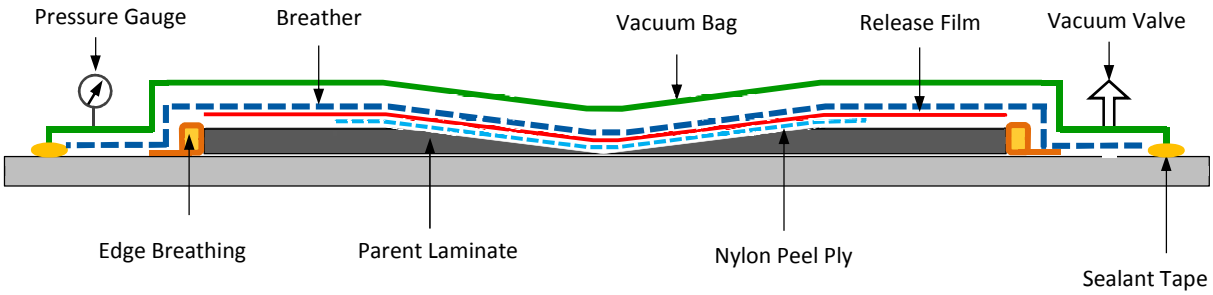


**Figure 3.1:** Schematic showing the bagging arrangement used for the manufacture of the parent laminate with the integrated scarfed cavity.

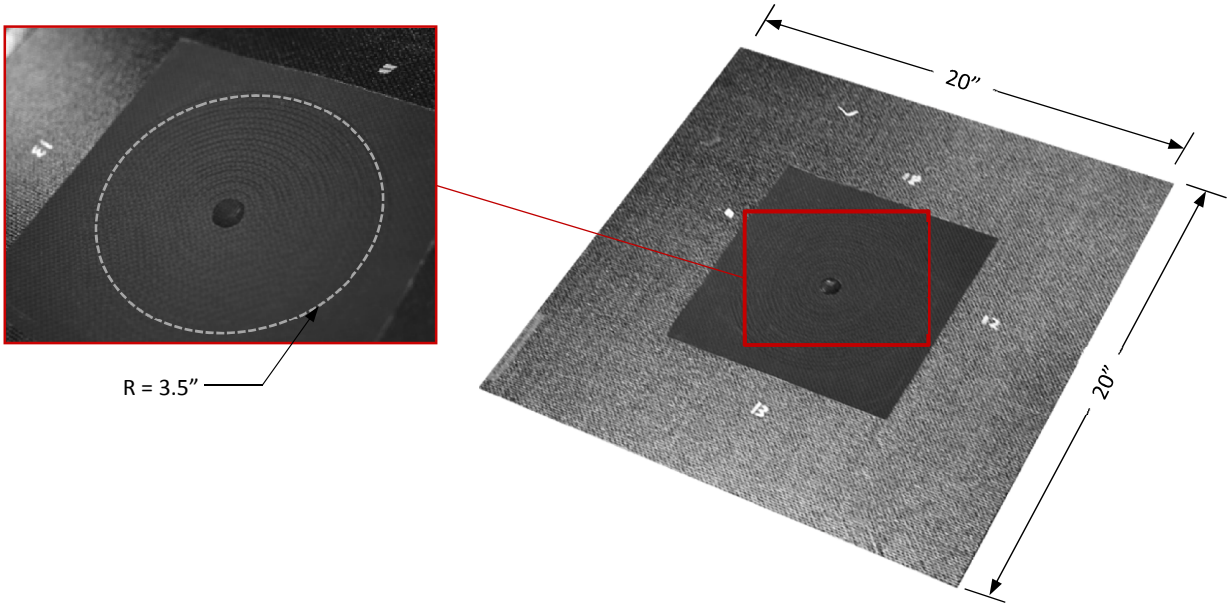


**Figure 3.2:** Picture showing the cured parent structure with the integrated scarfed cavity which was manufactured using the ply drop off technique. The close-up area of the scarfed cavity shows the rough terraced texture obtained from the ply drop off and the use of a peel ply.

### 3.1.3 Preparation of Repair Patch and Adhesive Film

The repair patch was manufactured using the same uncured OOA prepregs as that of the parent laminate. The lay-up sequence and the number of plies also matched the parent structure. The geometry of the repair patch consisted of concentric circular plies cut to different diameters and stacked together to form a scarf repair patch as shown in Figure 3.3 (a).

One layer of adhesive film was cut in a ring–shape to match the scarfed area on the parent laminate. It was placed between the repair patch and the scarfed area on the parent laminate when the repair process was implemented. Figure 3.3 (b) shows a picture of the adhesive film cutout.

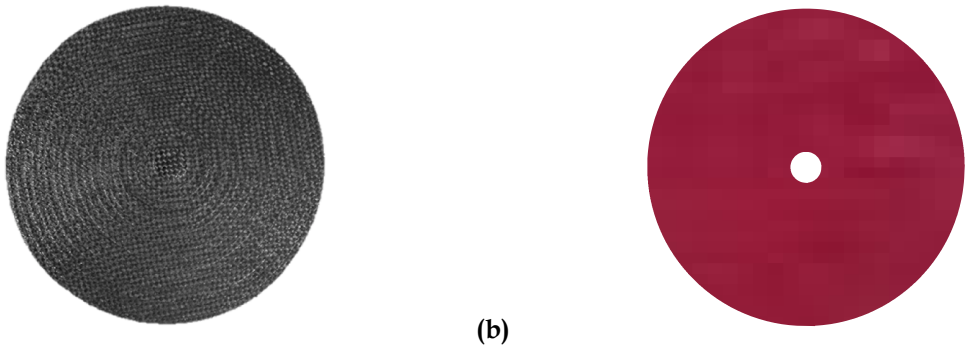

**(a)** **(b)**

**Figure 3.3:** Picture showing **(a)** the uncured repair patch used for the in-situ bonded repair. **(b)** The ring shaped adhesive film that was placed between the repair patch and the scarfed cavity.

## 3.2 Apparatus and Instrumentation

The in-situ bonded repair process was implemented and monitored using various types of equipment, which are described in this section. The equipment consisted of a laboratory scale temperature controlled heating blanket, also known as a hot-bond system, for the curing process and a data acquisition system to monitor the thermal response of the repair patch.

### 3.2.1 Hot-Bond System

#### Temperature Controller

A hot-bond system is commonly used to provide the heat required for curing the repair patch and the adhesive film. It consists of a proportional-integral-derivative (PID) temperature controller

that imposes a specific temperature cycle onto the repair patch via the heating blanket. To do so, a feedback thermocouple, placed directly above the repair patch, is used as an input to the PID controller which in turn regulates the amount of current though the heating blanket and hence the temperature imposed.

The hot-bond system used for the repair process, is an in-house built repair equipment. The PID controller is a Ramp and Soak Omega Controller (CN7800 series) which has a thermocouple input and a direct current (DC) output. The DC current signal generated by the PID controller controls the current going through the heating blanket via a solid state relay (SSR). The main principle of a SSR is to switch on a higher amperage circuit when a small activation DC current signal is applied across it. A SSR has the ability to switch on and off at high frequency enabling the temperature control to be fine-tuned. A layout of the hot-bond system circuitry and it various components are shown in Figure 3.4.

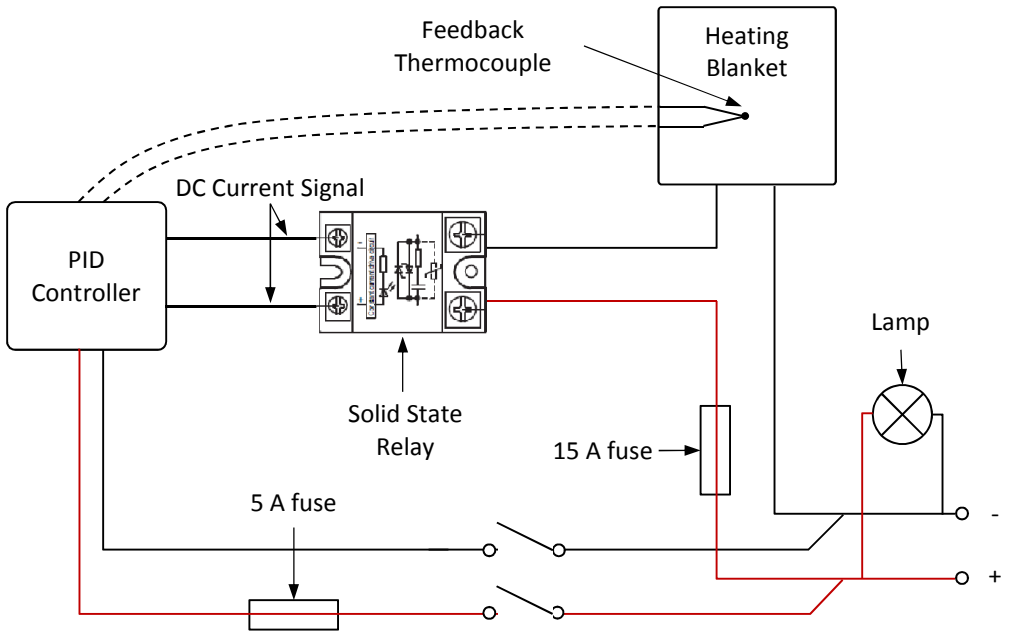


**Figure 3.4:** Schematic showing the layout of the electrical circuit for the hot bond system. The PID controller is used to control the temperature of the heating blanket via a solid state relay.

The hot-bond system operates by sensing the surface temperature and comparing it to the set point value entered by the user in the controller. To match these two temperatures, the PID controller sends (or not) a DC current signal to the SSR which close/open the heating blanket

circuit to provide heat or let the repair patch to cool down. The controller can be programmed such that the set point value follows a specific cure cycle with ramps and soaks (dwells).

**Heating Blanket**

The heat required for the curing process was supplied by a fibreglass-reinforced silicone rubber heating blanket. The heating blanket measured 12" x 12" with a thickness of 0.07", and was rated at a power density of 10 W/in$^2$ and maximum temperature rating of 232 °C. It operates with a 115V AC, single phase power supply and has an amperage of 12.52 A [46]. The structure of the heating blanket consists of flat resistive wires embedded between two thin flexible glass fibre reinforced silicone sheets, which are sealed together. Heat is generated when current passes through this network of resistive wires via the two external leads.

### 3.2.2 Data Acquisition System

The thermal response of the repair patch was monitored using thermocouples connected to a data acquisition system (DAQ) during the curing process. Type K thermocouples (Omega, 40 AWG, ±2 °C) were inserted at different locations in the repair patch to capture the temperature evolution. A National Instruments SCIX-1000/1102 with 20 thermocouple inputs was used to record the thermocouple readings in LabView Signal Express throughout the repair process.

## 3.3 Experimental Setup

Validation experiments for the in-situ bonded repair process were performed in a laboratory environment. An experimental setup was designed to replicate the in-field repair scenarios. This apparatus consisted of a clamped holder, which positioned the parent laminate structure vertically to simulate a fuselage structure undergoing repair as shown in Figure 3.5 and Figure 3.6. This experimental setup allowed the repair process on one side; the other side simulated inaccessibility (which is common during in-field repairs) and the heat flux exchange with ambient air. This stand-alone configuration was also chosen to avoid any thermal contact with other materials/structures that could influence the validation experiments. Furthermore, a combination of the relatively low in-plane thermal conductivity of the material and the

sufficiently big size of the parent structure ensured that the aluminum frame used as the holder (see Figure 3.6) did not influence the heat transfer phenomenon. Additionally, the criteria for ensuring a 1D heat conduction involving the overlap distance of the heating blanket (as previously discussed in Chapter 2) was satisfied for both experimental case studies. The corresponding $\lambda$ was 63.5 mm for the experimental case studies.

The setup also included a vacuum hose, which was connected to a vacuum pump, and was used to consolidate the repair patch onto the parent structure from one side. Vacuum pressure was applied onto the bagged area on the parent structure via a metallic valve, which was situated close to the repair zone. To prevent this valve from acting as a heat sink during the curing process, a thick insulating breather material was placed between the vacuum valve and the parent laminate. This insulating material significantly reduced conduction of heat from the heated repair zone to the metallic valve. It must be noted that for the experimental case studies, an additional vacuum bag was placed on the non-heated side to provide consolidation of the repair patch.

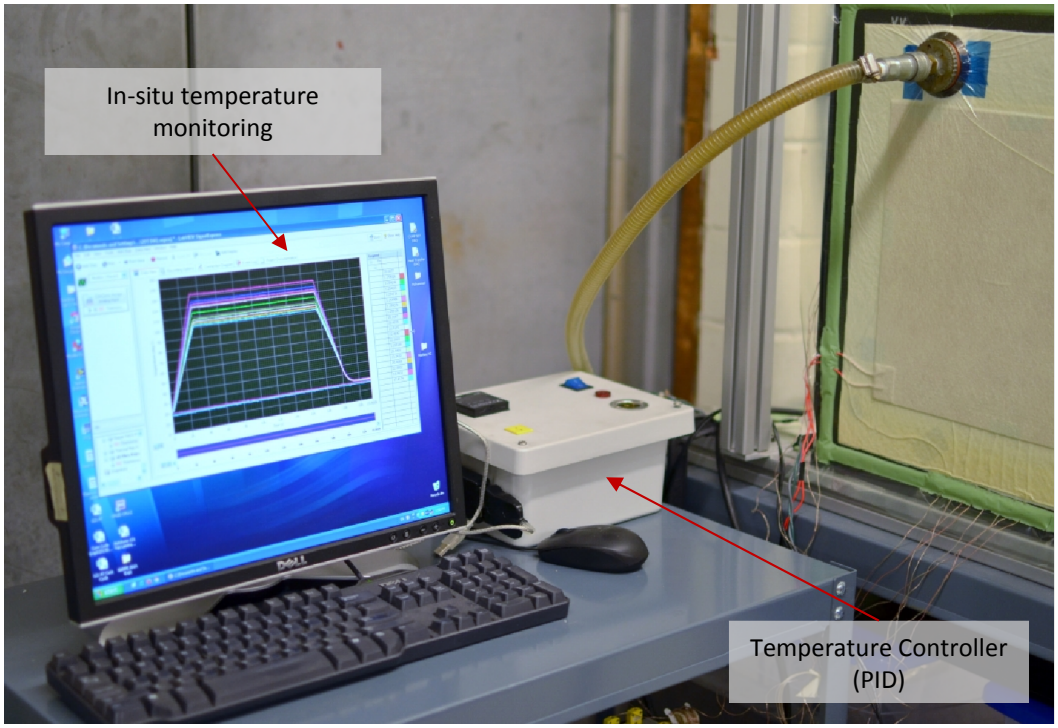


**Figure 3.5:** Picture of the experimental setup used to perform the in-situ bonded repair for the validation of the heat transfer model.

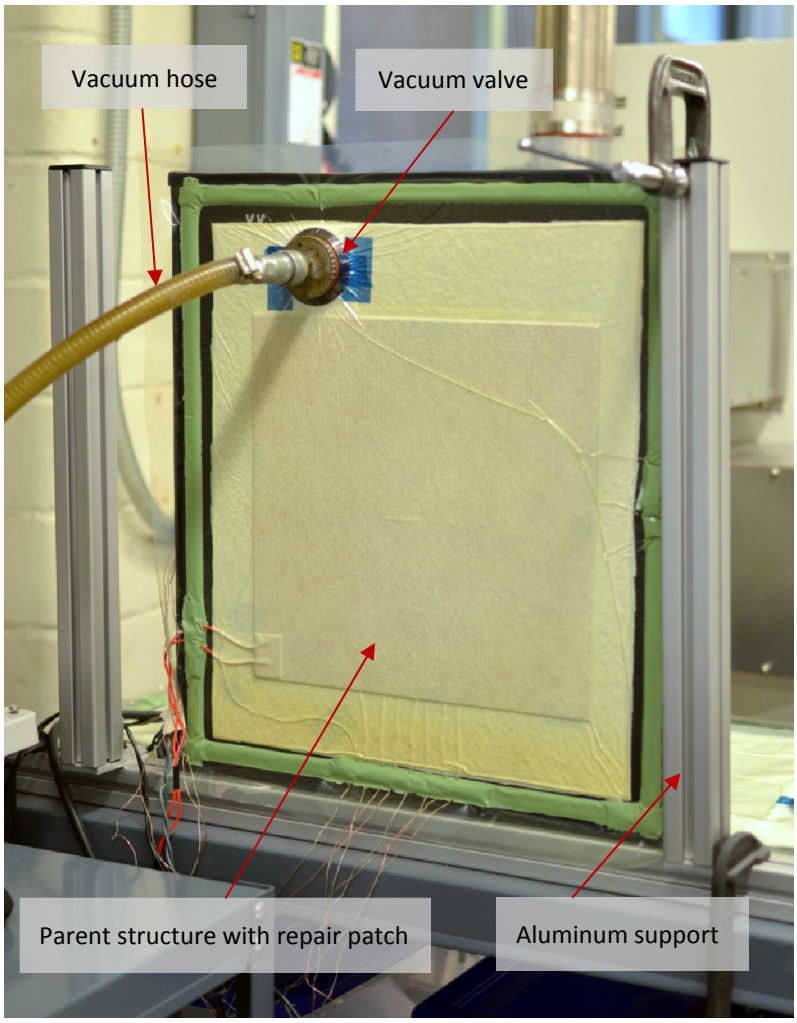


**Figure 3.6:** Picture of the parent laminate vertically supported in the experimental setup. The heating blanket was applied on one side and the other side was exposed to ambient air.

## 3.4 Measurement of Heat Transfer Coefficient

The heat transfer coefficient, *h*, is a quantity which is used to represent the heat flux exchange with the surrounding air; this heat exchange takes place on the non-heated side of the parent structure. It is a governing parameter in the heat transfer phenomena and must be determined experimentally prior to performing the repair. A direct way to extract this parameter is to use a commercially available heat flux sensor. However, these are usually expensive. There are various ways in which the value of *h* can be estimated indirectly [50]. In this section, a simple, economical yet reliable methodology is presented to indirectly measure the magnitude of *h*. This technique uses a setup, which is similar to that used for bonding the repair patch. Consequently,

this in-situ measurement technique is able to determine an effective heat transfer coefficient of the heat transfer phenomenon taking place during the implementation of the repair bonding process. A detailed description of this method for estimating the heat transfer coefficient for the in-situ bonded repair process is given in the next section.

### 3.4.1 Thermal Map Methodology

The heat transfer coefficient for the one sided in-situ bonded repairs can be estimated by measuring the heat flux throughout the parent structure which is subjected to a known heat source. The heat flux through a surface is defined as the heat flow per unit area through that surface [51]. For a unidirectional steady state heat transfer through a solid plate of thickness $L$, the heat flux is obtained by applying Fourier's law, which can be expressed using Equation (3.1). Equation (3.2) describes an external heat flux exchange with a fluid. According to the first law of thermodynamics, the heat flux is constant under steady-state conditions [52]. This characteristic of the heat flux simplifies the computation of the heat transfer coefficient, which is the main objective of this analysis.

$$q'' = -k\frac{dT}{dx} = k\frac{(T_1 - T_2)}{L} \tag{3.1}$$

$$q'' = h(T_w - T_\infty) \tag{3.2}$$

In Equations (3.1) and (3.2), $k$ is the thermal conductivity of the material, $h$ is the heat transfer coefficient, $T_1 - T_2$ is the temperature difference between the two surfaces of the plate, $T_w$ the surface temperature of the solid in direct contact with the fluid and $T_\infty$ is the temperature of the fluid, which is ambient air in this case.

It can be observed from Equations (3.1) and (3.2) that it is essential to measure the temperature difference across two points in space throughout the parent laminate to calculate the heat flux. However, for the one sided repair configuration under study, only one side of the parent structure can be accessed; it is also not possible to embed a thermocouple throughout the thickness of the cured parent laminate to probe the temperature. Subsequently, an additional plate with embedded

thermocouples is placed between the heat source (heating blanket) and the accessible side of the parent structure as shown in Figure 3.7 (a).

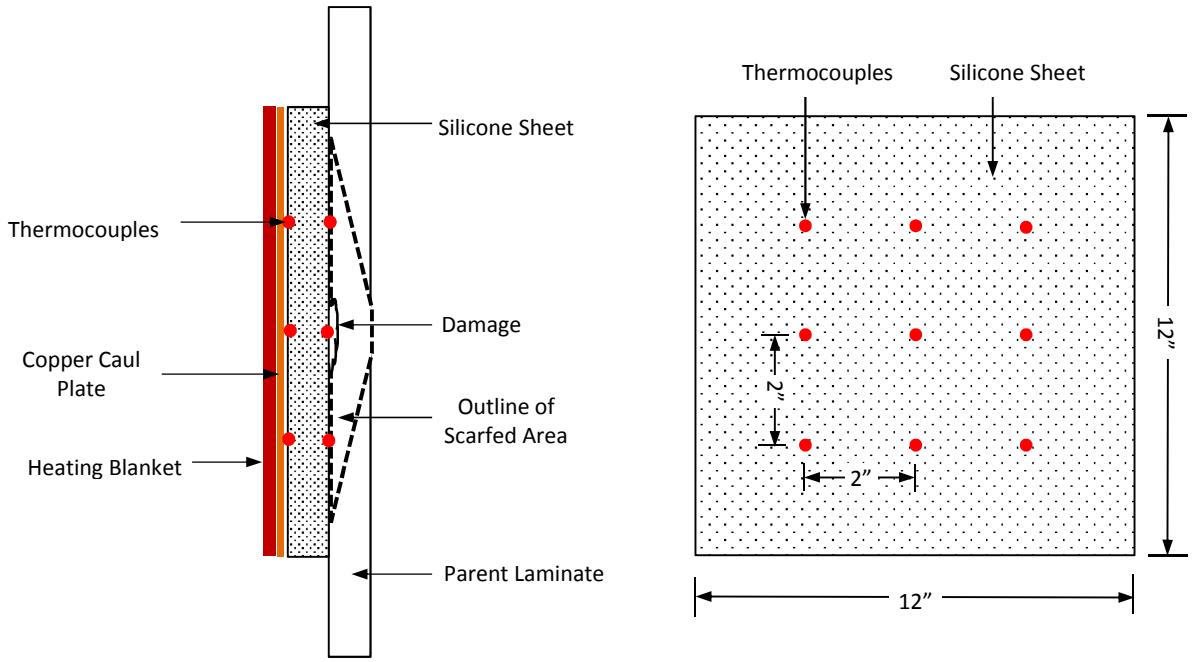


**Figure 3.7: (a)** Cross section of the representative thermal map setup used to estimate the transverse heat flux through the parent laminate subjected to a one sided heat source. **(b)** Thermocouple layout onto both sides of the silicone sheet

The material chosen for the additional plate was a piece of extreme temperature silicone rubber sheet which measured 12" x 12"x ¼" (its durometer hardness is 50A). Thermocouples were positioned at different locations on both sides of the silicone sheet. To ensure a good thermal contact on the parent laminate and the heat source, grooves were cut on the sheet surface to place the thermocouple wiring, creating a flush interface. A layout of the thermocouples on both the sides of the silicone sheet is shown in Figure 3.7 (b).

Since the heat flux is constant throughout the transverse direction at steady state condition, it is now possible estimate the magnitude of the heat flux by measuring the difference in temperature between the two surfaces of the silicone sheet. To extract the heat transfer coefficient with the air, a one-dimensional steady state heat transfer modelling of the parent laminate along with the silicone sheet is considered.

**One-Dimensional Steady State Modelling**

The heat transfer through the silicone sheet and the parent laminate under steady state condition is modeled using the concept of thermal resistance [52]. When a temperature is imposed on one side of the silicone sheet, as shown in Figure 3.7 (a), heat is transferred by conduction from the heat source through the silicone sheet and the parent laminate, and by convection from the other side of the parent laminate to the surrounding air of lower temperature. Under steady state conditions the heat flux is constant throughout the silicone sheet and the parent laminate at location *i* and is given by,

$$q_i'' = \frac{T_{iT} - T_\infty}{\frac{L_s}{k_s} + \frac{L_c}{k_c} + \frac{1}{h}} \tag{3.3}$$

where $L_s$ and $k_s$ are the thickness and thermal conductivity of the silicone sheet respectively, $L_c$ and $k_c$ are the thickness and transverse thermal conductivity of the composite parent structure respectively, and $T_{iT} - T_\infty$ is the difference in temperature between the surface of the silicone sheet (which is in contact with the heating blanket) and the ambient air on the back side of the parent laminate.

Similarly, the heat flux throughout the silicone sheet can be calculated from the measured temperatures across the two surfaces using,

$$q_i'' = \frac{T_{iT} - T_{iB}}{\frac{L_s}{k_s}} \tag{3.4}$$

where $T_{iT} - T_{iB}$ is the temperature difference across the silicone sheet at steady state condition.

Now that an estimate of the magnitude of the heat flux is obtained, the heat transfer coefficient, $h_i$, can be back calculated by plugging in the value of the heat flux in Equation (3.3) which can be rewritten as Equation (3.5).

$$\frac{1}{h_i} = \frac{\left(T_{iT} - T_\infty\right)}{q_i''} - \left(\frac{L_s}{k_s} + \frac{L_c}{k_c}\right) \tag{3.5}$$

Similarly, a value for the heat transfer coefficient is calculated from the nine temperature differences measured using the embedded thermocouples across silicone sheet. Using these values, an average estimate is calculated for the heat transfer coefficient using Equation (3.6).

$$\overline{h} = \frac{1}{n}\sum_{i}^{n} h_i \tag{3.6}$$

where $n = 9$ in this case.

**Concluding Remarks of the Thermal Map Method**

The thermal map provides a simple technique to estimate the heat transfer coefficient for bonded repairs. This technique has several advantages. For example, it involves a simple setup, which can be easily implemented for in-field applications. Furthermore, since a similar in-situ setup is used during the curing process, the thermal map method gives a good in-situ estimate of the heat transfer coefficient. Finally, the flexible silicone rubber sheet used in this method allows the evaluation of heat transfer coefficient on curved surfaces.

However, the thermal map technique is sensitive to the temperature measurement across the two surfaces of the silicone sheet. Since the difference in temperature at the surfaces of the silicone sheet is used to compute the heat flux, any small fluctuations in the temperature measurement are reflected in the final value of the heat transfer coefficient. To mitigate this effect and ensure an adequate degree of precision in the estimation of $h$, the heat flux was calculated by measuring the temperature at various locations over the repair patch zone; these measurements were made using nine pairs of thermocouples. Using these measurements, an average value of $h$ was computed. It is reiterated that the criteria corresponding to the 1D heat conduction formulation was satisfied for the experiments; however, slight temperature differences in the thermal mapping suggest possibility of minor edge effects.

The estimate of the heat transfer coefficient, $h$, can be further refined by placing a third thermocouple at the mid cross-section of the silicone sheet, in addition to the surface thermocouples. This configuration allows us to compute the heat fluxes with two different through thickness temperature differences (Figure 3.8). This technique increases the accuracy of $h$ since two independent readings are used to compute its value.

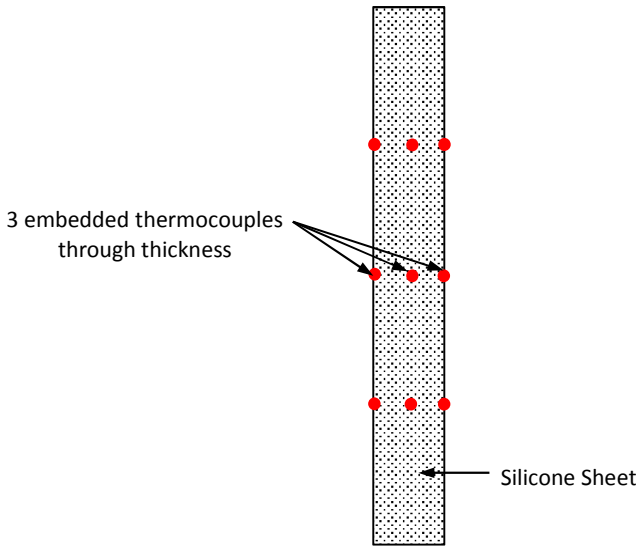


**Figure 3.8:** Schematic of the cross-section of the silicone sheet showing three different thermocouples embedded throughout the silicone blanket for the thermal map application. This configuration aims at reducing the percentage error in estimating the value of the heat transfer coefficient.

The thermal map procedure developed here was used to perform an in-situ measurement of the heat transfer coefficient prior to performing the bonded repair for the validation experiments. The corresponding details are described in the next section

### 3.4.2 In-Situ Estimation of the Heat Transfer Coefficient

In this section, an experimental implementation of the thermal map procedure is described to estimate the heat transfer coefficient on the non-heated side of the parent laminate. The experimental setup used here is similar to the one used for the repair process and was carried out as follows.

First, the silicone sheet with the embedded thermocouples was placed onto the non-scarfed parent structure; a 1.02 mm thick cooper caul plate and the heating blanket were placed next. To

ensure good thermal contact between each layer of material, the whole assembly was vacuum bagged, similar to the bonded repair process, and is shown in Figure 3.9 [40].

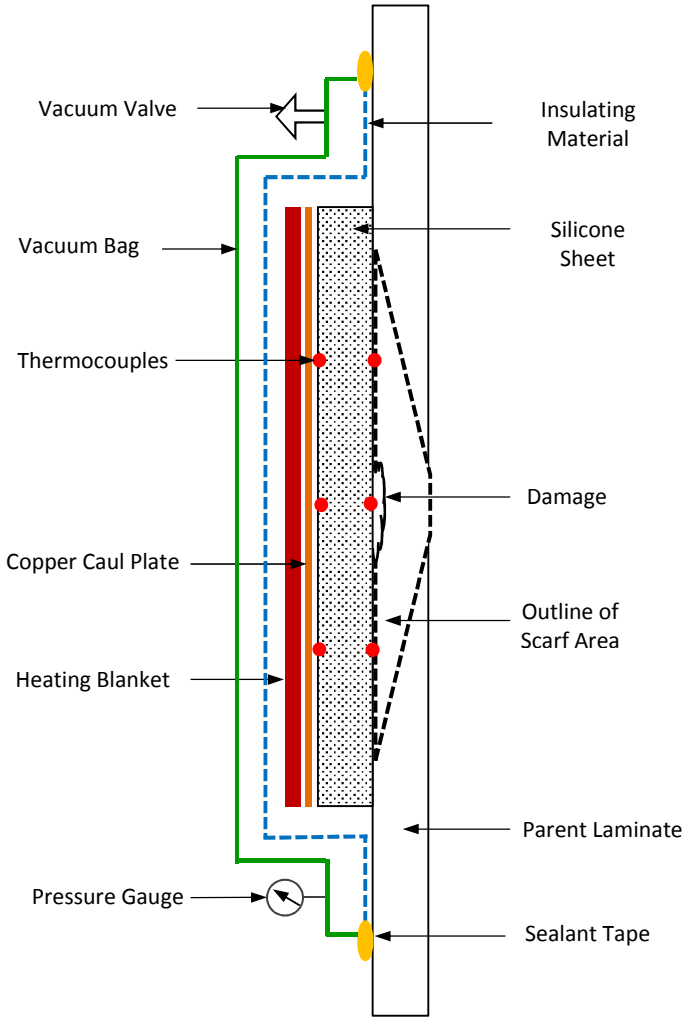


**Figure 3.9:** Schematic of the cross-section of the damaged parent structure showing the bagging arrangement used for the thermal map assembly.

Using a PID controller, the desired temperature profile was imposed onto the silicone sheet by means of the heating blanket. The temperature profile consisted of an initial ramp from ambient temperature to 100 °C over a period of 15 minutes, after which the temperature was maintained at 100 °C until steady state condition is reached. During the experiment, the temperature readings were monitored continuously using a National Instruments data acquisition system to determine the onset of steady state, which occurs when no change in temperature is observed. The heating blanket was then switched off to naturally cool down the system. Figure 3.10 shows the typical

measurement of the 18 different thermocouples embedded in the silicone sheet when the temperature profile was imposed.

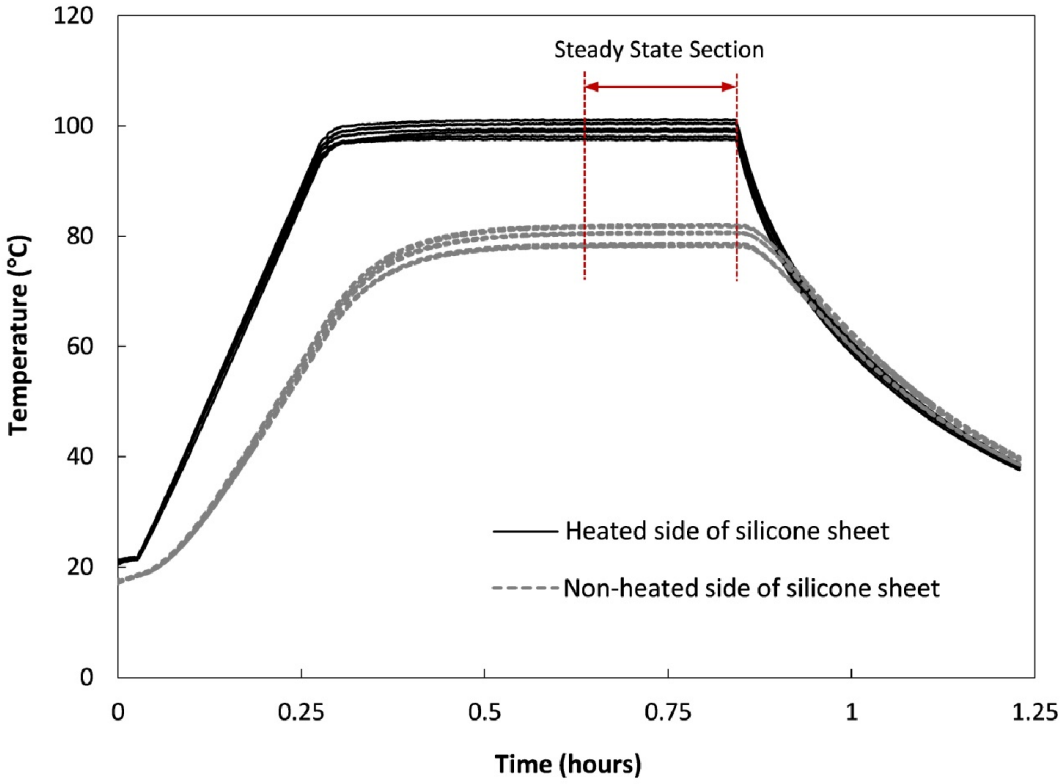


**Figure 3.10:** Graph showing the typical measurements of the 18 embedded thermocouples within the silicone sheet during the thermal map sensing process.

### Calculation of the Heat Transfer Coefficient, *h*

To illustrate the thermal map methodology for estimation of heat transfer coefficients, a case study is considered, namely, the repair Case Study 1 ( refer to Section 3.5) is presented. The average temperature of the 18 thermocouples is first calculated during the steady state portion of thermal response graph (Figure 3.10). Using Equation (3.4), the heat flux across the nine different locations on the silicone sheet is computed; the corresponding local heat transfer coefficients, $h_i$, are calculated using Equation (3.5). These results are presented in Table 3.3.

**Table 3.3:** Sensing data for post processing of thermal-map for repair Case Study 1.

| **Repair Configuration: Case Study 1** $T_\infty$ **= 18°C ,** $k_s$ **= 0.14 W/m·K ,** $L_s$ **= 6.3mm,** $k_c$ **= 0.21 W/m·K ,** $L_c$ **= 4.1mm** | | | | |
|---|---|---|---|---|
| **Thermocouple Location ,** $i$ | $T_{iT}$ (°C) | $T_{iB}$ (°C) | $q_i''$ (W/m$^2$) | $h_i$ (W/m$^2$·K) |
| 1 | 100.4 | 82.0 | 409 | 7.3 |
| 2 | 101.1 | 81.7 | 431 | 7.8 |
| 3 | 100.5 | 81.5 | 422 | 7.6 |
| 4 | 99.3 | 80.5 | 418 | 7.7 |
| 5 | 99.0 | 80.5 | 410 | 7.5 |
| 6 | 99.4 | 80.6 | 417 | 7.7 |
| 7 | 97.5 | 78.2 | 429 | 8.3 |
| 8 | 98.1 | 78.6 | 433 | 8.3 |
| 9 | 98.2 | 78.3 | 442 | 8.6 |

Using the values of $h_i$ from Table 3.3, the average representative value of the heat transfer coefficient of the back side of the parent laminate is calculated (equation (3.7)).

$$\bar{h} = \frac{1}{9}\sum_{i}^{9} h_i = \frac{70.7}{9} = 7.9 \tag{3.7}$$

The approach used to estimate the average value of *h* must be implemented each time, prior to the sanding process on the damaged parent structure. This procedure sequence is necessary to ensure good thermal contact between the silicone sheet and the parent laminate without forcing the silicone sheet to conform the scarfed cavity.

Once the heat transfer coefficient of the backside of the parent structure has been determined, the repair process can be implemented.

## 3.5 In-Situ Bonded Repair Experiment

To validate the model using experiments, two parent laminates with two different thicknesses were considered. The important characteristics of the two parent laminates are summarized in Table 3.4.

**Table 3.4:** Specifications of the parent laminates used for the experimental validation.

| Parent Laminate Specification | Case 1 | Case 2 |
|---|---|---|
| Material | 5320/PW | 5320/8HS |
| Dimension | 20" x 20" | 20" x 20" |
| Average Thickness | 4.1(mm) | 14(mm) |
| Scarf Angle | 3° | 10° |
| Number of Plies | 20 | 40 |

It is reiterated that prior to performing the in-situ bonded repair, the heat transfer coefficient of the backside of each parent structure was determined using the thermal map technique. For Case Study 1, an effective value of 8 $W/m^2 \cdot K$ was obtained; for Case Study 2, the heat transfer coefficient was 6 $W/m^2 \cdot K$.

### 3.5.1 Implementation of Repair Process

There are numerous steps involved in performing an in-situ bonded repair as mentioned in Chapter 1. The first step is surface preparation of the scarf area of the parent laminate. This is carried out to enhance the adhesivity of the surface. Since our goal is to capture the thermal response of the repair patch during curing, the surface preparation step is not a determining factor for it and can therefore be avoided. The next step involves applying the repair patch and bagging the assembly for the curing process. The ring shape adhesive film was first placed on the scarfed area; the repair patch plies were then carefully positioned onto the cavity to match the ply orientation of the parent laminate. Once the repair patch was in place, the parent laminate was vacuum bagged. The bagging configuration consisted of a perforated release film (model number: A4000RP-001-60-41 7-SHT, supplier: Airtech) on top of the repair patch, a glass fabric (to absorbed the excess resin), a non-perforated release film (model number: A4000R-001-60-41 7-SHT, supplier: Airtech), a breather (Airweave N10, 340g/$m^2$, supplier: Airtech), a 12" x 12" copper caul plate of thickness 1.02 mm (to minimize the temperature variation over the repair patch during heating), and a heating blanket. The entire assembly was vacuum sealed with a vaccum bag (model number: WL7400-002-60-1000-SHT, 0.002" thick) and sealant tape. A

schematic of the bagging arrangement used for the in-situ bonded repair process is shown in Figure 3.11.

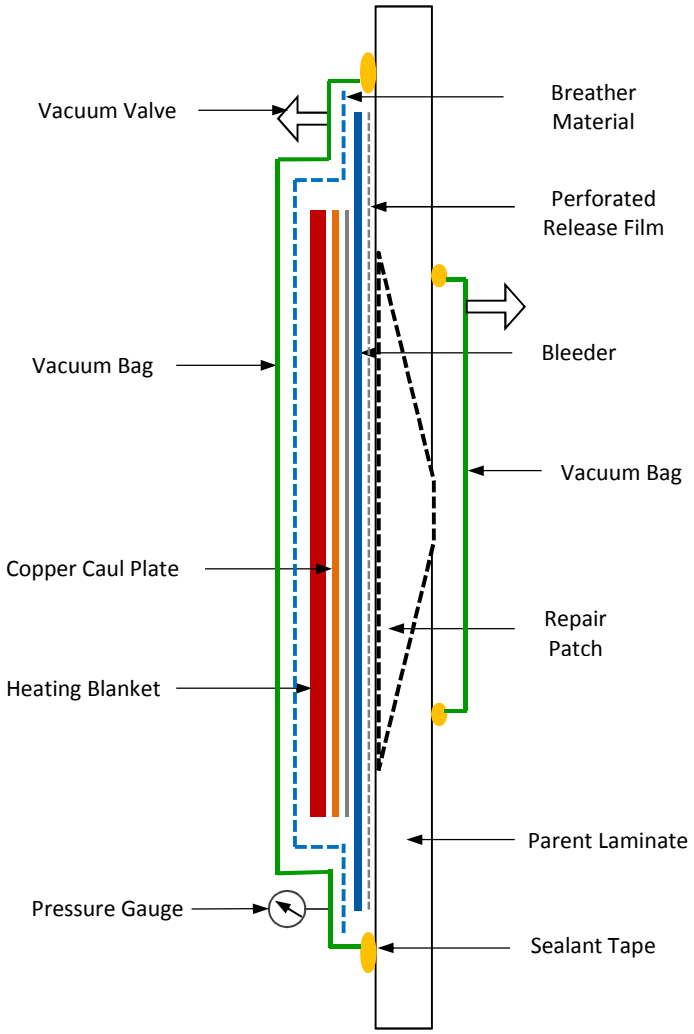


**Figure 3.11:** Schematic of the cross-section of the parent structure showing the bagging arrangement for the in-situ bonded repair process. It is noted that a vacuum bag was also placed on the non-heated side to provide consolidation pressure for the repair patch and prevent the flow of air through the repair patch.

### In-Situ Thermal Response Monitoring

For experimental validation, it is essential to the capture the thermal response of the repair patch during the curing process. This was achieved by embedding thermocouples at different locations in the repair patch and the parent laminate, as shown in Figure 3.12. Thermocouples 1, and 2 were placed at the centre of the repair patch. The remaining thermocouples 3, 4, 5, and 6 were

positioned at the extremities of the repair patch. Type K 40 AWG thermocouples were used along with the National Instruments data acquisition system.

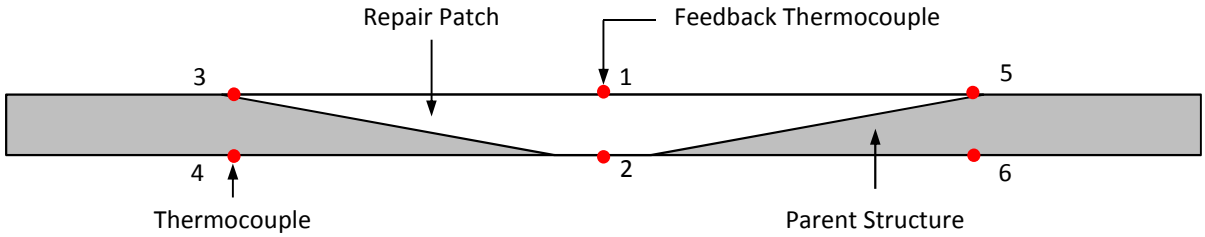


**Figure 3.12:** Schematic of the repair patch and parent laminate showing the locations of the thermocouples used to capture the thermal response of the repair patch during curing.

It must be noted that the feedback thermocouple was placed on the middle of the repair patch and was connected to the PID controller to control the temperature profile of the heating blanket.

### Curing Process

Before applying any heat to the system, the repair patch was first debulked under vacuum pressure at ambient temperature for a period of 4 hours. The cure cycle for the repair patch was then programmed within the PID controller, which controlled the temperature of the heating blanket. A similar cure cycle, which was used to manufacture the parent laminate was chosen for the repair patch. It involved an initial ramp of 2 °C/min to achieve a dwell temperature of 121 °C. The imposed temperature was maintained at 121 °C for 4 hours and then cooled to ambient temperature at a rate of 2 °C/min. During the curing process, the temperature throughout the repair patch was monitored. This experimentally determined temperature field within the repair patch is presented in the next section.

## 3.5.2 Comparison of Experimental Results and Analytical Solution

The temperature field at different locations throughout the repair patch, as shown in Figure 3.12, was monitored during the curing process. The experimental data are shown in Figure 3.13 and Figure 3.14 for case studies 1 and 2 respectively. The extracted temperature field for each case study was also compared to the corresponding analytical solution presented earlier. Table 3.5 summarizes the different input model parameters for each case study.

**Table 3.5:** Material properties of CYCOM 5320 and the heat transfer parameters for the two case studies [25]

| **Material Properties** | | |
|---|---|---|
| Transverse Thermal Conductivity, (W/m·K) | 0.21 | |
| Density, (kg/m$^3$) | 1310 | |
| Specific Heat Capacity, (J/kg·K) | 1260 | |
| **Thermal Response Parameters** | **Case 1** | **Case 2** |
| Laminate thickness, (mm) | 4.1 | 14 |
| Heat Transfer Coefficient, (W/m$^2$·K) | 8 | 6 |
| Ambient Temperature, (°C) | 18 | 21 |
| Ramp Rate, (°C/min) | 2.06 | 2 |
| Dwell Temperature, (°C) | 123 | 124 |

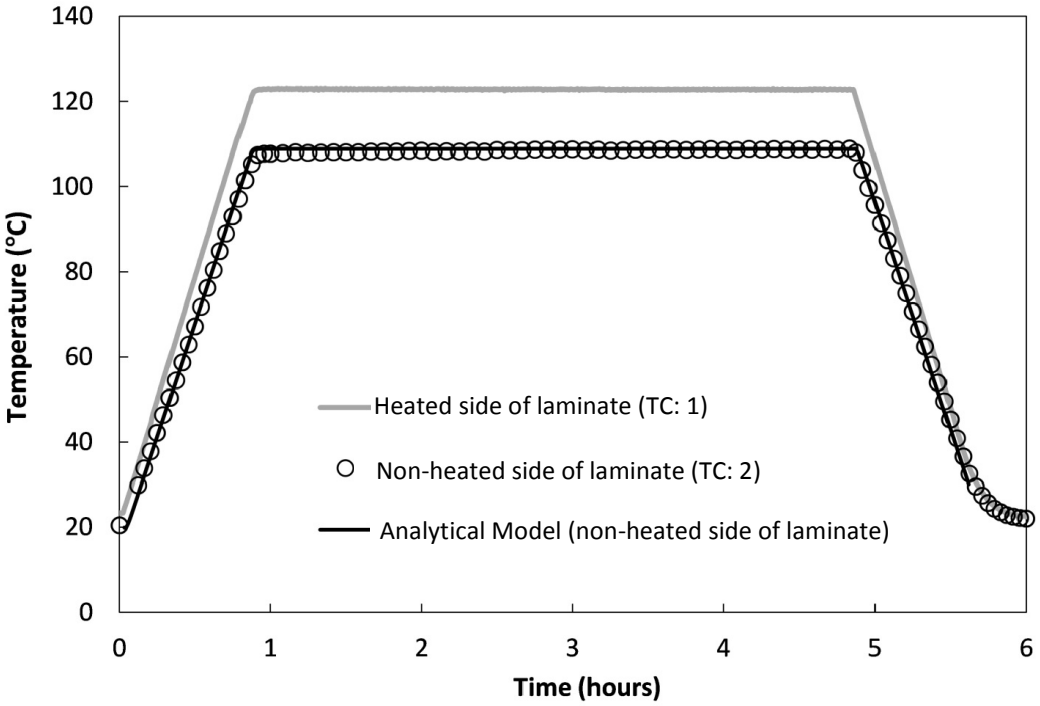


**Figure 3.13:** A temperature plot showing the temperature distribution through the thickness of the repair patch during the curing process for Case Study 1 (4.1 mm thick); the thermocouple measurements were collected every second. For better clarity, the temperature at locations 1 and 2 of the repair patch is shown. The temperature at the rest of the thermocouple locations are shown in the Appendix.

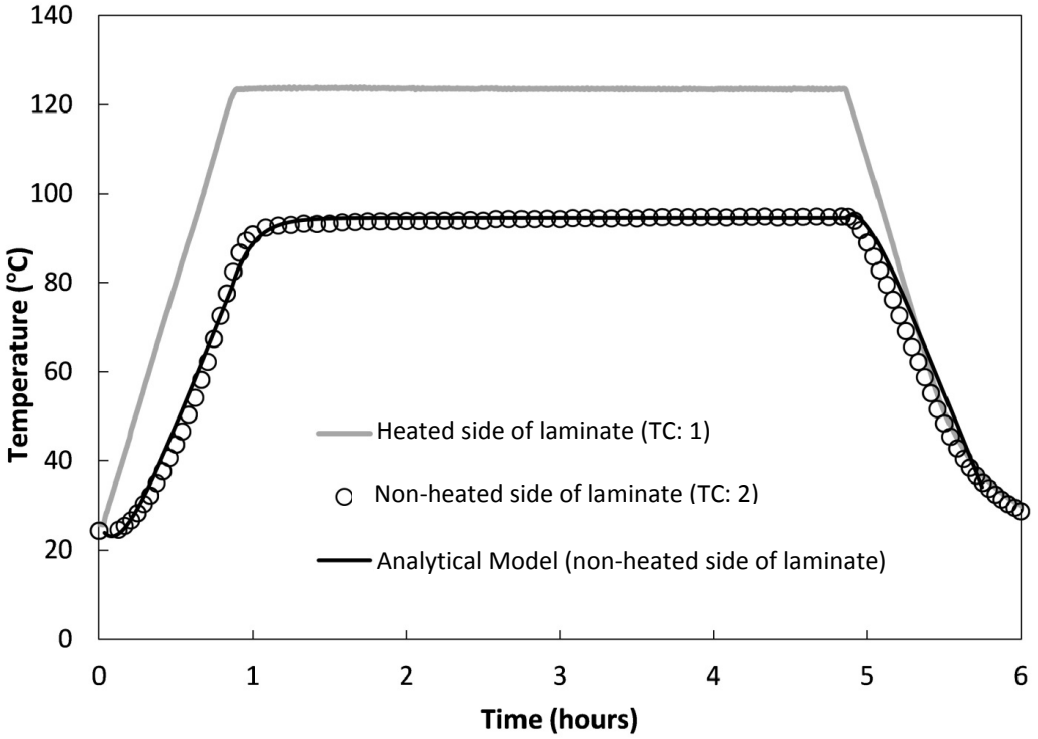


**Figure 3.14:** A temperature plot showing the temperature distribution through the thickness of the laminate during the cure of the repair patch for Case Study 2 (14mm thick) ); the thermocouple measurements were collected every second. For better clarity, the temperature at locations 1 and 2 of the repair patch is shown. The temperature at the rest of the thermocouple locations are shown in the Appendix.

Figure 3.13 and Figure 3.14 compare the experimentally determined values with the predicted thermal response of the repair patch during the curing process. These plots show a good correlation between the model solution and measured temperature. This holds true for both of the case studies, which consider two different thicknesses of the repair patch.

For completeness, the remaining temperature plots corresponding to locations 3, 4, 5, and 6 are shown in the Appendix for both Case Studies 1 and 2. Slight deviations from the analytical model can be observed in these plots. This could be due to non-uniformity in the temperature across the heating blanket leading to small variations in the temperature distribution across the repair patch. Minor edge effects may also cause the observed slight deviations in temperature distribution.

### Comparison of Experimental Thermal Response with Heat Charts

The four key characteristics of the thermal response of an in situ repair patch as described in Chapter 2 were extracted from the experimental data and compared with the values predicted by the heat charts. To obtain the key characteristics of the thermal response ($\Delta T$, $R_L$, $t_{ss}$ and $T_{ss}$) from the heat charts, the dimensionless parameters and numbers were first calculated for the two different case studies. These dimensionless parameters and numbers in addition to further details of the heat charts for each case study are presented in Appendix A. Table 3.6 summarizes the important aspects of the experimental and predicted thermal response data.

**Table 3.6:** Thermal response data for the two case studies. Both the experimental and predicted values are shown for comparison.

| Thermal Response Data | Case Study 1 | | | Case Study 2 | | |
|---|---|---|---|---|---|---|
| | Experiment | Heat Charts | Absolute Difference | Experiment | Heat Charts | Absolute Difference |
| $\Delta T$ (°C) at *t=3000s* | 15.5 | 14.5 | 1.0 | 40.3 | 42.8 | 2.5 |
| $R_L$ (°C/min) | 1.7 | 1.8 | 0.1 | 1.4 | 1.4 | 0.0 |
| $t_{ss}$ (min) | 0.0 | 0.0 | 0.0 | 10.1 | 11.6 | 1.5 |
| $T_{ss}$ (°C) | 108.7 | 108.8 | 0.1 | 94.5 | 94.6 | 0.1 |

The small absolute difference between the experimental and heat chart values shows that there is a close match between them for both case studies. This comparison shows that the heat charts are able to capture the key characteristics of the thermal response of an in-situ bonded repair patch.

The proposed heat transfer model and heat charts were validated using experiments. Two different thicknesses of repair patch were considered. In both cases the analytical model and the heat charts were able to capture the thermal response of the repair patch subjected to a one-sided heat source.

## 3.6 Summary

A methodology to validate the heat transfer model for the in-situ bonded repair process was described and implemented. An experimental setup was designed on a laboratory scale with the necessary equipment to best replicate this repair configuration. Furthermore, a simple technique to characterize the heat transfer coefficient on the non-heated side (inaccessible) of the parent structure was derived and applied experimentally. The in–situ bonded repair process was performed on two parent laminates with different thicknesses. During the curing process, the thermal response of the repair patch was captured by embedding thin thermocouples within the laminate. To validate the solution to the analytical model and the values extracted from the heat charts, a direct comparison was made between the predicted and the measured thermal response from experiments. A good correlation was observed between the model and the experiment for the two case studies. It is thereby demonstrated that the presented heat transfer model as well as the heat charts are able to predict the thermal response of the repair patch for the in-situ bonded repair process for monolithic composite panels.

# Chapter 4

# Analysis of Thermo-Chemical Phenomena and Heat Sinks

The first part of this chapter focuses on investigating how the thermo-chemical phenomena of the thermoset resin are dictated by the thermal response of the repair patch for the in-situ bonded repair configuration. The resin cure kinetics, viscosity, degree of impregnation and glass transition temperature models are used in conjunction with the analytical heat transfer model to study the effect of the induced temperature gradient on the final quality of the repair patch.

In the second part of this chapter, the influence of heat sinks on the thermal response is studied experimentally. Two metallic heat sinks with two different geometries and shapes are attached to the parent laminate and the thermal response of the repair patch is monitored during the in-situ bonded repair process.

## 4.1 Thermo-Chemical Analysis

It has been well established that the final quality of a composite laminate is significantly dependent on its processing conditions [22, 25, 44]. In the case of in-situ bonded composite repairs, the thermo-chemical processes of both the composite patch and the adhesive film greatly

dictate the strength restoration of the parent structure. Furthermore, the temperature gradient induced during the one-sided heated consolidation, generates a through thickness variation in thermo-chemical properties of composite patch and the adhesive film which severely influences the repair patch quality.

To improve the repair patch quality (with minimum void content and without compromising any mechanical properties), it is therefore essential to accurately predict many key thermo-chemical processes of the material that dictate the formation of voids and mechanical strength [2]. These thermo-chemical properties include degree of cure, degree of impregnation, resin viscosity and glass transition temperature. The coupling of these thermo-chemical characteristics with the thermal response of the repair patch during the curing process can be used to study the effect of processing conditions on in-situ bonded repairs as well as in designing and optimizing the cure cycle.

This coupling study is undertaken in the next section with the thermal model of the prepreg resin system (Cycom 5320) as the main focus. The adhesive behavior during cure is not incorporated due to lack of appropriate models. However, the given study can be easily extended once suitable adhesive models are developed.

### 4.1.1 Cure Kinetics

The epoxy resin systems of OOA prepregs considered for this study are thermosets. Initially, in their uncured state, thermosets consist of small molecules and other additives, including a catalyst. Upon heating, this catalyst accelerates an ongoing chemical process called polymerization which is responsible for cross-linking the small molecules [2]. The rate of this polymerization process increases initially when the resin viscosity is lowered; the rate eventually decreases when the molecular mobility is increasingly constrained by the evolving cross-linked network. The degree of cure, $\alpha(t)$, of a thermoset resin is a measure of the polymerization process with time. This polymerization process is generally characterized by the ratio of the heat of reaction released up to a time *t*, to the total heat of reaction such that $0 < \alpha(t) < 1$. During the curing of an in-situ repair patch, it is crucial that the degree of cure throughout the patch is

sufficiently high at the final stages of the process in order to exhibit maximum strength restoration of the parent laminate [25]. The temperature gradient induced throughout the repair patch due to the one-sided heat source introduces further challenges, which additionally mandate the study of the cure kinetics.

The evolution of the degree of cure during curing is studied using the thermal model in conjunction with the cure kinetics model of the material (Cycom 5320) developed by Kratz et al. [25].

The cure kinetics model was developed using a combination of models proposed by Kamal and Sourour [53] and by Cole et al. [54]. The degree of cure evolution with time is given by Equation (4.1),

$$\frac{d\alpha}{dt} = K_1 \alpha^{m_1} \left(1-\alpha\right)^{n_1} + \frac{K_2 \alpha^{m_2} \left(1-\alpha\right)^{n_2}}{1+\exp\left(D\left(\alpha-\left(\alpha_{C0}+\alpha_{CT}T\right)\right)\right)} \tag{4.1}$$

where $K_i$ is the Arrhenius temperature dependency,

$$K_i = A_i \exp\left(-E_{Ai}/\left(RT\right)\right) \tag{4.2}$$

The different constants in Equations (4.1) and (4.2) are summarized in Table 4.1.

**Table 4.1:** Cure kinetics model parameters for Cycom 5320 [25].

| Cure Kinetics Model Parameters | Value | Cure Kinetics Model Parameters | Value |
|---|---|---|---|
| $A_1$ | $8.23 \times 10^7$ | $m_2$ | 0.9 |
| $E_{A1}$ | 82375 | $n_2$ | 2.07 |
| $m_1$ | 0.75 | $D$ | 40.4 |
| $n_1$ | 12.46 | $\alpha_{C0}$ | -1.12 |
| $A_2$ | $1.04 \times 10^5$ | $\alpha_{CT}$ | $4.53 \times 10^{-3}$ |
| $E_{A2}$ | $6.2 \times 10^4$ | | |

The thermal response of the two case studies considered in Chapter 3 (experimental validation) is coupled with Equation (4.1) and the evolution of the degree cure of the repair patch is depicted in Figure 4.1.

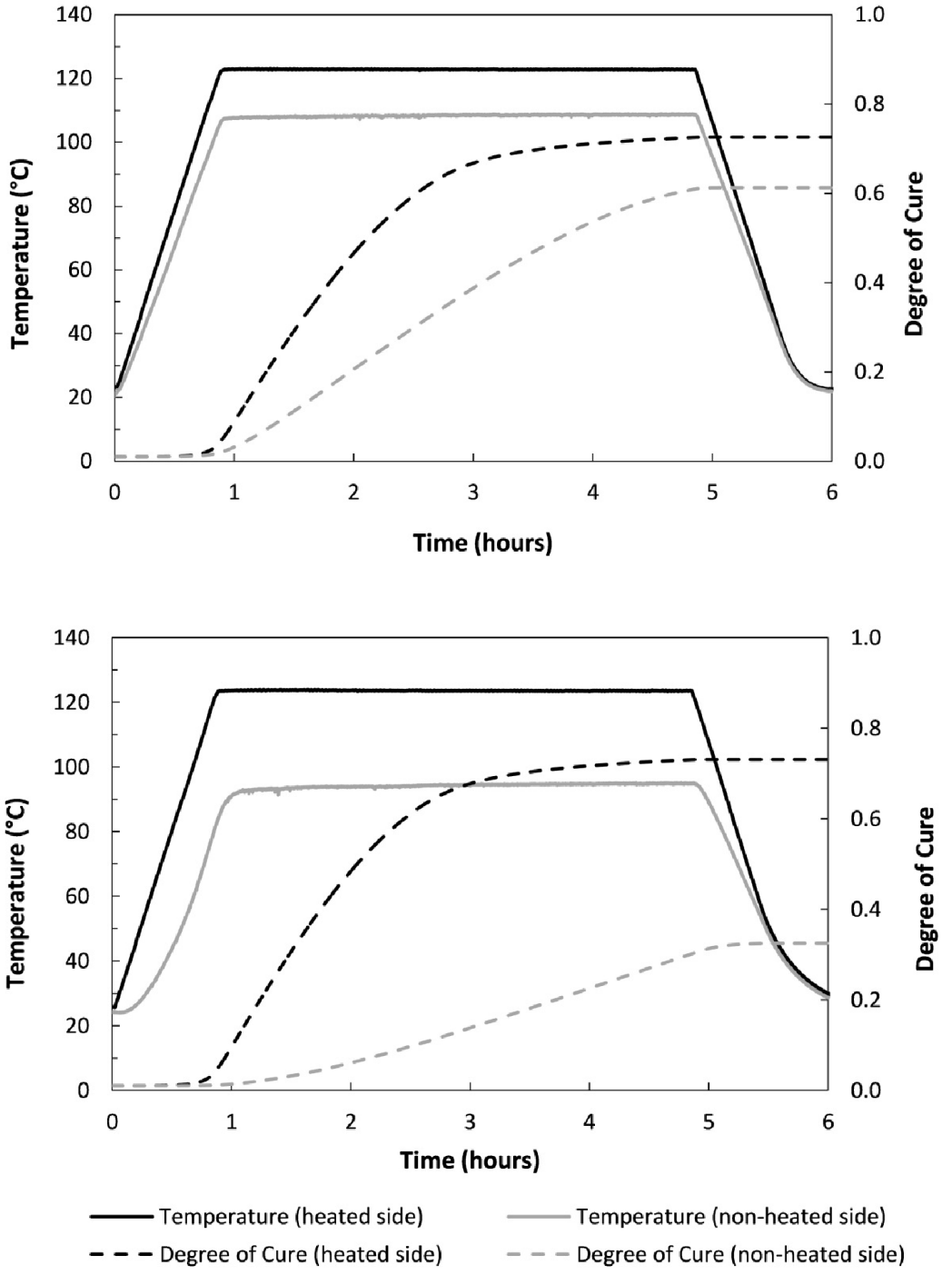


**Figure 4.1:** Graph showing the temperature and the predicted degree of cure of the heated and non-heated side of the repair patch during the curing process for Case study 1**(top)** and Case Study 2**(bottom)**. Case Study 1 and 2 involve a 4.1mm thick (5320/PW) and 14mm thick (5320/8HS) parent laminate respectively.

**Analysis of Cure Kinetics**

Figure 4.1 clearly shows that a cure gradient is induced throughout the repair patch for both the case studies considered. This is a direct consequence of the inevitable temperature gradient that is developed throughout the repair patch during the in-situ curing process. The cure gradient has several implications on the patch part quality, which can in turn be detrimental to its overall mechanical properties.

The cure kinetics for both case studies show that the resin gels ($\alpha = 0.48$ according to the thermal models developed by Kratz et al.[25]) at different instants in time. The surface in contact with the heat source always gels first while the surface furthest from the heat source gels last. However, if the surface in contact with the heat source gels prematurely, the through thickness permeability of the repair patch is decreased since gelation of the resin closer to the heat source can block the air channels. This behavior can prevent the escape of volatiles that are generated furthest from the heat source, subsequently resulting in void formation.

Another consequence of this cure gradient, particularly for the repair of thick laminates is shown by Case study 2 in Figure 4.1(bottom), where the resin did not gel throughout the curing process when the recommended cure cycle was applied. To mitigate this problem, one has to revisit the design of the imposed temperature profile in addition to the cure kinetics in order to accommodate for the effects of the temperature gradient for thick laminates. Since curing is happening at a much lower temperature furthest from the heat source, the time duration of the dwell must be extended or the dwell temperature must be higher so that the degree of cure is sufficiently high.

In addition to these direct consequences on the quality of the repair patch, the gradient in the resin cure kinetics has other ramifications. For example, it significantly dictates other thermo-chemical properties of the material such as the resin viscosity, which is a function of the degree of cure. To assess this aspect of the thermo-chemical behavior, the viscosity of the resin is discussed in the following section.

### 4.1.2 Resin Viscosity and Degree of Impregnation

Out-of–autoclave prepregs are engineered to feature a combination of dry permeable and resin coated (rich) areas. This is characteristic to the OOA prepreg where the relatively permeable areas allow gas evacuation when vacuum is applied to the bag at the beginning of the cure cycle which is also referred as the debulking process. When heat is applied to the laminate, the consolidation pressure provided by the vacuum bag forces the resin to flow into the dry regions. This impregnation process is greatly dependent on the state of the resin viscosity. There are two competing factors that dictate the viscosity of the resin: initially, thermal effects result in a low viscosity, however, eventually, the growth of the molecular chains (as degree of cure increases) leads to high viscosity [2]. During the initial stage of the cure cycle, the resin viscosity must be sufficiently low in order to fully impregnate the dry fibre regions. If the resin begins to gel prematurely without full impregnation, the underlying phenomenon may contribute to void formation in the laminate [2]; it must be noted that there are several other factors that can cause voids, however, in this study, the focus is on the flow-induced voids formed during the impregnation process. Consequently, it is important to obtain the right evolution of viscosity during curing to minimize this flow-induced void content (fully impregnated) of the repair patch. To fulfill this requirement for achieving high quality bonded repair, the thermal response of the in-situ bonded repair patch is coupled with a model of resin viscosity and the degree of impregnation to predict the evolution of the viscosity and the impregnation of the dry fibres for the repair process. The degree of impregnation is referred to as a measure of the dry tow filling during the resin infiltration process [2].

Kratz et al. developed the resin viscosity model for the Cycom 5320 material using techniques presented by Khoun et al. [43]. This viscosity model is given by Equation (4.3).

$$\mu = \mu_1 + \mu_2 \left( \frac{\alpha_{gel}}{\alpha_{gel} - \alpha} \right)^{A+B\alpha+C\alpha^2} \tag{4.3}$$

where , $\alpha$ is the instantaneous degree of cure and $\alpha_{gel}$ is the degree of cure at gelation. $\mu_i$ is the Arrhenius temperature dependency given by:

$$\mu_i = A_{\mu i} \exp\left(E_{\mu i} / (RT)\right) \tag{4.4}$$

A summary of the constants in Equations (4.3) and (4.4) is summarized in Table 4.2.

**Table 4.2:** Viscosity model parameters for Cycom 5320 [25].

| Viscosity Model Parameter | Value | Viscosity Model Parameter | Value |
|---|---|---|---|
| $A_{\mu 1}$ | 8.0 x $10^{-13}$ | $\alpha_{gel}$ | 0.48 |
| $E_{\mu 1}$ | 93931 | $A$ | 3.2 |
| $A_{\mu 2}$ | 2.9 x $10^{-11}$ | $B$ | 12.7 |
| $E_{\mu 1}$ | 8.3 x $10^{4}$ | $C$ | -29.6 |

The degree of impregnation was also predicted for the bonded repair process using a model developed by Centea et al. [22], which is given by,

$$\frac{d\beta}{dt} = \frac{K}{\mu R_{tow}^2 (1 - V_f)} \left( \frac{P_\infty - P_f}{(1-\beta)\ln(1/(1-\beta))} \right) \tag{4.5}$$

where $\beta$ is the degree of impregnation, $0 < \beta < 1$ , and $P_f = P_{gas} - P_c$ .

The different constants used in Equation (4.5) are summarized in Table 4.3.

**Table 4.3:** Degree of impregnation model parameters for Cycom 5320/PW and Cycom 5320/8HS [2].

| Degree of Impregnation Model Parameter | 5320/PW | 5320/8HS |
|---|---|---|
| $V_f$ | 0.71 | 0.74 |
| $R_{tow}$ (mm) | 0.0917 | 0.118 |
| $P_\infty$ (Pa) | 101325 | 101325 |
| $P_{gas}$ (Pa) | 0 | 0 |
| $P_c$ (Pa) | 0 | 17833 |
| $K$ ($m^2$) | $2.1 \times 10^{-15}$ | $9 \times 10^{-16}$ |

To study the evolution of the resin viscosity and the degree of impregnation, the thermal response of the repair patch during the in-situ bonded repair process for Case study 1 and 2 are used in conjunction with Equation (4.3) and (4.5) as shown in Figure 4.2 and Figure 4.3.

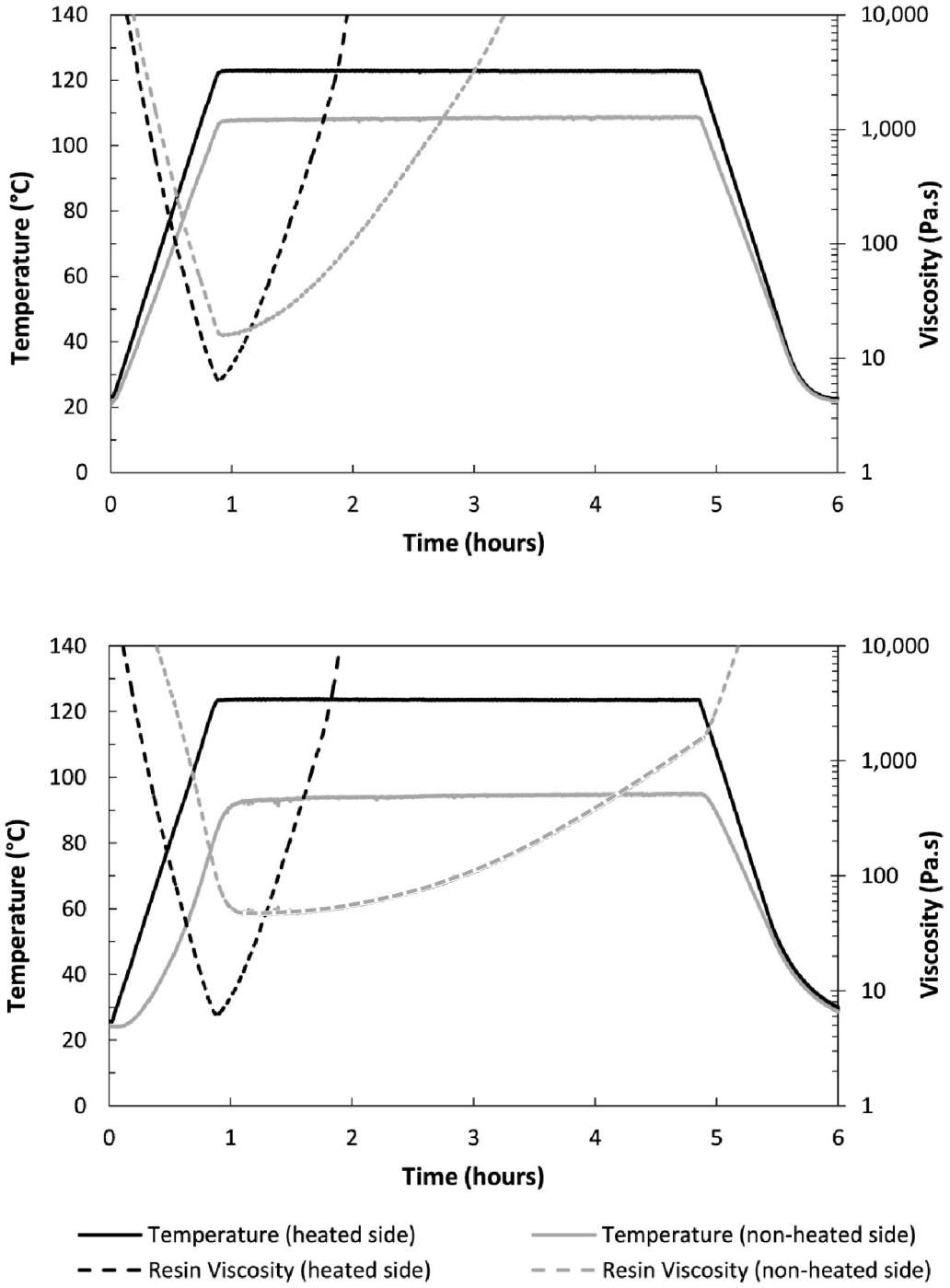


**Figure 4.2:** Graph showing the temperature and the predicted resin viscosity of the heated and non-heated side of the repair patch during the curing process for Case study 1**(top)** and Case Study 2**(bottom)**. Case Study 1 and 2 involve a 4.1mm thick (5320/PW) and 14mm thick (5320/8HS) parent laminate respectively.

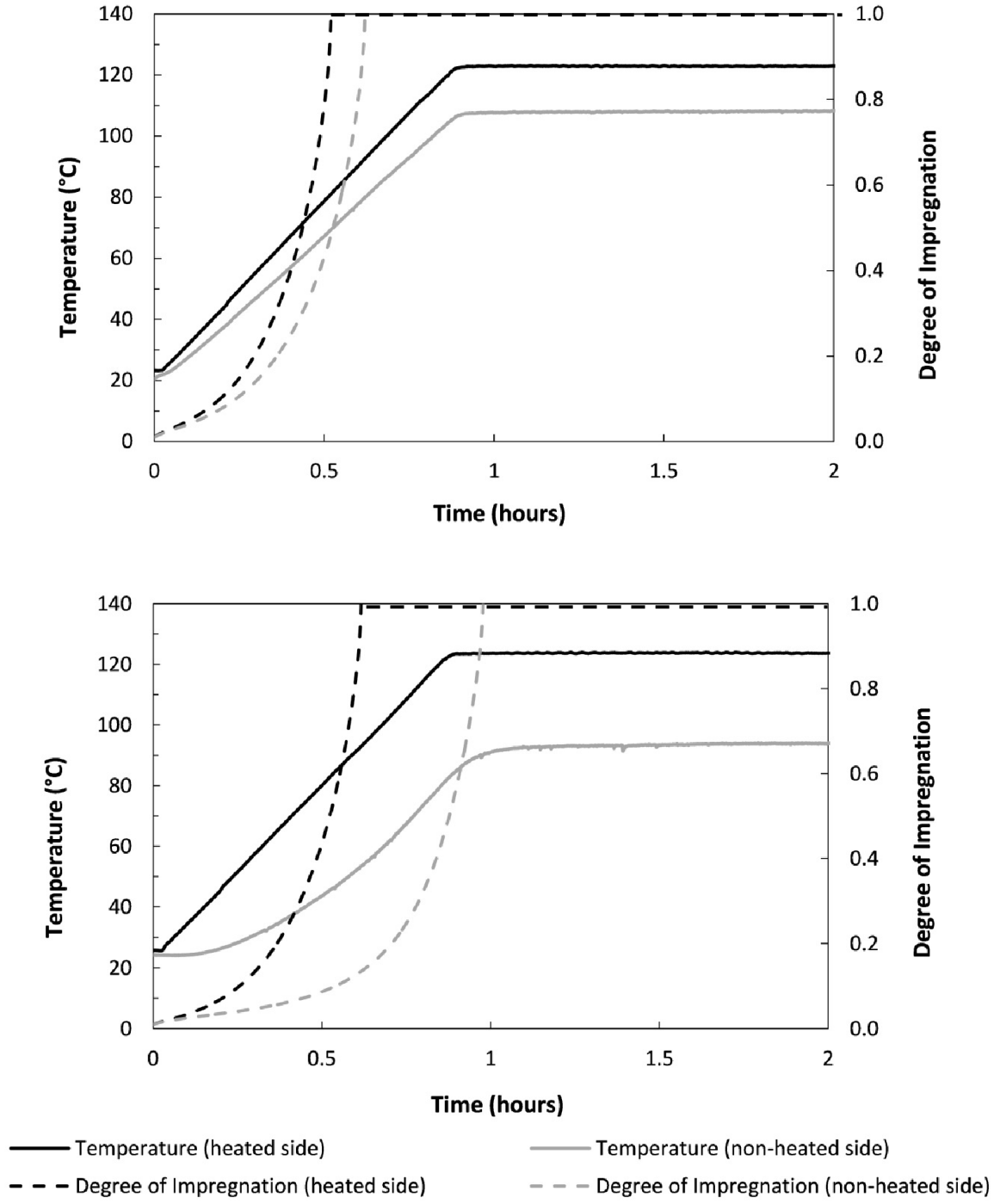


**Figure 4.3:** Graphs showing the temperature and the predicted degree of impregnation of the heated and non-heated side of the repair patch during the curing process for Case study 1**(top)** and Case Study 2**(bottom)**. Case Study 1 and 2 involve a 4.1mm thick (5320/PW) and 14mm thick (5320/8HS) parent laminate respectively.

**Analysis of Resin Viscosity and Degree of Impregnation**

The results presented by Kratz et al. show that the time-temperature cycle has a significant impact on resin viscosity, suggesting that cure cycle selection is a critical step in the processing of OOA prepregs [25]. This trend can also be seen in Figure 4.2 where the resin viscosity is shown as a function of temperature and time for a typical in-situ bonded repair process. For the case of this one-sided repair configuration, the constant temperature gradient throughout the repair patch represents additional complexity in designing an appropriate cure cycle. During the heating process, the resin viscosity changes throughout the thickness of the repair patch as shown in Figure 4.2 for the two case studies. The main consequence of this viscosity gradient is that the full impregnation of the dry fibres and gelation of the resin happen at different times throughout the repair patch.

Figure 4.3 shows the evolution of the impregnation process during the cure. This impregnation process is significantly dependent on the resin viscosity where a lower viscosity greatly favors a faster impregnation process and vice versa. As a consequence of the viscosity gradient throughout the repair patch, more time is required for the resin to fully impregnate the dry fibres furthest from the heat source, as shown in Figure 4.3. However, if the resin flow time is less than the time it takes to fully impregnate the dry fibres, this may potentially result in incomplete impregnation at gelation and result in flow induced micro-voids in the repair patch.

Consequently, to avoid these processing induced defects in the repair patch, sufficient amount of flow time must be allowed so that the dry fibres further away from the heat source can be fully saturated with resin. Alternatively, the time required to fully impregnate the resin can be reduced by using faster ramps and higher dwell temperatures. This will significantly reduce the resin viscosity furthest from the heat source leading to a faster impregnation process before the resin gels. Considering these guidelines can prove valuable when designing a cure cycle for the in-situ bonded repair process to achieve a final high quality repair patch.

This degree of impregnation model was validated by the experimental work done by Centea et al. [22], which considers the processing of OOA prepreg materials (Cycom 5320/PW and

5320/8HS) under similar processing conditions. Nonetheless, to complete the analysis of the degree of impregnation, the final quality of the repair patch can be assessed using microscopic observations of the cross sections of the cured repair patch and their comparison with predictions from models to detect any flow-induced voids. This additional analysis was not performed in this research work but it highlights the next steps for the repair patch quality assessment and ultimately, the validation of the models.

### 4.1.3 Glass Transition Temperature

Out-of-Autoclave composite materials are polymeric based structures. Their strengths and elastic properties are significantly dependent on their operating temperature [25]. An important physical property that defines the maximum operating temperature of this type of polymeric based structure (before it loses its structural integrity) is the glass transition temperature, $T_g$. In other words, the glass transition temperature defines the temperature at which the polymer transitions from a hard glassy state to a rubbery state. For the case of in-situ bonded repairs, it is essential for the $T_g$ of the repair patch to be greater than the upper operating temperature of the parent structure to achieve full structural restoration.

The glass transition temperature is dependent on the temperature profile of the repair as well as on its cure kinetics (as defined earlier). In early stages of the cure cycle, $T_g$ is below the processing temperature, but as soon as the resin has completely gelled, $T_g$ surpasses the processing temperature: this is referred to as the vitrification point. During the post cure zone, the final degree of cure of the composite material is increased and its mechanical properties are subsequently increased. In general, $T_g$ is kept higher than the processing temperature during the post-cure section to minimize any thermal-induced stresses that might result from the different coefficients of thermal expansion between the fibres and the resins. The current best practice entails a careful selection of the ramp for the post cure section according to the thermal response of the repair patch such that $T_g$ remains above the processing temperature after the vitrification point [25].

To study the evolution of $T_g$ during the processing of in-situ bonded repairs, a model developed by Kratz et al. to capture the $T_g$ of OOA prepreg material Cycom 5320 is used in conjunction

with the thermal response of the repair patch in Case Study 1 and 2 [25]. Additionally, to illustrate where the influence of $T_g$ matters the most, an additional post cure is implemented to Case Study 1 and 2 where the imposed temperature is ramped at 2°C/min to reach a dwell temperature of 180°C. The temperature profile recommended by the manufacturer was used for the post cure.

The glass transition temperature model is given by Equation (4.6),

$$\frac{T_g - T_{g0}}{T_{g\infty} - T_{g0}} = \frac{\lambda\alpha}{1-(1-\lambda)\alpha} \tag{4.6}$$

where $\alpha$ is the instantaneous degree of cure, $T_{g0}$ is the glass transition temperature of the uncured resin = -8.4°C, $T_{g\infty}$ is glass transition temperature of the fully cured resin = 212 °C and $\lambda$ is a constant = 0.66 [25].

The evolution of $T_g$ and the thermal response for Case Study 1 and 2 are plotted in Figure 4.4.

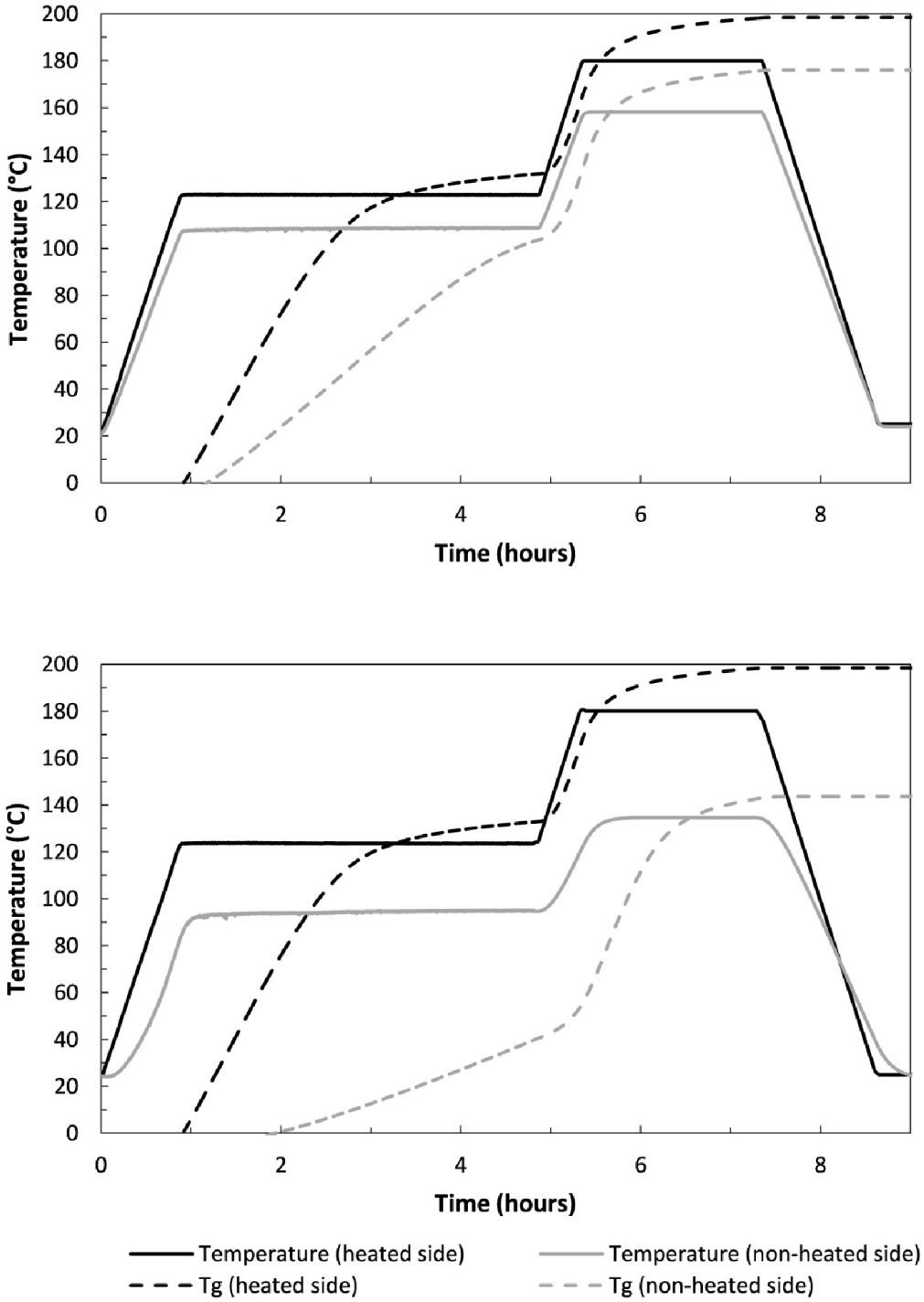


**Figure 4.4:** Graph showing the temperature and the predicted glass transition temperature of the heated and non-heated side of the repair patch during the curing process for Case study 1**(top)** and Case Study 2**(bottom)**. Case Study 1 and 2 involve a 4.1mm thick (5320/PW) and 14mm thick (5320/8HS) parent laminate respectively.

**Analysis of Glass Transition Temperature**

Figure 4.4 shows an effect of the temperature gradient induced within the repair patch. It leads to a through thickness variation in the evolution of the $T_g$ during the curing process. In both case studies, the vitrification point is not reached at the location furthest from the heat source when the manufacturer's recommended cure cycle is used. As a consequence of this lag in the evolution of $T_g$, there is an induced phase gradient within the repair patch at the end of the initial cure cycle: the side closer to the heat source is in a glassy state and the side furthest from the heat source is still in a rubbery state. Furthermore, during the recommended post cure section, the $T_g$ curve is below the temperature profile of the repair patch for both the heated and the colder side, which does not correspond to the general practice of maintaining the $T_g$ above the post-cure temperature.

To account for the temperature gradient induced variation in the glass transition temperature evolution, the imposed cure cycle must be modified for this in-situ bonded repair configuration. The first step requires extending the dwell duration in the initial cure such that $T_g$ crosses the temperature of the repair patch and the vitrification point is achieved across the entire repair patch. Next, the ramp rate during the post cure section must be adjusted according to the thermal response of the repair patch such that the temperature of the repair patch remains below the glass transition temperature. By combining the thermal response solution with the $T_g$ model, the discussed guidelines can be enforced in designing a robust cure cycle for the in-situ bonded repair process.

### 4.1.4 Summary of Thermo-Chemical Analysis

By studying the key thermo-chemical phenomena which dictate the repair patch quality, the cure cycle requirements for the in-situ bonded repair process were identified.

This simple analytical thermo-chemical approach can be used to design and optimize cure cycles for the in-situ bonded repair patch process. Additionally, since every repair process is different in terms of the thermal response of the system, the cure cycle must be revisited for each repair scenario. Therefore, having the ability to predict the thermal response as well as the thermo-

chemical phenomena for the any repair of this kind can prove valuable for quickly designing customized and robust cure cycles that best fit the processing requirements, especially for in-field applications. Next, a potential cure cycle is designed to incorporate all the thermo-chemical requirements as defined and explained above for the in-situ bonded repair configuration under study.

### 4.1.5 Modified Cure Cycle for Repair

The cure cycle for an in-situ bonded repair patch is designed by considering both the thermal response and the thermo-chemical requirements of the repair patch during processing. It was previously demonstrated that the cure cycle recommended by the manufacturer is not optimized to accommodate for any temperature gradients developed throughout the repair patch during curing. By studying the thermo-chemical behavior of the Cycom 5320 prepreg and enforcing the essential design guidelines, the cure cycle is modified accordingly for Case Study 1 as a representative application.

To adapt the manufacturer's recommended cure cycle of the Cycom 5320 prepreg for in-situ bonded repair, several modifications were made based on the thermal response and the chemical effects of the repair patch, as shown in Figure 4.5 and Figure 4.6. First, the initial ramp rate was increased to 10 °C/min to increase the minimum viscosity furthest away from the heated side, enabling a faster impregnation process before any gelation of the resin. It is worth mentioning that a ramp rate of 10 °C/min is feasible with this direct contact heat conduction technique of the in-situ bonded repair process, as opposed to an oven, where such ramp rates are not possible because of the large thermal mass of the oven. Next, the time duration of the first dwell is increased to 5 hours to ensure that the vitrification point is reached at the region furthest from the heat source. To maintain the glass transition above the processing temperature throughout the repair patch after the vitrification point, the ramp rate was set to 0.2 °C/min for during the post cure section of this case.

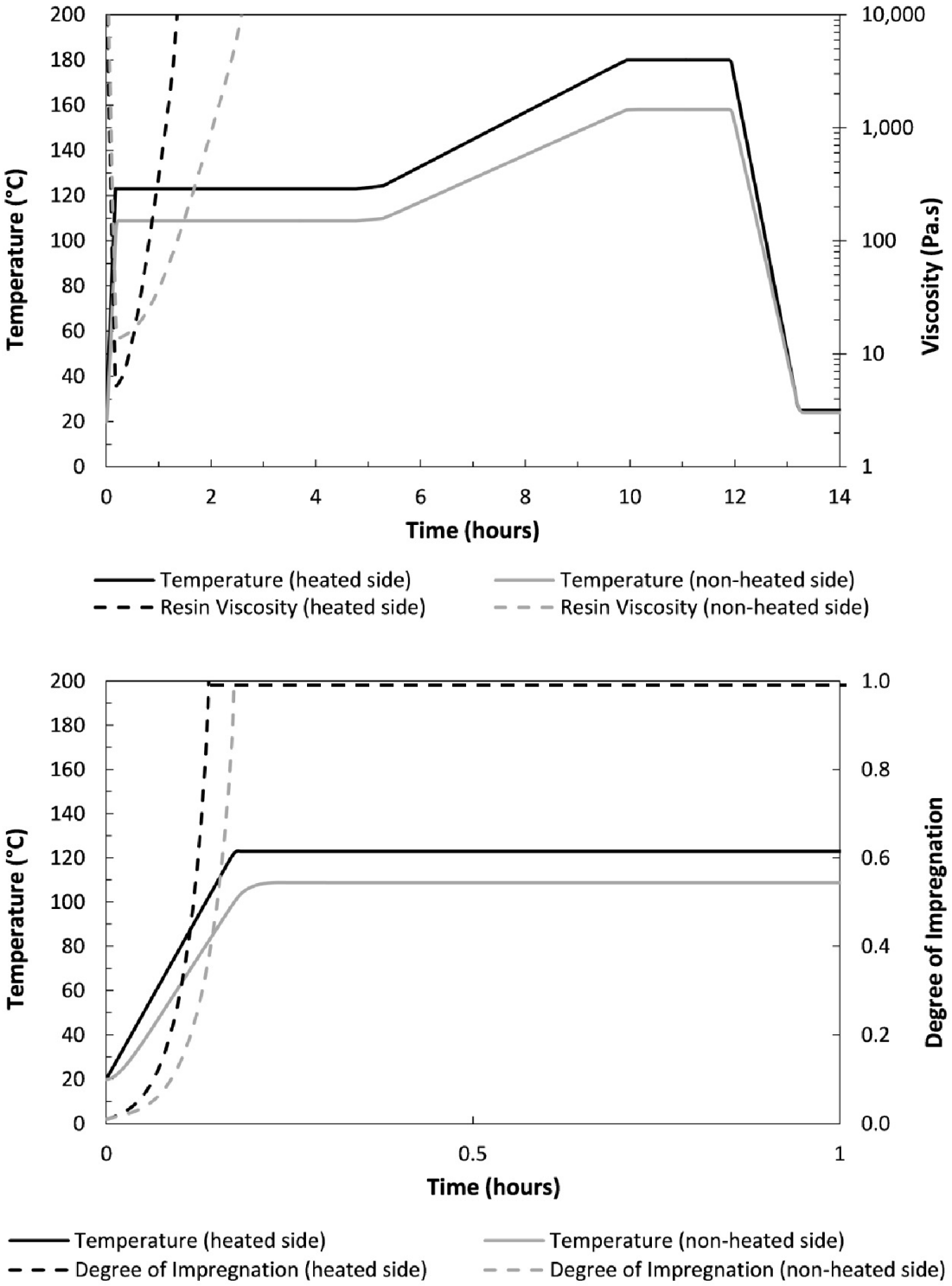


**Figure 4.5:** Graph showing the temperature evolution, the predicted resin viscosity **(top)** and degree of impregnation **(bottom)** of the heated and non-heated side of the repair patch when the modified cure cycle is imposed for Case Study 1. It involves a 4.1mm thick (5320/PW) parent laminate.

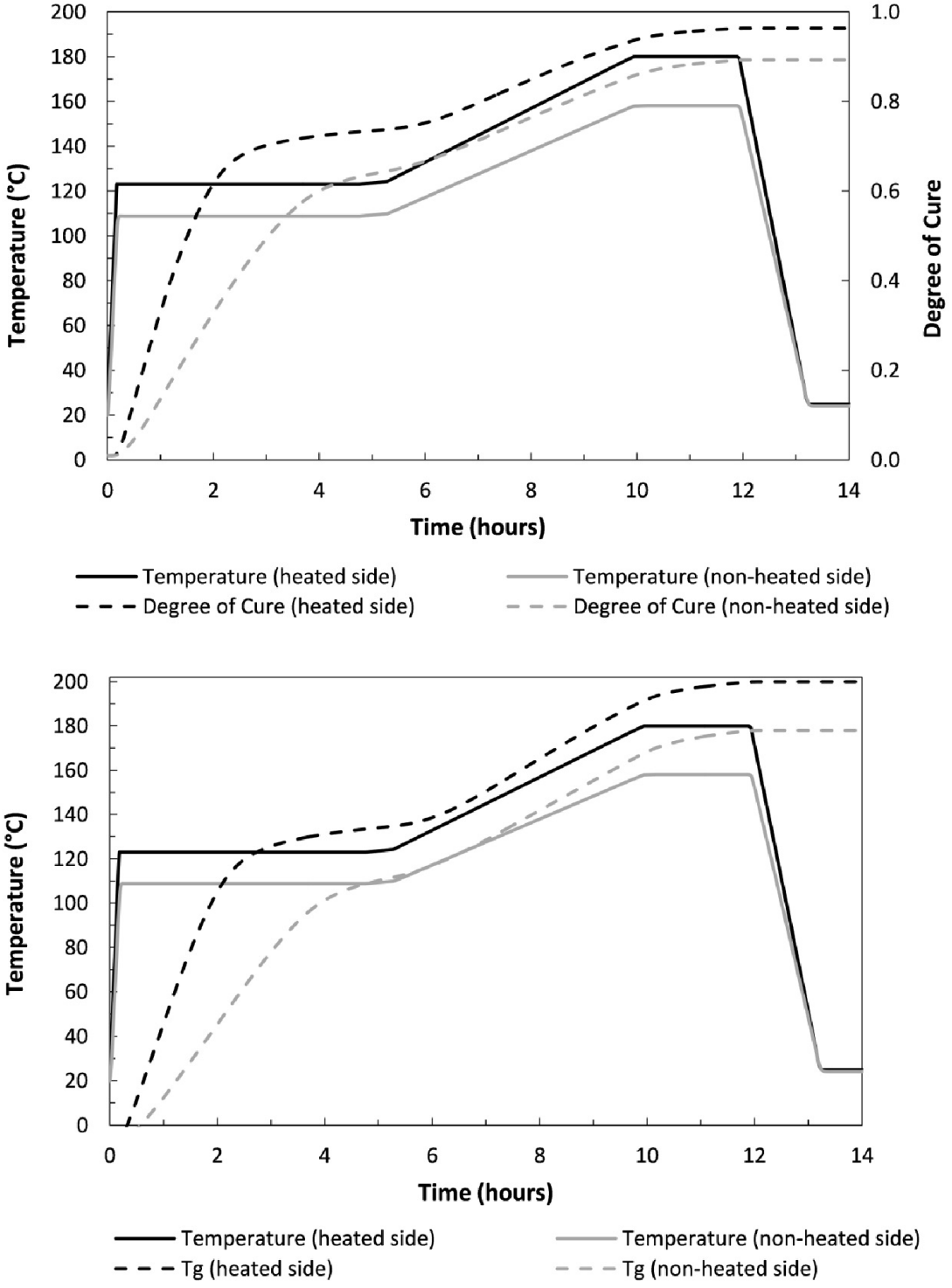


**Figure 4.6:** Graph showing the temperature evolution, the predicted degree of cure **(top)** and glass transition temperature **(bottom)** of the heated and non-heated side of the repair patch when the modified cure cycle is imposed for Case Study 1. It involves a 4.1mm thick (5320/PW) parent laminate.

All these amendments to the recommended cure cycle are necessary to accommodate for the temperature gradient induced within the repair patch. Incorporating these changes make the processing of in-situ bonded repair patch more robust by improving the final quality of the repair. Figure 4.7 shows a representative example of a repair that has been undertaken using optimized processing conditions.

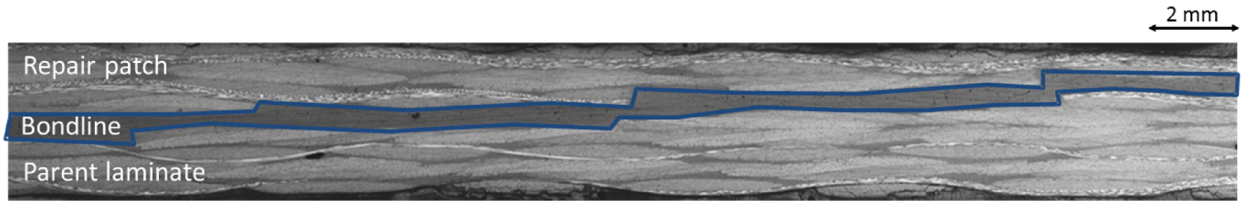


**Figure 4.7:** A micrograph of the cross-section of the monolithic panel (Case Study 1) restored using the in-situ bonded repair technique. The low void content (less than 1%) in the bondline and within the repair patch indicate a good quality repair.

Using a low resin viscosity ensured full impregnation of the dry fibres, particularly further from the heat source; this has also been illustrated by simulations, as discussed in Section 4.12. Additionally, enough time was allowed for the air to escape throughout the repair patch before premature gelation of the resin closer to the heat source, which can block the air passage and reduce the through-thickness permeability of the material, leading to void formation.

## 4.2 Thermal Response Analysis with Heat Sinks

In this section, the influence of metallic heat sinks on the thermal response of the repair patch is studied. This scenario is often seen in aircraft structures where relatively thin composite monolithic panels are reinforced using metallic spars and stiffeners. These types of structures are often referred to as stiffened panels. In-situ bonded repair process can be a potential one-step technique to repair these stiffened panels when they undergo damage. However, it is necessary to study the implication of these stiffeners on the heat transfer that takes place during the one-sided heating process to assess the feasibility of the repair.

Metallic stiffeners act as heat sinks during heating and the extent to which they influence the heat transfer depends on the materials, dimensions and shape of the stiffeners [33]. Sometimes, these stiffeners have a fin like shape, which provide good heat dissipation to the surrounding air during the heating process. However, this is undesirable for this repair process since it aggravates the temperature gradient within the repair patch.

### 4.2.1 Experimental Study of the Influence of Heat Sinks

In this study, two aluminum stiffeners with two different shapes and dimensions are considered. The first study involves a short flat stiffener and the second study consists of a longer L shaped stiffener. The effect of these two stiffeners was investigated by performing an in-situ bonded repair on a 4.1mm thick parent structure (similar to Case Study 1 in Section 3.1). During curing, the metallic stiffeners were attached on the backside of the parent laminate to simulate the structure of a stiffened panel. The two different shapes of the stiffeners considered in this experimental study are shown in Figure 4.8 and Table 4.4 shows their respective dimensions.

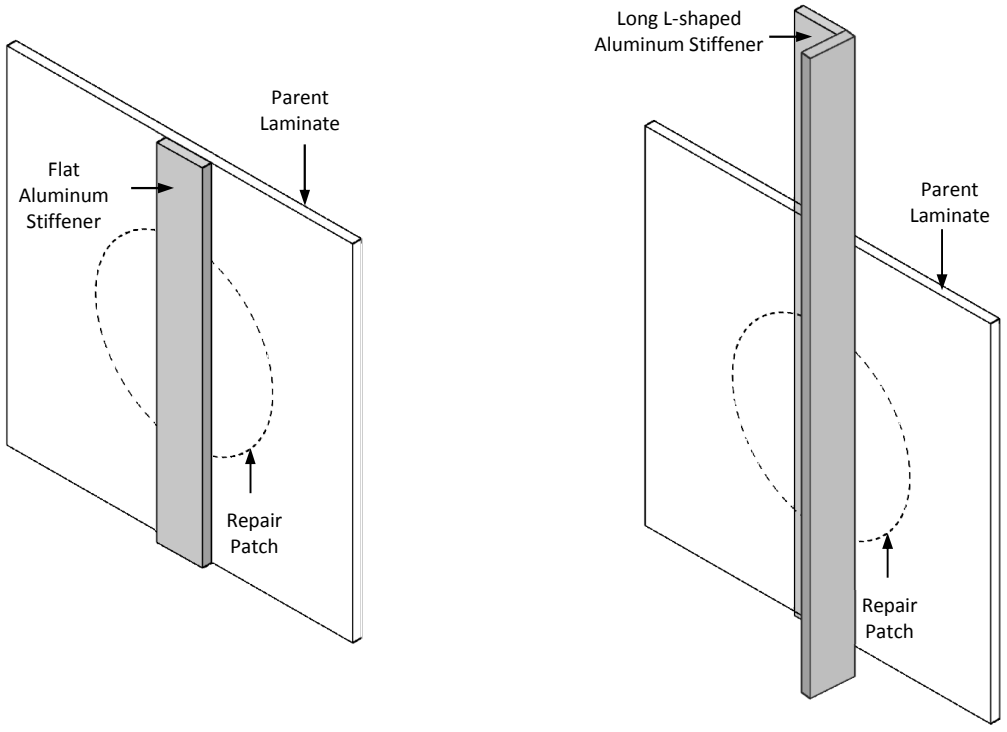


**Figure 4.8:** Schematic showing the two different types of aluminum stiffeners attached to the parent laminate:**(a)** represents a flat stiffener (Heat Sink Case Study 1) and **(b)** represents a long L-shaped stiffener (Heat Sink Case Study 2).

**Table 4.4:** Dimensions of the two types of metallic stiffener.

| **Dimensions** | **Heat Sink Case Study 1** Flat Stiffener | **Heat Sink Case Study 2** L-shaped Stiffener |
|---|---|---|
| Length (mm) | 360 | 1060 |
| Width (mm) | 48 | 38 |
| Thickness (mm) | 3.25 | 3.25 |

**Experimental Setup**

The experimental setup and procedures used for investigating the influence of heat sinks on the thermal response of the repair patch was similar to the one described in Chapter 3 where the two case studies were considered. First, a 20 plies (4.1mm thick) parent laminate as described in Section 3.1 was manufactured using Cycom 5320/PW prepreg according to the recommended procedure. The repair patch and the adhesive film were positioned in place on the parent structure and bagged according to repair procedures described in Section 3.1. Prior to performing the experiment, the heat transfer coefficient was measured experimentally using the thermal map technique.

Once the setup was in place (with the stiffener attached to the center on the non-heated side using clamps), the experiment was initiated by imposing the recommended cure cycle onto the repair patch using the heating blanket. During the curing process the temperature evolution throughout the repair patch was monitored using the data acquisition system. The locations of the thermocouples are shown in Figure 4.9.

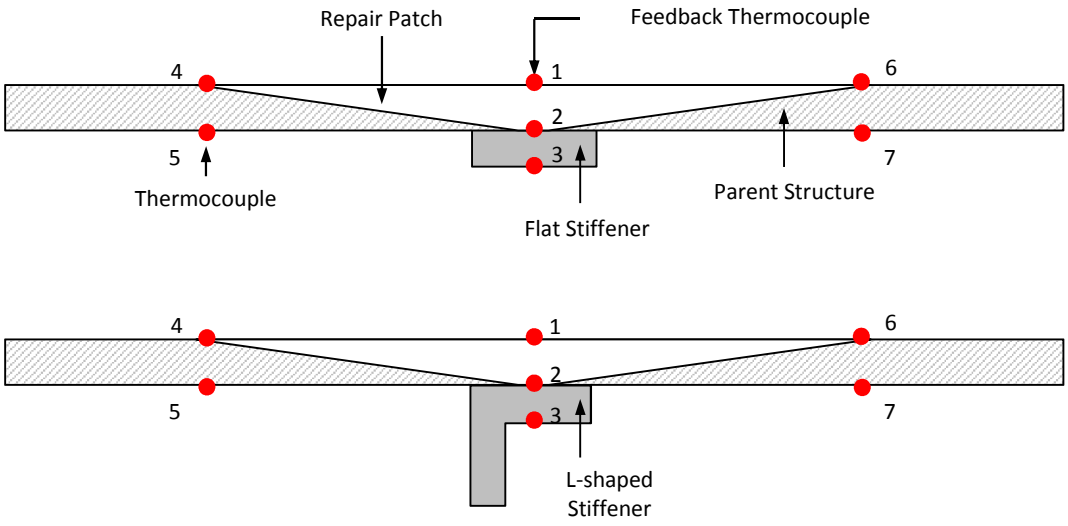


**Figure 4.9:** Schematic of the cross section of the repair patch showing the locations of the thermocouples used to capture the thermal response of the repair patch for the two heat sink case studies: Heat Sink Case Study 1 **(top)** and Heat Sink Case Study 2 **(bottom)**

In the next section, the experimental results of the temperature variation throughout the repair patch in the presence of heat sinks (metallic stiffeners) are presented and analyzed.

### 4.2.2 Experimental Results

The temperature at the various locations throughout the repair during the curing process is presented in Figure 4.10. To clearly represent the results within one graph for each case study involving a heat sink, the temperature evolution at the most critical locations are shown: **1, 2, 3 and 7**.

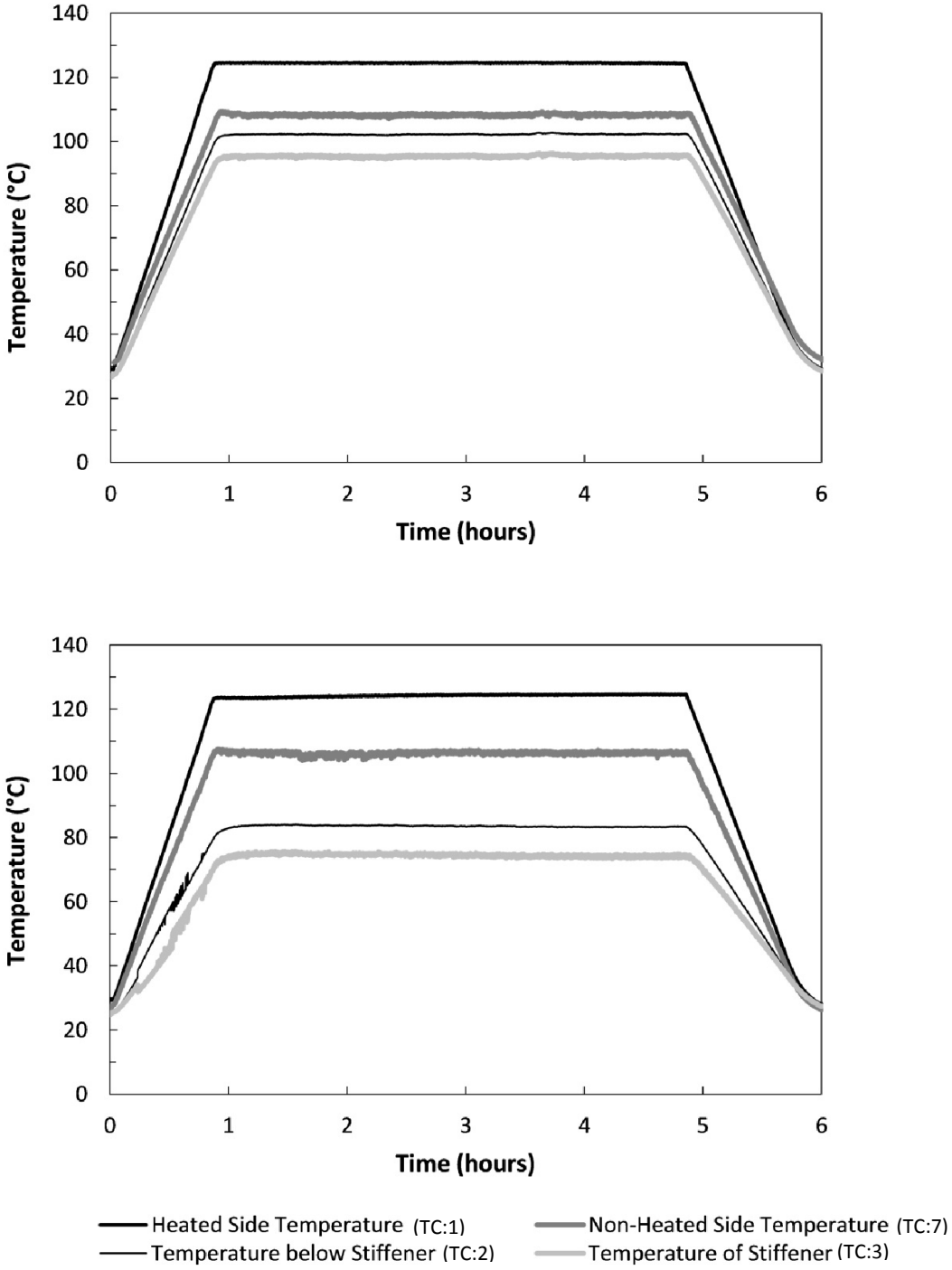


**Figure 4.10:** Graphs showing the thermal response of the repair patch for a 4.1mm thick parent laminate (5320/PW) in the presence of two different kinds of metallic stiffeners: a thin flat stiffener in Heat Sink Case Study 1 **(top)** and a long L-shaped stiffener in Heat Sink Case Study 2 **(bottom)**.

Figure 4.10 clearly shows that the thermal response of the repair patch above the metallic stiffener is affected by the presence of the heat sink. In the next section, this behavior (based on the two different types of stiffeners) is further analyzed.

### 4.2.3 Analysis of Heat Sinks

Metallic stiffeners in composite structures can significantly affect the heat transfer during the in-situ bonded repair process, as illustrated by the experimental study and results (Figure 4.10). The magnitude of this influence of the stiffeners on the heat transfer is dependent on their shape and size, as seen in the two heat sink case studies.

Heat Sink Case Study 1 considered a short, thin flat aluminum stiffener; its influence on the thermal response of the repair patch was determined experimentally. By comparing the temperature evolution directly below the metallic stiffener (location 2) to the temperature behavior at a region where there is no stiffener (location 7), it can be observed that the presence of the metallic stiffener increases the temperature gradient throughout the repair patch. This behavior can be explained by considering steady state heat conduction, which dictates the heat flux through the repair patch in the presence of a metallic heat sink. The governing 1D steady state heat flux equation for this heat transfer scenario is given by,

$$q'' = \frac{T_{imp} - T_{\infty}}{\frac{L_c}{k_c} + \frac{1}{h_c} + \frac{L_{ms}}{k_{ms}} + \frac{1}{h}} \tag{4.7}$$

where $T_{imp}$ is the imposed cure cycle, $T_{\infty}$ is the ambient temperature, $L_c/k_c$ and $L_{ms}/k_{ms}$ is the thickness to thermal conductivity ratio of the composite repair patch and the metallic stiffener respectively, $1/h_c$ is the thermal contact resistance and $1/h$ is the heat transfer coefficient of the ambient air.

Equation (4.7) shows that if the thickness to thermal conductivity ratio ($L_{ms}/k_{ms}$) of the stiffener is much lower than the same ratio for the composite material ($L_c/k_c$) due to the high thermal conductivity of its metallic nature, the presence of the stiffener will barely affect the overall heat

flux through the composite repair patch. However, $1/h_c$ , the thermal contact resistance between the non-heated sided of the repair patch with the metallic stiffener, plays a key role in the magnitude of the overall heat flux. When the contact resistance is high due to high surface roughness and rigidity at the interface, the overall heat flux is significantly increased throughout the repair patch and subsequently the temperature gradient is increased. Therefore, to ensure adequate heating during the repair of this kind of stiffened panels, it is crucial to take into account the thermal contact resistance when designing the repair.

Heat Sink Case Study 2 looked at the influence of a long and "fin-like" metallic stiffener on the repair process; the results are shown in Figure 4.10. The temperature evolution throughout the repair patch shows that this shape and geometry of the stiffener significantly alters the heat transfer within the system in addition to the thermal contact resistance. The temperature gradient is amplified during the curing process as shown by the temperature evolution at a point underneath the stiffener (thermocouple location 2). This behavior can be explained using a combination of two main heat transfer phenomena. First, the length and the high thermal conductivity of the metallic stiffener significantly contribute to the conduction and dissipation of the localized heat to the surrounding air under the repair patch along the full length of the stiffener. For instance, during the experiment, the temperature at the other extremity of the stiffener was relatively high. Secondly, the "fin-like" geometry of the stiffener behaves as a cooling system which enhances the heat exchange with the ambient air by increasing the surface area for heat convection [55]. Consequently, the heat transfer phenomena throughout the repair patch is greatly dominated by the fast cooling effect occurring due to the presence of this stiffener; the heat transfer is a function of the shape, dimensions and the thermal contact resistance of the stiffener.

### 4.2.4 Summary of Heat Sink Analysis

The influence of the metallic stiffeners on the in-situ bonded repair process was studied experimentally. It was demonstrated that the shape, dimension and the thermal contact resistance between the repair patch and the stiffener significantly alters the heat transfer phenomena leading to an amplified temperature gradient throughout the repair patch. To achieve efficient bonded

repairs on stiffened panels, it is therefore essential that these deviations in the heat transfer phenomena in the presence of heat sinks are taken into account during the design stage of the repair process. Based on the geometry and the shape of the stiffener, the relative influence on the thermal response can be assessed to be critical or negligible as demonstrated in the two heat sink case studies previously studied. The different contribution of various types of stiffeners on the heat transfer phenomena can be predicted by modelling. However, it deviates to more complicated models for which numerical tools are required to predict the thermal response of the repair patch. This was beyond the scope of the current research work; nevertheless, since this aspect of heat transfer modelling has not been considered yet, it opens an avenue for further modeling work. The presented experimental results, identification of key factors that dictate the heat transfer in the presence of stiffeners, and given explanations for the observed physical phenomena, provides preliminary steps for further studies.

# Chapter 5

# Conclusions and Future Work

## 5.1 Conclusions and Contributions

The prime objective of this work was to bridge the gap between the existing tools of heat analysis and the processing of bonded repairs to meet the demands of in-field repairs for developing robust and optimized repair processes. The main conclusions and contributions of this research work are summarized as follows:

1. **The heat transfer phenomenon of the in-situ bonded repair process was modeled analytically.**

   During the curing process of in-situ bonded repairs, the heat source is applied to only one side of the repair, leading to a non-negligible, transverse temperature gradient in the patch. To overcome the inability of in-situ instrumentation and monitoring, a modeling approach was undertaken to predict this induced temperature variation. It was found that a transient 1D heat transfer model was sufficient to capture the temperature evolution within the patch and an analytical solution was derived.

2. **Heat charts were developed as a design and optimization tool to facilitate the repair process for in-field repairs.**

   To ease the design and optimization process of in-field repairs, the solution to the heat transfer model was depicted graphically in the form of heat charts. By performing a dimensional analysis, it was found that the thermal response of the repair patch could be represented on a 2D graph. The heat charts are able to predict the thermal response of any general repair case, thus offering a valuable repair tool for in-field applications.

3. **An experimental setup to study the repair process was designed and both the analytical model and the heat charts were validated using experiments.**

   The repair experiments were performed on a laboratory scale. To best replicate the scenario for in-field repairs, a setup was designed and used to study different repair cases. A simple in-situ technique to measure the heat transfer coefficient of air was also outlined. The solution to the analytical model was validated experimentally and a close match was observed between the measured and the predicted thermal response.

4. **The repercussion of the induced thermal gradient on the key thermo-chemical phenomena of Cycom 5320 prepregs was analyzed.**

   A clearer understanding of the implications of the temperature variation on the repair patch quality was achieved by studying the evolution of the governing thermo-chemical phenomena. It was found that the recommended cure cycle for Cycom 5320 requires alteration to mitigate the effect of the temperature gradient and be optimized for the repair process. High initial ramp rates, extended dwell periods and carefully picked ramp rates for the post cure section summarise the general guidelines to adjust the cure cycle for producing high quality repair patches.

5. **The effect of the metallic stiffener on the thermal response of the repair patch was studied experimentally and the key heat transfer phenomena were identified.**

   The presence of metallic stiffener was shown to be detrimental to the curing process of in-situ bonded repair. It was found that metallic stiffeners significantly amplify the temperature gradient and also conduct heat to other areas of the structure. Furthermore, it was found that this induced temperature gradient is greatly dependent on the stiffener shape and dimensions and the thermal contact resistance with the repair patch.

## 5.2 Future Work

In addition to the main conclusions and contributions presented in this thesis, the current research work can be extended to address other aspects of processing for in-situ bonded repair process. The potential areas for further studies are discussed below.

1. **The analytical heat transfer platform can be extended to account for the thermally induced residual stresses phenomenon.**

   The temperature gradient throughout the repair patch and at the bondline inevitably generates residual stresses, which can potentially affect the shape and the strength restoration efficiency of the final repair. Djokic et al. studied the effect of residual stresses in a composite patch onto metallic structure and was able to provide guidelines on how to minimize their detrimental effects [56]. Similarly, using the developed heat transfer platform, a model to assess the effects of the temperature gradient on the residual stresses for this repair configuration, could be studied. Consequently, one of the mechanical aspects for the repair patch would be incorporated in the design and optimization process of the repair, henceforth making the process more robust.

2. **The heat transfer model can be adapted for the in-situ repair process of honeycomb structures.**

   Honeycomb structures that undergo damage represent numerous challenges to restore their structural strength using in-situ bonded repairs. One key aspect in implementing a bonded repair on a honeycomb structure is the drying process of existing honeycomb prior to bonding. When damaged honeycomb structures are exposed to a humid and fluctuating environmental cycle, they absorb a lot of humidity. This moisture content has a detrimental effect; it creates voids in the bondline and the repair patch and can also lead to pressure build when heated locally [57]. Consequently, to avoid such pervasive effects, it is required that the honeycomb structure is locally dried to achieve minimum moisture content. Therefore, the heat transfer fundamentals could be applied in a similar manner to study the drying process of the honeycomb structures, where the heat transfer model would be used in conjunction with the mass flow for humidity and pressure phenomena. The coupled heat and mass flow model would henceforth provide an insight on the repair approach for honeycomb structures.

3. **The in-situ repair process can be implemented on a representative structure to validate the developed analytical tools for optimizing the processing of the repair.**

   The in-situ bonded repair procedure devised is this thesis could be implemented on a real-life damaged structure with the modified cure cycle and the final quality of the repair patch could be assessed. It would involve determining the final degree of the cure of the entire repair patch using differential scanning calorimetry (DSC) and the flow induced void content which is dictated by the impregnation process. These characteristics of the repair patch would then be compared to predicted models.

# References


[1] P. K. Mallick, *Fiber-reinforced composites : materials, manufacturing, and design*. New York: M. Dekker, 1993.

[2] T. Centea, "Material - processing - quality relationships during the consolidation of ou-of-autoclave prepregs," PhD, Mechanical engineering, McGill University, Canada, 2012.

[3] W. D. Callister, *Materials science and engineering : an introduction*. New York: Wiley, 2000.

[4] S. W. Tsai and H. T. Hahn, *Introduction to composite materials*. Westport, Conn.: Technomic Pub., 1980.

[5] W. G. Roeseler, B. Sarh, and M. U. Kismarton, "Composite structures: The first 100 years," in *16th International Conference on Composite Materials, ICCM-16 - "A Giant Step Towards Environmental Awareness: From Green Composites to Aerospace", July 8, 2007 - July 13, 2007*, Kyoto, Japan, 2007.

[6] H. Kawakami and P. Feraboli, "Lightning strike damage resistance and tolerance of scarf-repaired mesh-protected carbon fiber composites," *Composites Part A: Applied Science and Manufacturing,* vol. 42, pp. 1247-1262, 2011.

[7] K. B. Armstrong, L. G. Bevan, and W. F. Cole, *Care and Repair of Advanced Composites (2nd Edition)*: Society of Automotive Engineers, Inc., 2005.

[8] V. Faivre and E. Morteau, "Damage tolerant composite fuselage sizing : Characterization of accidental damage threat," *Flight Airworthiness Support Technology,* vol. 48, 2011.

[9] S. Black. (2013) Lightnight strike protection strategies for composite aircraft. *Composites World*. Available: www.compositesworld.com

[10] S. R. Hall, M. D. Raizenne, and D. L. Simpson, "A proposed composite repair methodology for primary structure," *Composites,* vol. 20, pp. 479-483, 1989.

[11] A. A. Baker and R. Jones, *Bonded repair of aircraft structures*. Dordrecht; Boston; Hingham, MA, USA: M. Nijhoff ; Distributors for the United States and Canada, Kluwer Academic, 1988.

[12] L. J. Hart-Smith, "Bonded-bolted composite joints," *Journal of Aircraft,* vol. 22, pp. 993-1000, 1985.

[13] A. A. Baker, "A Proposed Approach for Certification of Bonded Composite Repairs to Flight-Critical Airframe Structure," *Applied Composite Materials,* vol. 18, pp. 337-369, 2011.

[14] L. Dorworth and G. Gardiner, "Repair of composite structures - a review," *Journal of Advanced Materials,* vol. 39, pp. 3-13, 10/ 2007.

[15] A. J. Gunnion and I. Herszberg, "Parametric study of scarf joints in composite structures," *Composite Structures,* vol. 75, pp. 364-376, 2006.

[16] A. A. Baker, R. J. Chester, G. R. Hugo, and T. C. Radtke, "Scarf repairs to highly strained graphite/epoxy structure," *International Journal of Adhesion and Adhesives,* vol. 19, pp. 161-171, 1999.

[17] A. Harman, "Optimisation and Improvement of the Design of Scarf Repairs to Aircraft," PhD, School of Mechanical and Manufacturing Engineering, The University of New South Wales, Australia, 2006.

[18] N. S. Berring, M. P. Renieri, G. G. Bond, and D. J. Palmer Jr, "Autoclave vs. Non-Autoclave: A comparison of hat-stiffened subcomponents by static and fatigue testing and related non-destructive evaluations," in *2012 SAMPE International Symposium and Exhibition - Emerging Opportunities: Materials and Process Solutions, May 21, 2012 - May 24, 2012*, Baltimore, MD, United states, 2012.

[19] Sutter J.K., Scott W.K., Pelham L., Miller S.G., Polis D.L., Nailadi C.*, et al.*, "Comparison Of Autoclave And Out-of-autoclave Composites," in *42nd ISTC*, Salt Lake City, UT, 2010, p. 14.

[20] C. Dang, K. Bernetich, E. Carter, and G. Butler, "Mechanical comparison of out-of-autoclave prepreg part to conventional autoclave prepreg part," in *67th American Helicopter Society International Annual Forum 2011, May 3, 2011 - May 5, 2011*, Virginia Beach, VA, United States, 2011, pp. 1900-1910.

[21] L. K. Grunenfelder and S. R. Nutt, "Air Removal In Vbo Prepreg Laminates: Effects Of Breathe-Out Distance And Direction," presented at the 43rd ISTC, Ft. Worth, TX, 2010.

[22] T. Centea and P. Hubert, "Modelling the effect of material properties and process parameters on tow impregnation in out-of-autoclave prepregs," *Composites Part A: Applied Science and Manufacturing,* vol. 43, pp. 1505-1513, 9// 2012.

[23] L. Repecka and J. Boyd, "Vacuum-bag-only-curable prepregs that produce void-free parts," in *47th International SAMPE Symposium and Exhibition, May 12, 2002 - May 16, 2002*, Long Beach, CA, United states, 2002, pp. 1862-1874.

[24] C. Ridgard, "Out of autoclave composite technology for aerospace, defense and space structures," in *SAMPE '09 Spring Symposium Conference Proceedings, May 18, 2009 - May 21, 2009*, Baltimore, MD, United states, 2009.

[25] J. Kratz, K. Hsiao, F. Goran, and P. Hubert, "Thermal models for MTM45-1 and Cycom 5320 out-of-autoclave prepreg resins," *Journal of Composite Materials,* 2012.

[26] T. Centea and P. Hubert, "Measuring the impregnation of an out-of-autoclave prepreg by micro-CT," *Composites Science and Technology,* vol. 71, pp. 593-599, 2011.

[27] F. C. Campbell, "Repair," in *Structural Composite Materials*, ed: ASM International, 2010, pp. 517-535.

[28] J. E. Robson, F. L. Matthews, and A. J. Kinloch, "The bonded repair of fibre composites: Effect of composite moisture content," *Composites Science and Technology,* vol. 52, pp. 235-246, 1994.

[29] N. A. Laboratory. (24 June 2014). *Composites Repair*. Available: www.nlr.nl

[30] J. Kratz, "Processing Composite Sandwich Structures using Out-of-Autoclave Technology," M.Eng, Mechanical Engineering, McGill University, 2009.

[31] B. M. Louis, "Gas transport in Out-Of-Autoclave prepreg laminates," Master of Applied Science, Materials Engineering, University of British Columbia, 2007.

[32] M. Preau, K. Bujun, N. Auda, and P. Hubert, "Out-of-autoclave soft-patch breathing solutions for low porosity repairs," in *SAMPE Tech 2013 Conference and Exhibition, October 21, 2013 - October 24, 2013*, Wichita, KS, United States, 2013.

[33] M. Davis and J. Tomblin, "Best Practice in Adhesive-Bonded Structures and Repairs," U. S. D. o. Transportation, Ed., ed. Springfield, Virginia: National Technical Information Services, 2007.

[34] M. Davis and D. Bond, "Principles and practices of adhesive bonded structural joints and repairs," *International Journal of Adhesion and Adhesives,* vol. 19, pp. 91-105, 1999.

[35] M. N. Watson, "Using infrared technology thermal profiling of a repair area," in *SAMPE 2010 Conference and Exhibition "New Materials and Processes for a New Economy", May 17, 2010 - May 20, 2010*, Seattle, WA, United States, 2010, p. Seattle and Eastern Canada SAMPE Chapters.

[36] T. K. Papathanasiou, S. I. Markolefas, S. P. Filopoulos, and G. J. Tsamasphyros, "Heat Transfer in Thin Multilayered Plates—Part II: Applications to the Composite Patch Repair Technique," *Journal of Heat Transfer,* vol. 133, pp. 021303-1 - 021303-7, 2010.

[37] T. K. Papathanassiou, S. P. Filopoulos, and G. J. Tsamasphyros, "Optimization of composite patch repair processes with the use of genetic algorithms," *Optimization and Engineering,* vol. 12, pp. 73-82, 2011.

[38] A. N. Rider, C. H. Wang, and J. Cao, "Internal resistance heating for homogeneous curing of adhesively bonded repairs," *International Journal of Adhesion and Adhesives,* vol. 31, pp. 168-176, 2011.

[39] C. C. N. Bestley, S. G. R. Brown, and S. M. Alston, "Experimental validation of a thermal model of adhesively bonded scarf repairs for CFRP composite materials incorporating cure kinetics," in *5th International Conference on Computational Methods and Experiments in Materials Characterisation, MC11, July 13, 2011 - July 15, 2011*, Malta, 2011, pp. 351-362.

[40] A. F. Emery, "Preliminary results for estimating the backside heat losses of a composite panel," in *2010 14th International Heat Transfer Conference, IHTC 14, August 8, 2010 - August 13, 2010*, Washington, DC, United states, 2010, pp. 397-404.

[41] A. Rasekh, R. Vaziri, and A. Poursartip, "Simple techniques for thermal analysis of the processing of composite structures," in *36th International SAMPE Technical Conference - Materials and Processing:Sailing into the Future, November 15, 2004 - November 18, 2004*, San Diego, CA, United States, 2004, pp. 1089-1099.

[42] M. P. Heisler, "Temperature charts for induction and constant temperature heating," *Transactions of the ASME,* vol. 69, pp. 227-236, 04/ 1947.

[43] L. Khoun, T. Centea, and P. Hubert, "Characterization Methodology of Thermoset Resins for the Processing of Composite Materials — Case Study: CYCOM 890RTM Epoxy Resin," *Journal of Composite Materials,* vol. 44, pp. 1397-1415, June 1, 2010 2010.

[44] P. Hubert, A. Johnston, A. Poursartip, and K. Nelson, "Cure kinetics and viscosity models for Hexcel 8552 epoxy resin," in *46th International SAMPE Symposium and Exhibition -2001 a Materials and Processes Odyssey, May 6, 2001 - May 10, 2001*, Long Beach, CA, United States, 2001, pp. 2341-2354.

[45] M. N. Özisik, *Heat conduction*. New York: Wiley, 1993.

[46] McMaster. (June 2013). *Heating Blankets* Available: www.mcmaster.com

[47] W. A. Strauss, *Partial differential equations : an introduction*. New York: Wiley, 1992.

[48] Cytec Engineered Materials, "CYCOM 5320-1 Epoxy Resin System," *Technical Data Sheet,* vol. Revision 01–19.03.12, 2009.

[49] Cytec Engineered Materials, "FM® 300-2 film adhesive," *Technical Data Sheet,* vol. Revision 02–27.09.11, 2011.

[50] J. V. Beck, B. Blackwell, and C. R. St Clair, *Inverse heat conduction : ill-posed problems*. New York: Wiley, 1985.

[51] J. P. Holman, *Heat transfer*. Boston, [Mass.]: McGraw Hill Higher Education, 2010.

[52] Y. Yener and S. Kakaç, *Heat conduction*. New York: Taylor & Francis, 2008.

[53] M. R. Kamal and S. S., "Kinetics and thermal characterization of thermoset cure," *PEN Polymer Engineering & Science,* vol. 13, pp. 59-64, 1973.

[54] K. C. Cole, J. J. Hechler, and D. Noel, "New approach to modeling the cure kinetics of epoxy amine thermosetting resins. 2. Application to a typical system based on bis[4-(diglycidylamino)phenyl]methane and bis(4-aminophenyl) sulfone," *Macromolecules,* vol. 24, pp. 3098-3110, 1991.

[55] A. Bejan, *Heat transfer*. New York: John Wiley & Sons, 1993.

[56] D. Djokic, A. Johnston, A. Rogers, P. Lee-Sullivan, and N. Mrad, "Residual stress development during the composite patch bonding process: measurement and modeling," *Composites Part A: Applied Science and Manufacturing,* vol. 33, pp. 277-288, 2002.

[57] J. Kratz, "Transport Phenomena in Vacuum Bag Only Prepreg Processing of Honeycomb Sandwich Panels," PhD thesis, Mechanical Engineering, McGill university, 2013.

# Appendix

Thermocouples measurement data for the experimental Case Studies 1 and 2 considered in Chapter 3 for the experimental validation of the analytical model:

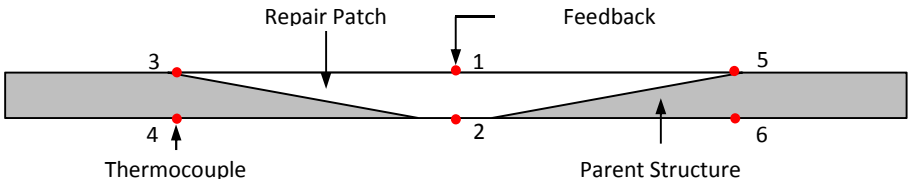


**Figure A.1:** Schematic of the repair patch and parent laminate showing the locations of the thermocouples used to capture the thermal response of the repair patch during curing.

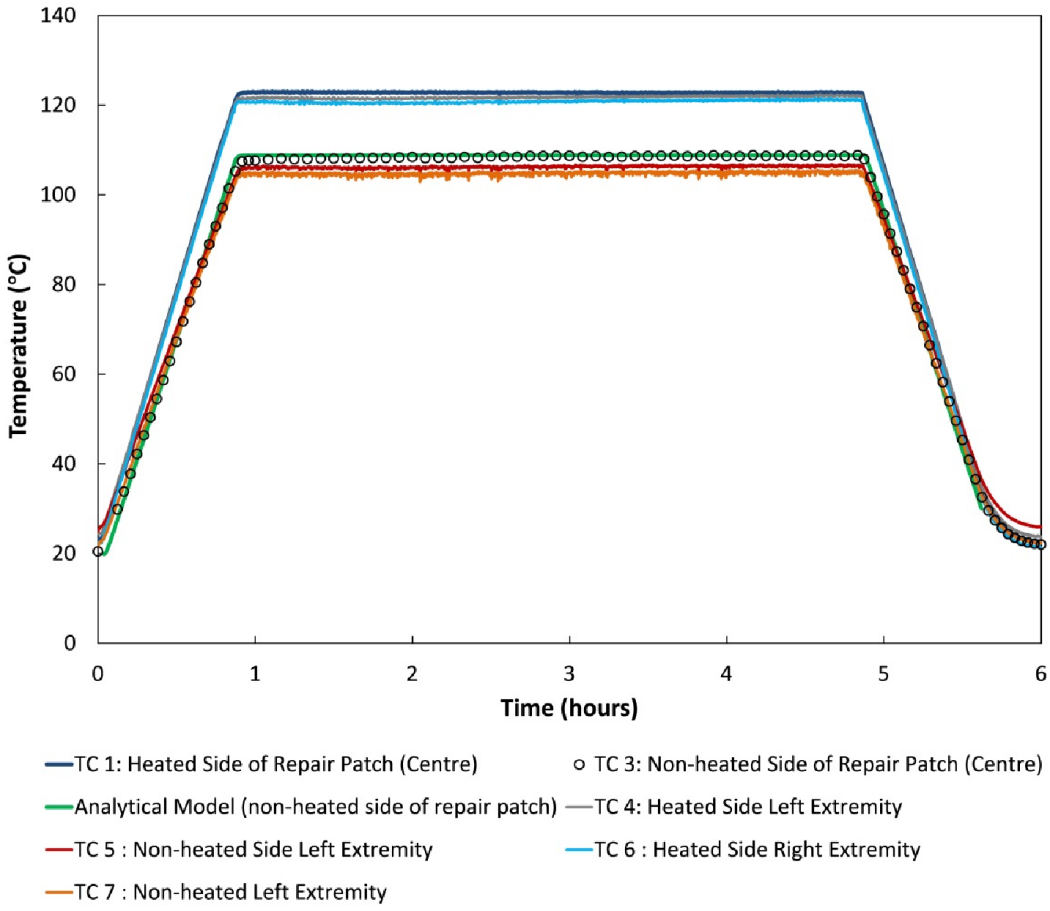


**Figure A.2:** A temperature plot showing the temperature distribution through the thickness of the repair patch during the curing process for Case Study 1 (4.1 mm thick). The temperature at locations 1, 2,3,4,5 and 6 of the repair patch is shown.

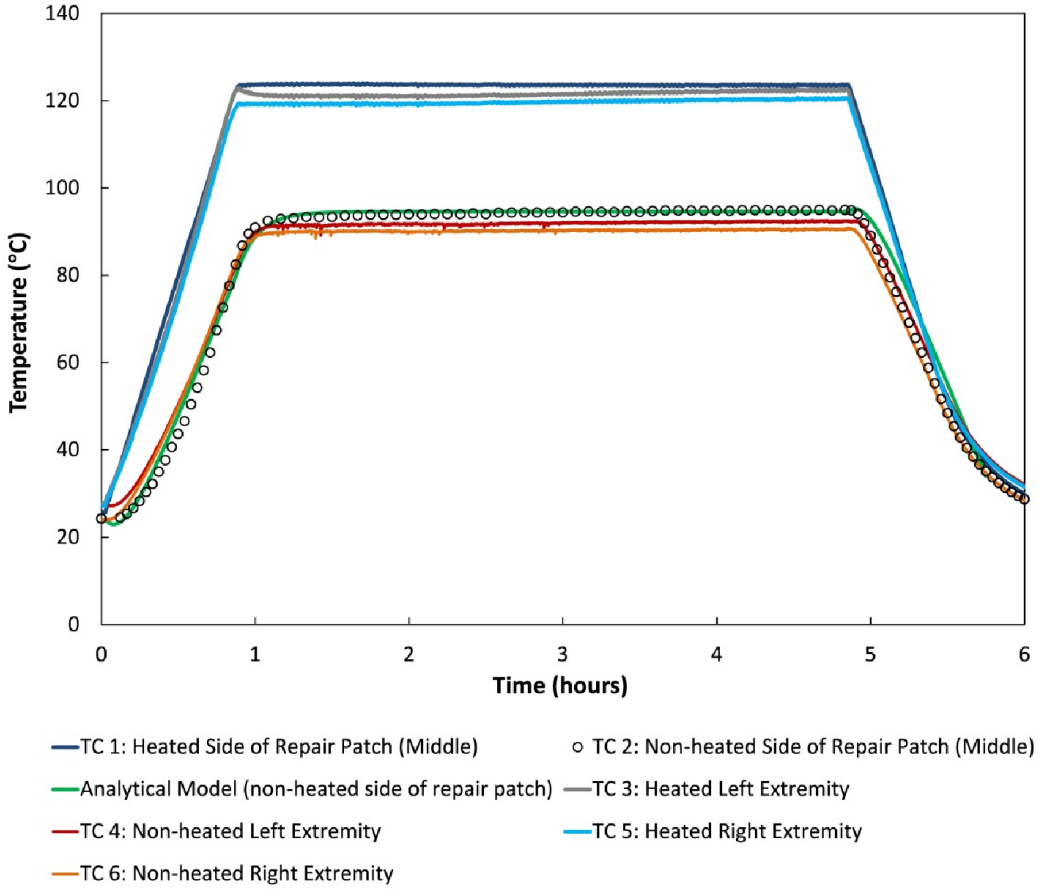


**Figure A.3:** A temperature plot showing the temperature distribution through the thickness of the repair patch during the curing process for Case Study 2 (14 mm thick). The temperature at locations 1,2,3,4, 5 and 6 of the repair patch is shown.

Heat chart sample illustration of the two experimental case studies presented in Chapter 3:

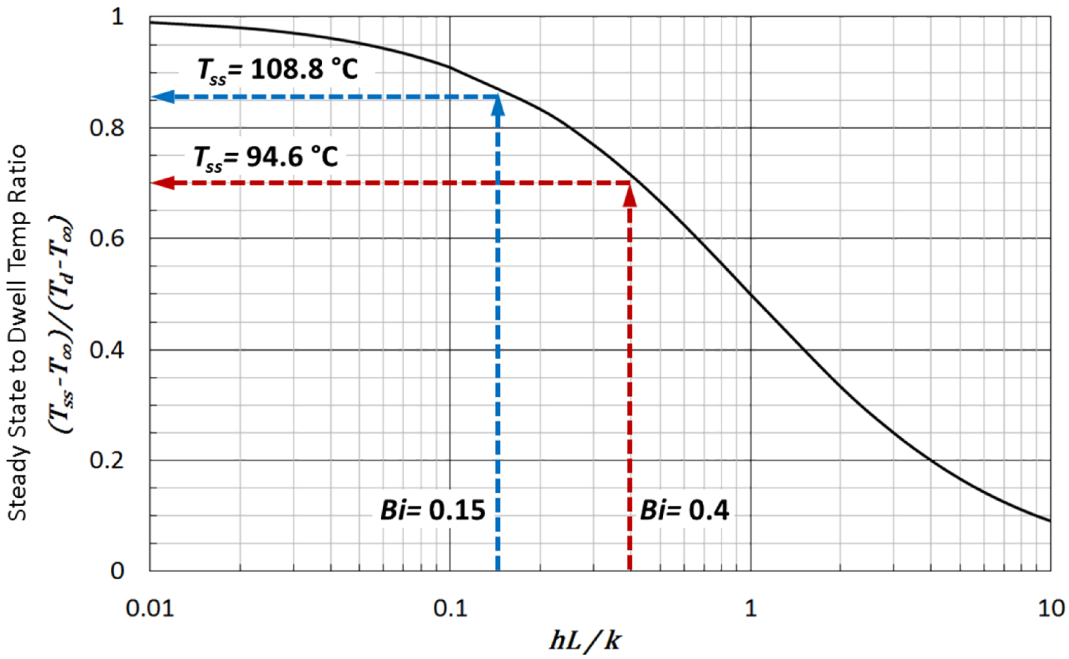


**Figure A.4:** Heat chart showing the extracted values of the steady state temperature for the non-heated side of the repair patch ($T_{ss}$) for the experimental Case Studies 1 and 2 discussed in Chapter 3.

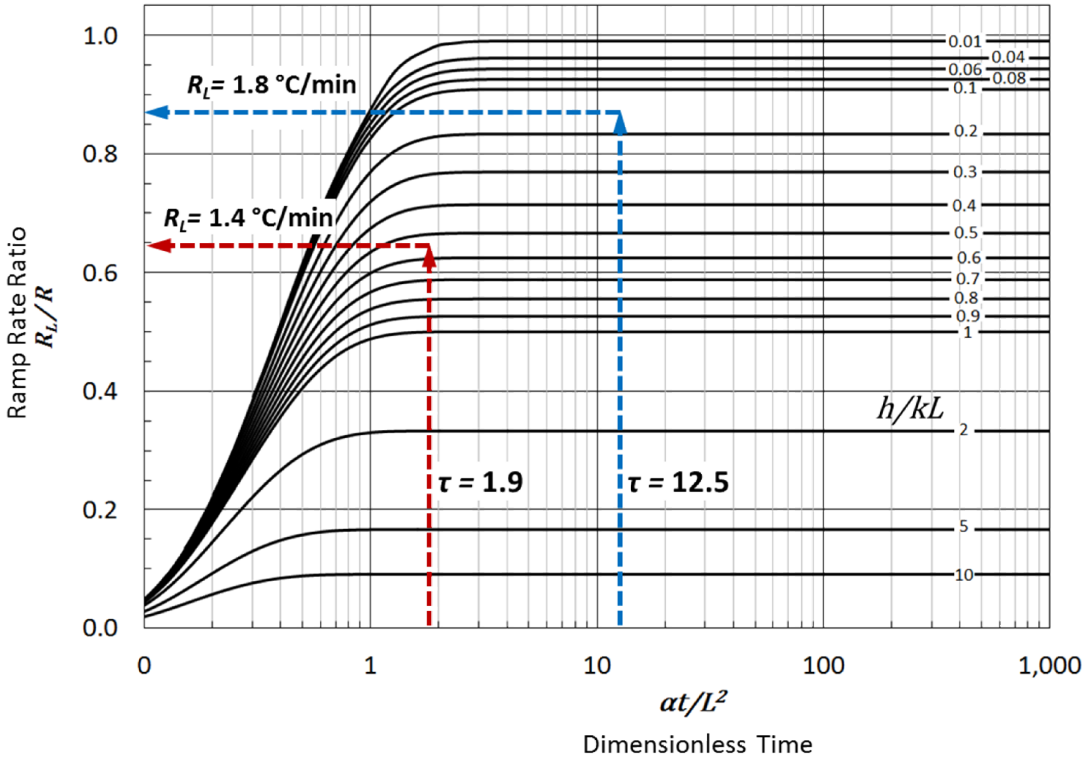


**Figure A.5:** Heat chart showing the extracted values of the ramp rate of the non-heated side of the repair patch ($R_L$) for the experimental Case Studies 1 and 2 discussed in Chapter 3.

Contour plots illustrating the trends of the influence of $h$ and $L$ on the two key characteristics of the thermal response, $\Delta T$, and $t_{ss}$:

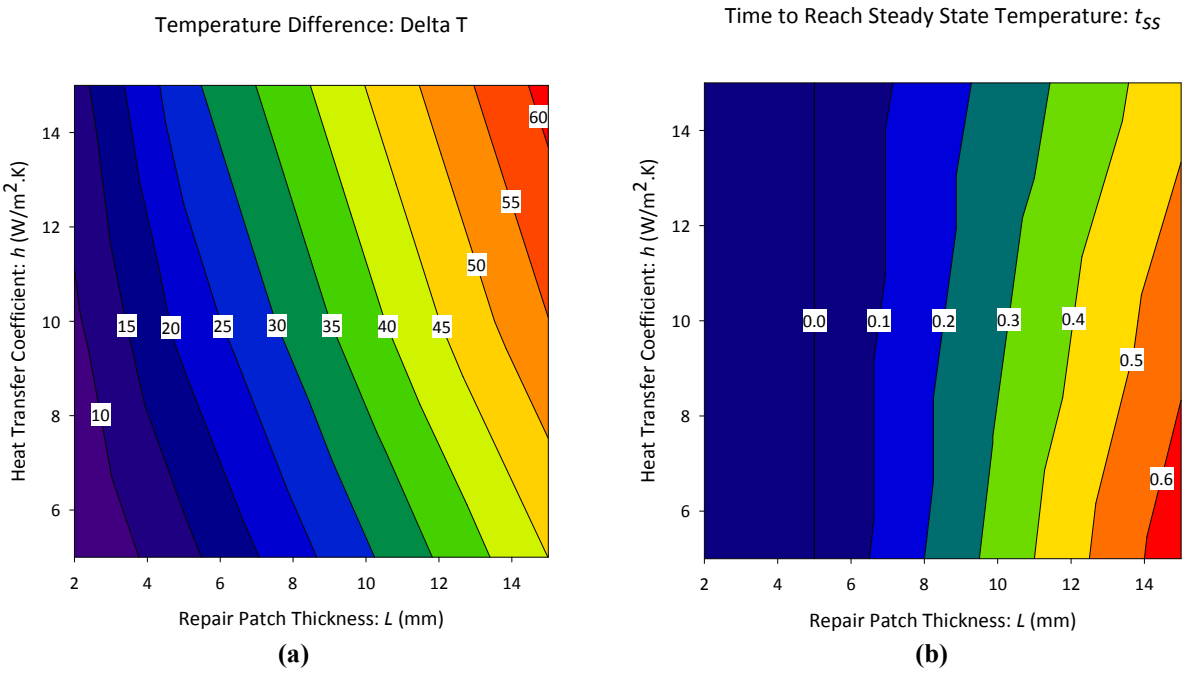


**Figure A.6:** A contour plot of the relative deviations in **(a)** $\Delta T$ ,in °C, and **(b)** $t_{ss}$ , in hours, from the baseline imposed cure cycle is shown for a range of values of heat transfer coefficient, $h$, and repair patch thickness, $L$.